

METAL-ORGANIC FRAMEWORKS (MOFs): SYNTHESIS,
CHARACTERIZATION, AND POTENTIAL APPLICATIONS

A THESIS SUBMITTED TO
THE GRADUATE SCHOOL OF NATURAL AND APPLIED SCIENCES
OF
MIDDLE EAST TECHNICAL UNIVERSITY

BY

SAEED AHMAD KHAN

IN PARTIAL FULFILLMENT OF THE REQUIREMENTS
FOR
THE DEGREE OF MASTER OF SCIENCE
IN
MICRO AND NANOTECHNOLOGY

AUGUST 2022

Approval of the thesis:

**METAL-ORGANIC FRAMEWORKS (MOFs): SYNTHESIS,
CHARACTERIZATION, AND POTENTIAL APPLICATIONS**

submitted by **SAEED AHMAD KHAN** in partial fulfillment of the requirements for
the degree of **Master of Science in Micro and Nanotechnology, Middle East
Technical University** by,

Prof. Dr. Halil Kalıpçılar
Dean, Graduate School of **Natural and Applied Sciences**

Prof. Dr. Deniz Üner
Head of the Department, **Micro and Nanotechnology**

Prof. Dr. Burcu Akata Kurç
Supervisor, **Micro and Nanotechnology, METU**

Examining Committee Members:

Prof. Dr. Necati Özkan
Polymer Science and Technology, METU

Prof. Dr. Burcu Akata Kurç
Micro and Nanotechnology, METU

Prof. Dr. Emren Nalbant
Chemistry, METU

Assoc. Prof. Dr. Selis Önel Kayran
Chemical Engineering, Hacettepe University

Assoc. Prof. Dr. Bahar İpek Torun
Chemical Engineering, METU

Date: 22.08.2022

I hereby declare that all information in this document has been obtained and presented in accordance with academic rules and ethical conduct. I also declare that, as required by these rules and conduct, I have fully cited and referenced all material and results that are not original to this work.

Name, Last name : Saeed Ahmad Khan

Signature :

ABSTRACT

METAL-ORGANIC FRAMEWORKS (MOFs): SYNTHESIS, CHARACTERIZATION, AND POTENTIAL APPLICATIONS

Khan, Saeed Ahmad
Master of Science, Micro and Nanotechnology
Supervisor : Prof. Dr. Burcu Akata Kurç

August 2022, 148 pages

Metal-organic frameworks (MOFs) are an emerging class of crystalline porous materials that consist of metal clusters (nodes) connected by organic linkers (struts) to form a three-dimensional molecular framework. MOFs have attracted considerable attention in recent years owing to their exceptional properties. Due to their remarkable design flexibility, ultra-high porosity, large specific surface area, and tunable chemistry, MOFs are indispensable for potential applications in clean energy, gas adsorption, and catalysis.

In this study, three types of MOFs were synthesized by the solvothermal method i.e. UiO-66 a zirconium-based MOF (Zr-MOF), MIL-125 a titanium-based MOF (Ti-MOF), and MIL-47 a vanadium-based MOF (V-MOF). The three MOFs synthesized in this study have different molecular framework structures and topologies. MOFs were synthesized by varying synthesis temperatures, precursor concentrations, reaction time, and using modulators.

UiO-66 MOF was synthesized at different synthesis temperatures (80°C, 100°C, and 120°C) and precursor (ZrCl₄ and H₂bdc) concentrations i.e. ZrCl₄ 8.6-19.1 mM and H₂bdc 8.6-36.1 mM. It was shown that the synthesis temperature and concentration of precursors have affected the synthesis (reaction) time for UiO-66 as well as the

size and morphology of the UiO-66 crystals. The use of modulators like HCl, acetic acid, and triethylamine changed the morphology and the size of the crystals. Moreover, the synthesis time was also affected by the introduction of modulators in the synthesis solution of UiO-66. The water adsorption capacity of UiO-66 MOF was also tested for relative humidity (%Rh) values of 25-80% at 30°C.

MIL-125 synthesis was achieved under different experimental conditions without the use of a glove box. MIL-125 was synthesized from 100°C, 130°C, 150°C, and 160°C, and it was observed that the synthesis temperature affected the morphology of MIL-125 crystals. The synthesis time (2 days and 3 days) changed the morphology of the synthesized MIL-125 crystals. The reactant concentrations (H₂bdc and titanium isopropoxide) and the impurities formed during the synthesis affected the MIL-125 MOF product. Furthermore, some variation in the MIL-125 crystal shape was observed from batch to batch even when synthesized at the same experimental conditions and precursor concentrations.

MIL-47 was synthesized at different synthesis temperatures (160°C and 220°C), reaction times (1 day, 3 days, and 5 days), and precursors (H₂bdc and VOSO₄.nH₂O) concentrations. The synthesis temperature affected the shape of the MIL-47 crystals as well as the synthesis (reaction) time. Different crystal morphologies were obtained for MIL-47 MOF at different experimental conditions.

Keywords: MOFs, Synthesis, UiO-66, MIL-125, MIL-47

ÖZ

METAL-ORGANİK ÇERÇEVELER (MOF'lar): SENTEZİ, KARAKTERİZASYONU VE POTANSİYEL UYGULAMALARI

Khan, Saeed Ahmad
Yüksek Lisans, Mikro ve Nanoteknoloji
Tez Yöneticisi: Prof. Dr. Burcu Akata Kurç

Ağustos 2022, 148 sayfa

Metal-organik çerçeveler (MOF'lar), üç boyutlu moleküler çerçeve oluşturmak için organik bağlayıcılar (destekler) ile bağlanan metal kümelerden (düğümlerden) oluşan, gelişmekte olan bir kristal gözenekli malzeme sınıfıdır. MOF'lar olağanüstü özellikleri nedeniyle son yıllarda büyük ilgi görmüştür. Dikkate değer tasarım esnekliği, ultra yüksek gözenekliliği, yüksek spesifik yüzey alanı ve ayarlanabilir kimyası nedeniyle MOF'lar temiz enerji, gaz adsorpsiyonu ve katalizör alanlarındaki potansiyel uygulamalar için vazgeçilmezdir.

Bu çalışmada, üç tip MOF: zirkonyum bazlı (Zr-MOF) UiO-66, titanyum bazlı (Ti-MOF) MIL-125 ve vanadyum bazlı (V-MOF) MIL-47 solvotermal yöntemle sentezlenmiştir. Bu çalışmada sentezlenen üç MOF, farklı moleküler çerçeve yapılarına ve topolojilerine sahiptir. MOF'lar, farklı sentez sıcaklıkları, öncül madde konsantrasyonları, reaksiyon süresi ve modülatörler kullanılarak sentezlenmiştir.

UiO-66 MOF, farklı sentez sıcaklıklarında (80°C, 100°C ve 120°C) ve farklı öncül madde (ZrCl₄ ve H₂bdc) konsantrasyonlarında yani ZrCl₄ 8.6-19.1 mM ve H₂bdc 8.6-36.1 mM'da sentezlenmiştir. Sentez sıcaklığı ve öncül madde

konsantrasyonunun, UiO-66'in sentez (reaksiyon) süresiyle birlikte UiO-66 kristallerinin boyut ve morfolojisini etkilediği gösterilmiştir. HCl, asetik asit ve trietilamin gibi modülatörlerin kullanımı, kristallerin morfolojisini ve boyutunu etkilemiştir. Ayrıca, sentez süresi, UiO-66'nın sentez çözeltisine modülatörlerin eklenmesinden de etkilenmiştir. UiO-66 MOF'un su tutma kapasitesi de 30°C'de %25-80 bağıl nem (%Rh) değerleri için test edilmiştir.

MIL-125 sentezi, eldivenli kabin kullanılmadan farklı deney koşulları altında gerçekleştirilmiştir. MIL-125, 100°C, 130°C, 150°C ve 160°C'de sentezlenmiş ve sentez sıcaklığının MIL-125 kristallerinin morfolojisini etkilediği gözlenmiştir. Sentez süresi (2 gün ve 3 gün), sentezlenen MIL-125 kristallerinin morfolojisini değiştirmiştir. Reaktant konsantrasyonları (H₂bdc ve titanyum izopropoksit) ve sentez sırasında oluşan safsızlıklar MIL-125 MOF ürününü etkilemiştir. Ayrıca, aynı deneysel koşullar ve öncül madde konsantrasyonlarında sentezlendiğinde bile MIL-125 kristal şeklinde bir partiden partiye bazı varyasyonlar gözlemlenmiştir.

MIL-47, farklı sentez sıcaklıklarında (160°C ve 220°C), reaksiyon sürelerinde (1 gün, 3 gün ve 5 gün) ve öncül madde (H₂bdc ve VOSO₄.nH₂O) konsantrasyonlarında sentezlenmiştir. Sentez sıcaklığı, MIL-47 kristallerinin şeklini ve ayrıca sentez (reaksiyon) süresini etkilemiştir. MIL-47 MOF için farklı deney koşullarında farklı kristal morfolojileri elde edilmiştir.

Anahtar Kelimeler: MOF'lar, Sentez, UiO-66, MIL-125, MIL-47

To my parents and all those who touched my life

ACKNOWLEDGMENTS

Foremost, it is my pleasure to express my deepest gratitude and appreciation to my supervisor, Prof. Dr. Burcu Akata Kurç, micro and nanotechnology program, METU, Ankara. I am thankful for her mentorship and continuous guidance throughout my research work. Without her sincere support and critique, this work would not have been possible. I am beholden to Dr. Burcu Akata Kurç for her confidence in me and for motivating me all along this journey.

I would like to thank and pay my regards to Assoc. Prof. Dr. Selis Önel Kayran, chemical engineering department at Hacettepe University, Ankara, for her valuable insights and constant guidance during my thesis and the TUBİTAK project. I truly appreciate Dr. Selis Önel Kayran for allowing me to work in her research lab and collaborate with her research group.

I would like to thank all my cohort members in the Nanodev research group, Cansu Gölboylu, Duygu Kuzyaka, Melda İşler Binay, Öyku Baltacı, Pelin Paşabeyoğlu, Ramona Davoudnezhad, Salih Kaan Kirdeciler, and Temel Burak Kutlu, for their encouragement, support, warm friendship, and great memories. I am thankful to them for motivating me whenever I felt low and stressed. Thanks to Ramona Davoudnezhad and Pelin Paşabeyoğlu for helping me with the FE-SEM and XRD characterization and analysis.

The financial support provided by the Scientific and Technological Research Council of Türkiye (TUBİTAK) under grant agreement 220M002 is greatly acknowledged. I am grateful to METU Central Laboratory for the support provided in the characterization and analysis of the samples.

I am very much thankful and indebted to my family for their lifelong support, and understanding, and for keeping up with my idiosyncrasies.

TABLE OF CONTENTS

ABSTRACT.....	v
ÖZ.....	vii
ACKNOWLEDGMENTS	x
TABLE OF CONTENTS.....	xi
LIST OF TABLES	xiv
LIST OF FIGURES	xv
LIST OF ABBREVIATIONS	xx
CHAPTERS	
1 INTRODUCTION	1
1.1 Metal-Organic Framework.....	1
1.1.1 UiO-66 (Zirconium-MOF)	5
1.1.2 MIL-47 (Vanadium-MOF)	7
1.1.3 MIL-125 (Titanium-MOF)	9
1.1.4 Properties and applications of Metal-Organic Frameworks.....	11
1.1.5 Nucleation and crystal growth of MOFs	16
2 LITERATURE REVIEW	21
2.1 Metal-Organic Frameworks: history and background	21
2.2 Synthesis of MOFs.....	24
2.2.1 UiO-66.....	26
2.2.2 MIL-47	30
2.2.3 MIL-125	32
2.3 Chemistry, nucleation, and functionalization of MOFs.....	35

2.3.1	UiO-66	35
2.3.2	MIL-47	41
2.3.3	MIL-125	42
2.4	Properties and applications of MOFs	44
2.4.1	UiO-66	44
2.4.2	MIL-47	46
2.4.3	MIL-125	48
2.5	Goals and Objective	50
3	EXPERIMENTAL SECTION	53
3.1	Synthesis of MOFs	53
3.1.1	Solvothermal synthesis of MOFs	54
3.1.2	Activation of MOFs	64
3.2	Characterization of MOFs	65
3.2.1	X-Ray Diffraction	65
3.2.2	Field Emission Scanning Electron Microscopy	65
3.2.3	Nitrogen adsorption-desorption analysis	66
3.2.4	Water adsorption studies	66
4	RESULTS AND DISCUSSION	67
4.1	UiO-66 (Zr-MOF)	67
4.1.1	Effect of reaction temperature on the synthesis of UiO-66	67
4.1.2	Effect of modulators on the synthesis of UiO-66	77
4.2	MIL-125 (Ti-MOF)	89
4.2.1	Effect of reaction temperature on the synthesis of MIL-125	92
4.2.2	Effect of reaction time on the synthesis of MIL-125	96

4.2.3	Effect of concentration of titanium-source on the crystal shape of MIL-125	98
4.3	MIL-47 (V-MOF)	103
4.3.1	Effect of reaction temperature on synthesis of MIL-47	103
4.3.2	Effect of reaction time on MIL-47 at synthesis temperature of 160°C	105
4.3.3	Effect of reaction time on MIL-47 at synthesis temperature of 220°C	108
4.3.4	Effect of concentration of precursors on the synthesis of MIL-47	111
4.4	Activation, surface characterization, and thermogravimetric analysis of UiO-66, MIL-125, and MIL-47	115
4.5	Water adsorption (uptake) by UiO-66	122
5	SUMMARY, CONCLUSIONS, AND SUGGESTIONS	127
5.1	Summary and Conclusions	127
5.2	Suggestions for future work	129
	REFERENCES	131
	APPENDICES	
A.	Particle size distribution of UiO-66, MIL-125, and MIL-47	147

LIST OF TABLES

TABLES

Table 3-1 Sample codes and experimental conditions for the solvothermal synthesis of UiO-66.....	58
Table 3-2 Sample codes for the AA-TEA co-modulation synthesis of UiO-66 at 120°C with precursor concentration C2 (sample U66-120-C2)	59
Table 3-3 Sample codes and experimental conditions for the solvothermal synthesis of MIL-47	62
Table 3-4 Sample codes and experimental conditions for the solvothermal synthesis of MIL-125	64
Table 4-1 Experimental parameters, the shape of crystals, and mean particle sizes for UiO-66 synthesized in the presence of acetic acid-TEA modulators at 120°C.....	81
Table 4-2 Surface characterization results from N ₂ adsorption-desorption isotherm data of UiO-66, MIL-125, and MIL-47	118

LIST OF FIGURES

FIGURES

Figure 1.1. A general schematic representation of MOF structure.....	1
Figure 1.2. Structure of UiO-66 MOF, its SBUs and organic linker (a), and atomic view of metal node (b) [3][4].....	2
Figure 1.3 Different types of MOFs and their corresponding SBUs i.e. metal nodes and organic linkers [2]	3
Figure 1.4 Schematic view of UiO-66 metal-organic framework from different angles. The red and green spheres represent octahedral and tetrahedral cavities in the framework, respectively [14].	5
Figure 1.5 The two types of cages (pores) in the UiO-66 framework, tetrahedral (7.5 Å) and octahedral (12 Å) [16].....	6
Figure 1.6 UiO family of MOFs [17].....	6
Figure 1.7 (a) The array of octahedral $V^{IV}O_6$ metal nodes connected by organic linkers (H_2bdc) to form (b) MIL-47 MOF [19], [20].....	8
Figure 1.8 (a) MIL-125 MOF unit cell with octahedral (12.5 Å) and tetrahedral (6 Å) cages represented by a yellow and green sphere, respectively, and (b) cyclic octamer [4], [25].	9
Figure 1.9 Molecular 3D framework of MIL-125. Cyclic octahedral metal nodes connected to form octamers (in blue) [26].....	10
Figure 1.10 A defect site in UiO-66 MOF due to a missing organic linker [3].....	13
Figure 1.11 Tuning defect sites for catalytic properties in UiO-66 [36].....	14
Figure 1.12 Functionalization of MOF [55].	16
Figure 1.13 Step-by-step evolution of UiO-66 SBUs into the 3D framework in precursor solution [61]	18
Figure 1.14 Formation of intermediate ($[ZrCl(OH)_2(DMF)_2]Cl$) and subsequent conversion into UiO-66 MOFs in the synthesis solution by using $ZrCl_4$ and $ZrOCl_2 \cdot 8H_2O$ as metal sources [62].....	19

Figure 2.1. BET surface areas of some MOFs with ultrahigh porosity compared with other conventional materials available in the porous material market. The values in parenthesis are pore volumes (cm ³ /g) of respective materials [10].....	23
Figure 2.2 Number of publications in different research areas related to MOFs [73].	23
Figure 2.3 Comparison of the ratio of publications in different research domains for Zeolites and MOFs [73].....	24
Figure 2.4 Schematic of MOF-5: The first MOF reported to have permanent porosity and stable framework structure [76].....	26
Figure 3.1 Synthesis of MOFs by different methods [108].....	53
Figure 3.2 Timeline of patented synthetic routes for MOFs [109].....	54
Figure 3.3 Solvothermal synthesis of MOFs [60].	55
Figure 3.4 Step-by-step solvothermal synthesis of UiO-66 MOF.....	57
Figure 3.5 A general schematic of the acid-base co-modulates solvothermal synthesis of UiO-66 [3].....	59
Figure 3.6 Step-by-step solvothermal synthesis of MIL-47 MOF	61
Figure 3.7 Step-by-step solvothermal synthesis of MIL-125 MOF	63
Figure 4.1 PXRD patterns of samples (a) U66-80-C1, (b) U66-100-C1, and (c) U66-120-C1 synthesized at 80°C, 100°C, 120°C, respectively, and (d) simulated XRD pattern of UiO-66 (COD ID 4512072)	68
Figure 4.2 SEM images of samples (a) U66-80-C1, (b) U66-100-C1, and (c) U66-120-C1 synthesized at 80°C, 100°C, and 120°C, respectively	70
Figure 4.3 PXRD patterns of samples (a) U66-80-C2, (b) U66-100-C2, and (c) U66-120-C2 synthesized at 80°C, 100°C, and 120°C, respectively, and the simulated XRD pattern of UiO-66 (COD ID 4512072)	72
Figure 4.4 SEM images of samples (a) U66-80-C2, (b) U66-100-C2, and (c) U66-120-C2 synthesized at 80°C 100°C 120°C, respectively	73
Figure 4.5 PXRD of UiO-66 MOF synthesized at 80°C (U66-80-C1) with reo-phase peak marked in red	76

Figure 4.6 PXRD patterns of UiO-66 samples (a) U66-120-C2, (b) U66-S1, (c) U66-S2, (d) U66-S3, (e) U66-S4, (f) U66-S5, (g) U66-S6, and (h) U66-S7. Samples (b) to (g) were synthesized using AA-TEA co-modulation route at 120°C with TEA concentrations 2 mM, 4 mM, 8 mM, 12 mM, 16 mM and 19 mM, respectively. (h) The U66-S7 sample was synthesized with only AA as a modulator. A simulated XRD pattern of UiO-66 is also given (COD ID 4512072).....	78
Figure 4.7 SEM images of samples (a) U66-S1, (b) U66-S2, (c) U66-S3, (d) U66-S4, (e) U66-S5 and (f) U66-S6 synthesized at 120°C using acid-base co-modulation route with TEA concentrations 2 mM, 4 mM, 8 mM, 12 mM, 16 mM and 19 mM, respectively	80
Figure 4.8 Evolution of UiO-66 mean crystal size with TEA concentration in the reacting solution.....	80
Figure 4.9 FE-SEM images of U66-120-C2 sample synthesize (a) without and (b) with only AA modulation	82
Figure 4.10 PXRD patterns of UiO-66 synthesized at 80°C (U66-80-C1) in the presence of HCl as a modulator. (a) 3 ml HCl (b) 1 ml HCl (c) without HCl.....	85
Figure 4.11 SEM images of UiO-66 synthesized at 80°C (U66-80-C1) in the presence of HCl modulator (a) 3m HCl (b) 1 ml HCl (c) without HCl.....	87
Figure 4.12 PXRD of MIL-125 MOF with (a) circular disc-shaped and (b) truncated octahedral crystals obtained at 150°C in 2 days (both samples are M125-150-2 synthesis in two different batches).....	89
Figure 4.13 XRD pattern of MIL-125 (as-synthesized) from the literature [119]..	90
Figure 4.14 SEM image of (a) circular disc-shaped and (b) truncated octahedral MIL-125 MOF crystals obtained at 150°C in 48 hours (both samples are M125-150-2 synthesis in two different batches).....	91
Figure 4.15 PXRD patterns of MIL-125 MOF obtained at (a) 100°C (M125-100-3), (b) 130°C (M125-130-3), (c) 150°C (M125-150-3), and (d) 160°C (M125-160-3). The simulated PXRD pattern of MIL125 (COD ID 7211159)	93

Figure 4.16 FE-SEM images of MIL-125 MOF obtained at (a) 100°C (M125-100-3), (b) 130°C (M125-130-3), (c) 150°C (M125-150-3), and (d) 160°C (M125-160-3).	94
Figure 4.17 PXRD patterns of MIL-125 MOF synthesized at 150°C in (a) 2 days (M125-150-2), and (b) 3 days (M125-150-3). The simulated PXRD pattern of MIL125 (COD ID 7211159)	96
Figure 4.18 SEM images of MIL-125 MOF synthesized at 150°C in (a) 2 days (M125-150-2), and (b) 3 days (M125-150-3).....	97
Figure 4.19 PXRD of MIL-125 MOF synthesized at 150°C in 2 days (M125-150-2) with (a) 87.72 and (b) 98.62 mM concentration of titanium isopropoxide in the reagent solution. The simulated PXRD pattern of MIL125 (COD ID 7211159)....	99
Figure 4.20 SEM image of MIL-125 MOF synthesized at 150°C in 2 days (M125-150-2) with (a) 87.72 mM and (b) 98.62 mM concentration of titanium isopropoxide in the reagent solution.	100
Figure 4.21 PXRD of MIL-47 MOF obtained at different temperatures (a) 160°C (M47-160-5) (b) 220°C (M47-220-5).....	103
Figure 4.22 PXRD pattern of MIL-47 as calculated (Calcd) and experimental (Exp) from Barthelet et al. (*peaks belong to aluminum sample holder) [19].....	104
Figure 4.23 SEM images of MIL-47 MOF synthesized at (a) 160°C (M47-160-5) (b) 220°C (M47-220-5)	105
Figure 4.24 PXRD patterns of MIL-47 MOF obtained at 160°C in (a) 1 day (M47-160-1), (b) 3 days (M47-160-3), and (c) 5 days (M47-160-5)	106
Figure 4.25 FE-SEM images of MIL-47 MOF obtained at 160°C at different reaction times (a) 1 day (M47-160-1), (b) 3 days (M47-160-3), and (c) 5 days (M47-160-5)	107
Figure 4.26 PXRD of MIL-47 MOF obtained at 220°C in (a) 1 day (M47-220-1) (b) 5 days (M47-220-5).....	109
Figure 4.27 FE-SEM images of MIL-47 MOF obtained at 220°C in (a) 1 day (M47-220-1) (b) 5 days (M47-220-5).....	110

Figure 4.28 PXRD of MIL-47 MOF obtained at 160°C with different precursors concentrations in 5 days (a) C2 (M47-160-5-C2) (b) C3 (M47-160-5-C3).....	112
Figure 4.29 FE-SEM images of MIL-47 MOF obtained at 160°C with different precursors concentrations in 5 days (a) C2 (M47-160-5-C2) (b) C3 (M47-160-5-C3)	113
Figure 4.30 Nitrogen adsorption-desorption isotherm for as-synthesized (black) and activated (orange) UiO-66 (U66-80-C1 sample)	115
Figure 4.31 Nitrogen adsorption-desorption isotherm for as-synthesized (black) and activated (orange) MIL-125 (M125-150-3 sample).....	116
Figure 4.32 Nitrogen adsorption-desorption isotherm for as-synthesized (black) and activated (orange) MIL-47 (M47-160-5 sample).....	117
Figure 4.33 TGA curves of activated UiO-66 (black), MIL-125 (red), and MIL-47 (blue) MOFs. Samples are U66-80-C1, M125-150-3, and M47-160-5, respectively	120
Figure 4.34 The water uptake bar chart of U66-80-C1 (a) without and (b) with HCl modulator	123
Figure 4.35 Water adsorption isotherm obtained at 30°C of U66-80-C1 synthesized in the presence of an HCl modulator.	124
Figure 4.36 Water adsorption capacities of UiO-66 synthesized in the presence of AA-TEA modulators (see Table 3-2)	125

LIST OF ABBREVIATIONS

ABBREVIATIONS

AA	Acetic Acid
BET	Brunauer-Emmett-Teller
BFDH	Bravais, Friedel, Donnay, Harker
CSD	Cambridge Structural Database
DEF	Diethyl formamide
DLS	Dynamic Light scattering
DMF	Dimethylformamide
FE-SEM	Field Emission Scanning Electron Microscopy
H ₂ bdc	1,4-benzodicarboxylic acid
H ₂ bpdC	Biphenyl-4,4-dicarboxylic acid
H ₂ tpdc	P-terphenyl-4,4-dicarboxylic acid
MOFs	Metal-Organic Frameworks
MIL	Matériaux de l'Institut Lavoisier
SBU	Secondary Building Units
TGA	Thermogravimetric Analysis
TEA	Triethylamine
UiO	Universitetet i Oslo
XRD	X-ray Diffraction

CHAPTER 1

INTRODUCTION

1.1 Metal-Organic Framework

Metal-Organic Frameworks (MOFs) are a new class of crystalline materials that consist of inorganic and organic components, known as secondary building units (SBUs), in the same chemical structure. In MOFs, the inorganic parts are connected by the organic linkers to form a 3D framework, as shown schematically in Figure 1.1. By choosing different types of inorganic components and organic linkers, nearly an infinite number of structural networks of MOFs can be designed. As of 2016, more than 70,000 different MOFs have been reported in Cambridge Structural Database (CSD) [1]. The metal atom-centered SBUs are also called metal clusters or nodes [2]. The type of SBUs in MOFs structure has a tremendous effect on the properties and the design of the MOFs network. The structure of a zirconium-based MOF with its corresponding SBUs is shown in Figure 1.2. Different types of MOFs with their corresponding metal nodes and organic linkers are shown in Figure 1.3.

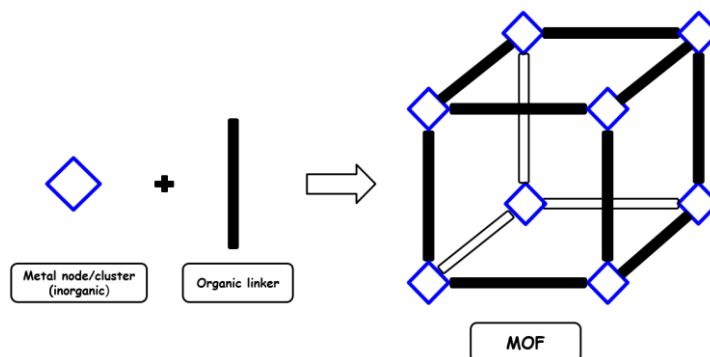


Figure 1.1. A general schematic representation of MOF structure.

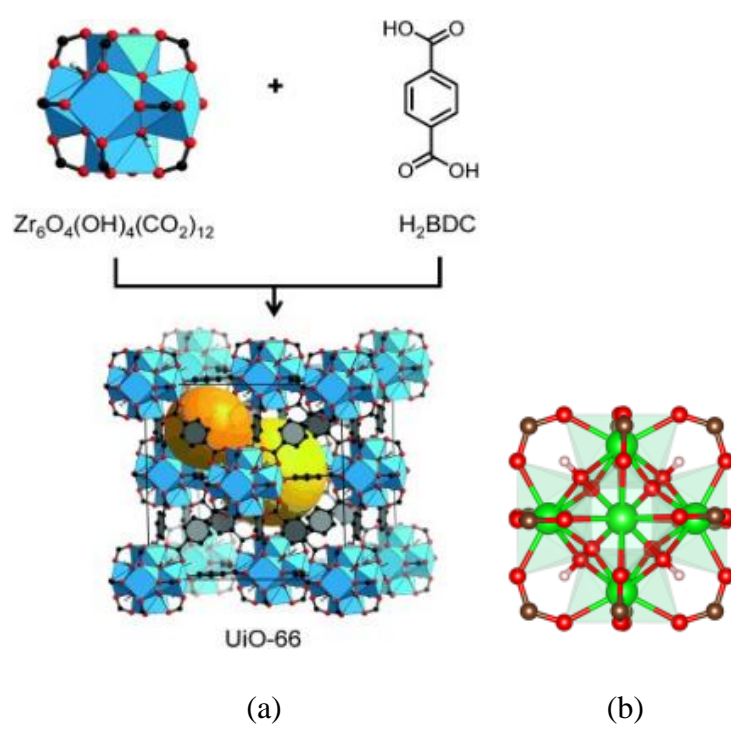


Figure 1.2. Structure of UiO-66 MOF, its SBUs and organic linker (a), and atomic view of metal node (b) [3][4].



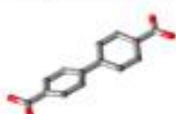
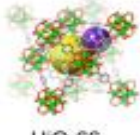

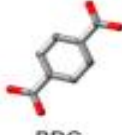




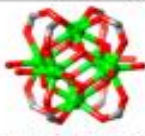
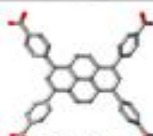


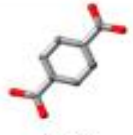
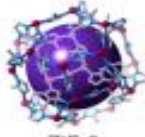




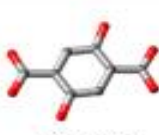



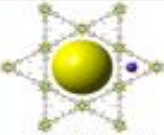
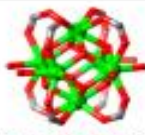
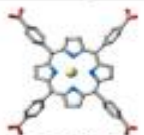
MOF	Metal Node	Organic Linker
 UiO-67	 $Zr_6O_4(OH)_4$	 BPDC
 UiO-66	 $Zr_6O_4(OH)_4$	 BDC
 PCN-600(M)	 $Fe_3O(OH)_3$	 M-TCPP
 NU-1000	 $Zr_6O_4(OH)_6(H_2O)_4$	 TBAPy
 Cr-MIL-101	 $Cr_3O(OH)_3$	 BDC
 ZIF-8	 Zn	 MelM
 Mg-MOF-74	 MgOH	 $BDC-(OH)_2$
 NU-125	 Cu_2	 LH ₆
 PCN-222(Fe)	 $Zr_6O_4(OH)_6(H_2O)_4$	 Fe-TCPP

Figure 1.3 Different types of MOFs and their corresponding SBUs i.e. metal nodes and organic linkers [2]

There is disagreement among the MOFs researchers on the number of MOFs entries in CSD due to ‘ambiguity’ in the definition of MOF. The term ‘Metal-Organic Framework’ (MOF) was first coined by Omar Yaghi et al. in 1995 [5], but there is still confusion in the definition of MOFs among researchers, and it is still debated [6], [7]. MOFs are considered a subgroup of “coordination networks” which are themselves a subset of coordination polymers [8]. MOFs are sometimes called ‘coordination polymers’ and are defined as “coordination polymers” (or coordination networks) with open framework having potential voids”, however, some scientists disagree with this definition [6]. Generally, researchers agree on the definition that “MOFs are crystalline materials consisting of metal-atom-centered clusters of atoms (metal nodes or SBUs) connected by organic linkers to form 2D or 3D structures based on ‘building block’ approach [1], [6], [7]. The metal clusters are bonded to organic linkers by a coordination covalent bond in which the electrons are shared by metal atoms in the metal clusters [6], [8], [9]. These coordination covalent bonds are generally weaker than most covalent bonds but are strong enough to maintain the permanent porous structure of MOFs [9].

Due to their high surface areas, flexible design, and exceptional tunable properties, MOFs have recently attracted considerable attention. In 2013, it was reported that the number of MOFs was 20,000 [10]. Then in 2016, 70,000 MOFs entries were recorded in CSD [1]; however, in 2019, this number swelled up to 100,000 [7]. The confusion in definition and the reporting of the large number of MOFs every year makes it very difficult to extract MOF crystallographic data from the databases like CSD [1].

The first metal-organic framework, MOF-5, with permanent porosity, was synthesized by Omar Yaghi and his coworkers in 1999 [11]. After Yaghi’s seminal work on MOFs, MOFs have attracted considerable attention in the last couple of decades due to their exceptional properties, e.g., design flexibility, ultrahigh porosity, surface area, and tunable properties [12]. The structures and properties of three MOFs i.e. UiO-66, MIL-47, and MIL-125, that were synthesized in this study are explained in the following paragraphs.

1.1.1 UiO-66 (Zirconium-MOF)

UiO-66 is a zirconium metal-based MOF, which means that the core atoms in metal nodes are zirconium atoms. UiO-66 is an archetypal MOF with high surface area, and chemical and thermal stability. First synthesized in 2008 by the Lillerud group at the University of Oslo [13], UiO-66 contains $Zr_6O_4(OH)_4$ clusters (SBUs or metal nodes) linked by 1,4-benzodicarboxylic acid (H_2bdc) organic linker (Figure 1.2). In the ideal UiO-66 framework, the metal node consists of six (6) Zr atoms bridged together by eight (8) oxygen atoms (four μ_3 -O and four μ_3 -OH), forming a polyhedral structure. The polyhedral metal node is then connected to twelve (12) other polyhedra via twelve (12) organic linkers (H_2bdc), thus forming a close-packed cubic unit cell of UiO-66. This unit cell then propagates into a 3D network of UiO-66 MOF, as shown in Figure 1.4.

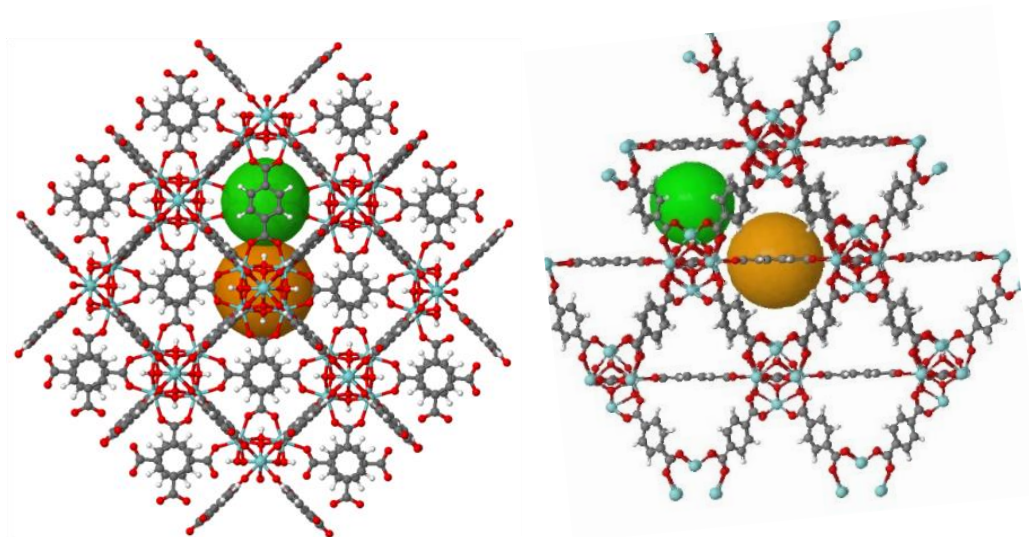


Figure 1.4 Schematic view of UiO-66 metal-organic framework from different angles. The red and green spheres represent octahedral and tetrahedral cavities in the framework, respectively [14].

There are two types of pores in the UiO-66 framework, which are 12 Å octahedral units and 7.5 Å tetrahedral units, as shown in Figure 1.5 [15]. The surface area of UiO-66 varies between 800-1500 m²/g.

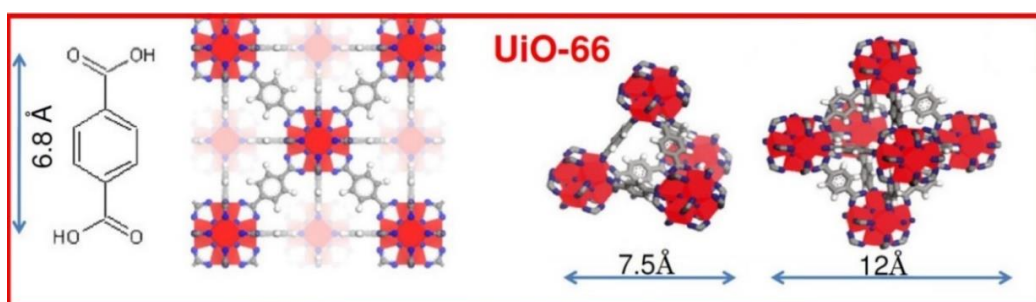


Figure 1.5 The two types of cages (pores) in the UiO-66 framework, tetrahedral (7.5 Å) and octahedral (12 Å) [16].

UiO family contains three types of MOFs i.e. UiO-66, UiO-67, and UiO-68. By replacing the organic linker in UiO-66 with two benzene rings containing linker (biphenyl-4,4-dicarboxylic acid (H₂bpdc)) and three benzene rings containing linker (p-terphenyl-4,4-dicarboxylic acid (H₂tpdc)), two new types of MOFs can be designed i.e. UiO-67 and UiO-68, respectively as illustrated in Figure 1.6 [13], [15].

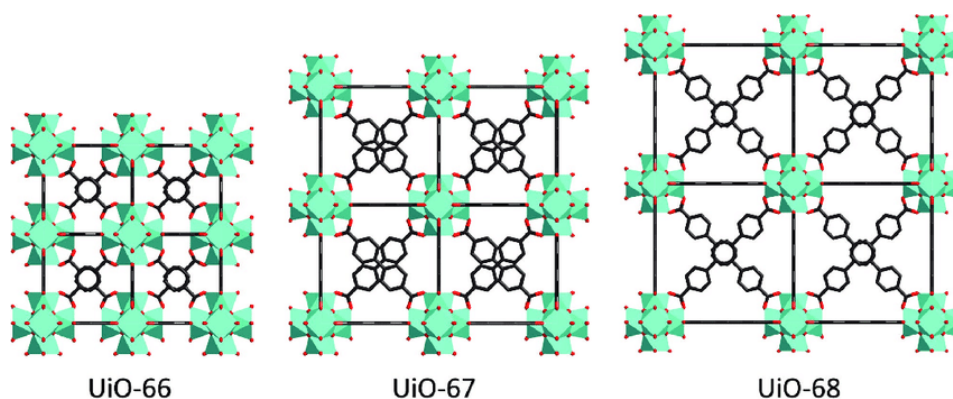
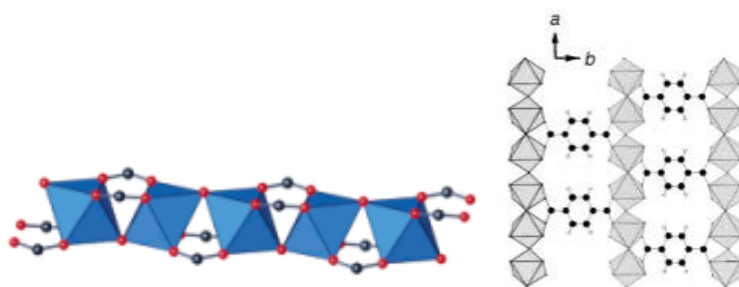


Figure 1.6 UiO family of MOFs [17]

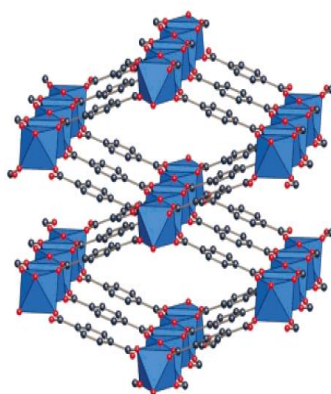
Increasing the length of organic linkers (i.e. number of benzene rings) in UiO-67 and UiO-68 results in larger cavities in the framework, and also the surface areas increase to around 3000 m²/g and 4000 m²/g, respectively [13]. One of the most important properties of UiO-66 is its thermal stability, as its framework is stable up to 500°C in the air; whereas most MOFs are thermally stable in the air only up to around 350°C. UiO-66 owes its remarkable stability to the strength of Zr-O bonds and the bonds between metal nodes and oxygen in the organic linkers [13]. The oxophilic nature of Zr^(IV) tends to form close packing coordination in SBUs and thus strong interaction with surrounding O atoms [18].

1.1.2 MIL-47 (Vanadium-MOF)

MIL-47 is a vanadium metal-based MOF. MIL-47 was first synthesized by the Gerard Ferey group from Matériaux de l'Institut Lavoisier (MIL) France and thus carries the name of that institution [19]. MIL-47 is a three-dimensional metal-organic framework with a Vanadium (V^{+IV}) atom center coordinated by four oxygen atoms from four carboxylate groups of organic linkers and two oxygen atoms in the O-V-O axis forming octahedral V^{IV}O₆ node (cluster/SBU). Octahedral V^{IV}O₆ metal nodes are connected at opposite corners via O atoms forming an array of metal clusters (or nodes). This array of metal clusters is linked by organic linkers (H₂bdc) to other arrays of metal clusters (Figure 1.7a), thus forming a 3D network of MIL-47 with long 1D channels like pores, as shown in Figure 1.7b.



(a)



(b)

Figure 1.7 (a) The array of octahedral $V^{IV}O_6$ metal nodes connected by organic linkers (H_2bdc) to form (b) MIL-47 MOF [19], [20]

Pore dimensions and BET surface area of MIL-47 are $10.5 \times 11 \text{ \AA}$ and $930 \text{ m}^2/\text{g}$, respectively. Some level of flexibility is also observed in the MIL-47 framework i.e. the dimensions of the pore change upon the introduction of guest molecules into the framework, which can be called the ‘breathing effect’ [19], [21], [22]. Flexibility (breathing effect) in the MIL-47 framework depends upon the oxidation state of the V atom in metal nodes [22]. MIL-47 framework shows the breathing effect when the vanadium atom is in V^{3+} oxidation state and shows no flexibility when in V^{4+} oxidation state [23].

1.1.3 MIL-125 (Titanium-MOF)

MIL-125 is a titanium metal based MOF which was first synthesized by the Gerard Ferey group from Matériaux de l'Institut Lavoisier (MIL) [24] (Figure 1.8a).

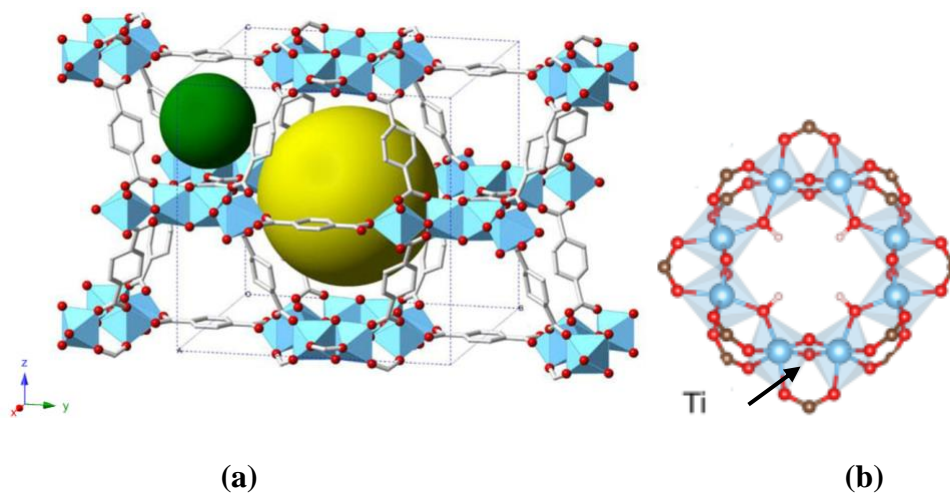


Figure 1.8 (a) MIL-125 MOF unit cell with octahedral (12.5 Å) and tetrahedral (6 Å) cages represented by a yellow and green sphere, respectively, and (b) cyclic octamer [4], [25].

In the MIL-125 structure, the Ti atom is bonded to six (6) surrounding oxygen atoms forming an octahedral cluster (or node). Eight octahedral Ti clusters are connected from corners to form circular (cyclic) octamers ($\text{Ti}_8\text{O}_8(\text{OH})_4(-\text{CO}_2)_{12}$) as shown in Figure 1.8b and Figure 1.9.

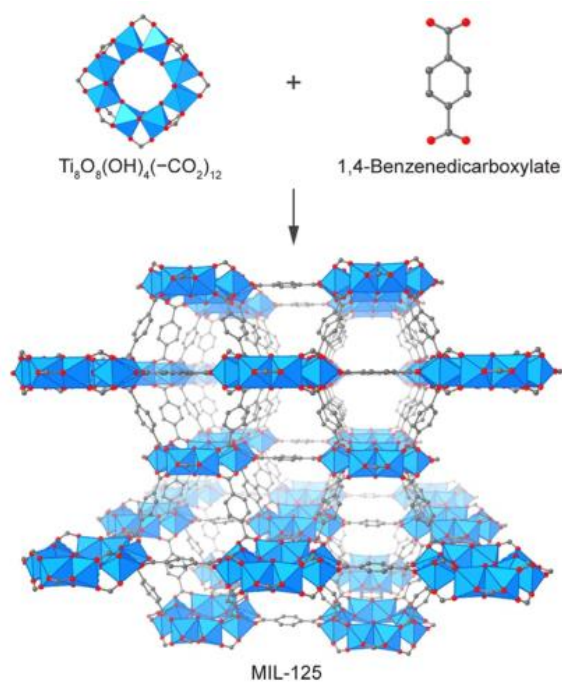


Figure 1.9 Molecular 3D framework of MIL-125. Cyclic octahedral metal nodes connected to form octamers (in blue) [26]

H₂bdc organic linkers connect these octamers to twelve (12) other octamers to form a 3D framework of MIL-125 as. A unit cell of MIL-125 MOF is shown in Figure 1.8 and an extended molecular 3D network of MIL-125 MOF is shown in Figure 1.9. MIL-125 framework contains two types of cages, octahedral (12.5 Å) and tetrahedral (6 Å) represented by yellow and green spheres in Figure 1.8, respectively. In the MIL-125 framework, twelve (12) organic linkers are connected to each octamer, four organic linkers are in the same plane as the cyclic octamer wheel, and four linkers each below and above the octamer plane (see Figure 1.9) [24], [27]. BET surface area of MIL-125 is around 1500 m²/g and is thermally stable in the air up to 350°C [24]. MOF-901, MOF-902, MUV-10, MUV-101, and PCN-22 are different types of titanium-based MOFs. Apart from the high surface area, porosity, and flexibility in design, the Ti-MOF family has three properties that distinguish them from other MOFs [26].

1. Ti-MOFs have photo-responsive properties, which can be engineered for specific photochemical reactions by tailoring the band gap and playing with the structure of MOF i.e. functionalization.
2. Ti-MOFs are stable in various harsh conditions, which is an important property for industrial applications.
3. Ti-MOFs have very low toxicity.

1.1.4 Properties and applications of Metal-Organic Frameworks

MOFs have attracted considerable attention in the last couple of decades owing to their exceptional properties. Due to their remarkable design flexibility, ultra-high porosity, large specific surface area and tunable properties, MOFs are indispensable for potential applications in clean energy [28], fuel cells [29]–[31], gas adsorption [32]–[34] and catalysis [21], [25], [35], [36], [37]. MOFs are microporous materials and the surface area of some MOFs can go as high as 10,000 m²/g, which is greater than the conventional porous materials used in industries these days [10]. The densities of MOFs are generally very low (0.13 g/cm³), and the non-framework-free volume can occupy up to 90% of the total volume [2].

Catalysis is the area that will be revolutionized by the introduction of MOFs. There are already a considerable number of studies on a laboratory scale about the use of MOFs as catalysts [10], [21], [25], [36]. The field of MOFs application in catalysis is still in its infancy due to some intrinsic limitations of MOFs e.g. lack of understanding of catalytic site quantifications, transport process in pores, thermal stability, and regeneration of MOF catalysts [2], [35], [38]. That is why no MOF-based catalyst has yet made it to industrial application. Despite these limitations, MOFs are ideal candidates for catalysts due to their high surface area, porosity, and tunable properties [10]. Different MOFs have been tested on a lab scale as catalysts for photocatalytic water splitting [39], reduction of carbon dioxide in useful chemicals [37], photocatalysis [40], and esterification reactions [27]. Zirconium-based MOF, UiO-66 is tested as a catalyst for nerve agent detection and its

subsequent conversion into a nontoxic chemical [41]. The prospective advantages and limitations of MOFs as practical catalysts are mentioned below [35], [42], [43].

Advantages of MOFs as catalysts:

- Surface areas and active site densities per unit volume are very high in MOFs.
- MOFs have tremendous flexibility in their structures for in-situ and post-synthetic modifications by various active catalytic groups.
- The pores in MOFs can be easily tailored for effective transport of reactants and products, for shape selective reactions, and for accommodating different catalytically active chemical species.

Limitations of MOFs as catalysts:

- Due to the presence of organic species, the thermal stabilities of MOFs are low compared to inorganic compounds, which limits their applicability in the harsh conditions of industrial processes.
- There is the possibility of the reaction of reactants or products with the MOFs causing their structures to unbundle.
- The presence of organic components in the structure makes MOFs difficult to regenerate after the deposition of organics inside the framework pores.
- Impurities in reactants can change the surface chemistry of MOFs and thus pacify their catalytic activity.

MOFs can be used for gas storage [44], as adsorbents [22], and for gas separation [45] due to their high surface area and porosity combined with flexibility in design and tunable properties. There is a possibility of methane gas storage in MOFs for transportation purposes at moderate pressures as an alternative to the high-pressure gas fuel tanks [44], [46]. BASF, one of the largest chemical manufacturing companies in the world, has already developed a prototype technology for MOF-based natural gas fuel systems for transport vehicles [47]. The affinity of the MOFs for gas adsorption can be altered by playing with the molecular framework structure through functionalization or the introduction of new chemical species [48]. Storage

and capture of carbon dioxide and hydrogen gases are very important for clean energy and the environment and MOFs can potentially play a huge role in this regard [12], [30].

Using MOFs as moisture sorbents in the air conditioning system of buildings can reduce energy consumption by 30-40% due to the elimination of latent cooling loads from the system [32]. One interesting potential use of MOFs is harvesting atmospheric water for drinking in some of the driest regions of the planet e.g. deserts [49].

Fuel cells and clean energy are other fields where MOFs have great potential to be game changers. MOFs can be incorporated into the polymer membrane of PEM fuel cells to enhance the proton (H^+) conductivity [50]. The ability to tune the chemistry of MOFs for designing new catalysts has opened up wide areas for their applications and one of them is using MOFs as oxygen reduction catalysts in fuel cells [31].

Defects in MOFs are the missing linkers in the framework, and sometimes the structural distortions or missing metal nodes are also referred to as defects [36],[51]. For example, in the ideal UiO-66 framework structure, twelve (12) H_2bdc organic linkers are attached to the metal nodes. However, the MOF is said to have defect sites when one or more organic linkers are missing in the framework (Figure 1.10) after synthesis.

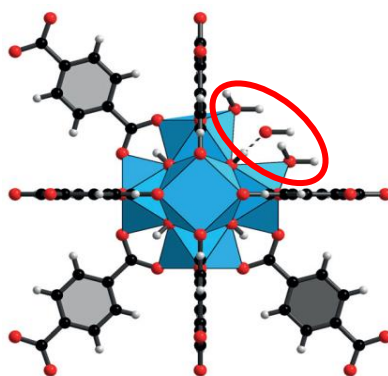


Figure 1.10 A defect site in UiO-66 MOF due to a missing organic linker [3].

The red circle in Figure 1.10 pinpoints a defect site created by one missing linker in the framework of UiO-66. These defects are not necessarily undesirable, and sometimes they can enhance the catalytic and adsorption properties of the MOF [36], [52]. The catalytic activity of defective UiO-66 MOF can be tuned for desired application by controlling the density of defective sites in the framework. In the UiO-66 framework, when the linker is missing, it leaves unsaturated Zr^{4+} sites on which water molecules are adsorbed, forming Brønsted acid sites. Upon the desorption of these water molecules, Lewis acid sites are generated [36]. The active catalytic sites in the UiO-66 framework can be switched between Brønsted and Lewis acid sites by hydrating and dehydrating the MOFs. The schematic of this mechanism is shown in Figure 1.11. Different functional groups can be introduced to these sites to tune the properties of MOFs for different catalytic and gas adsorption/storage applications [3].

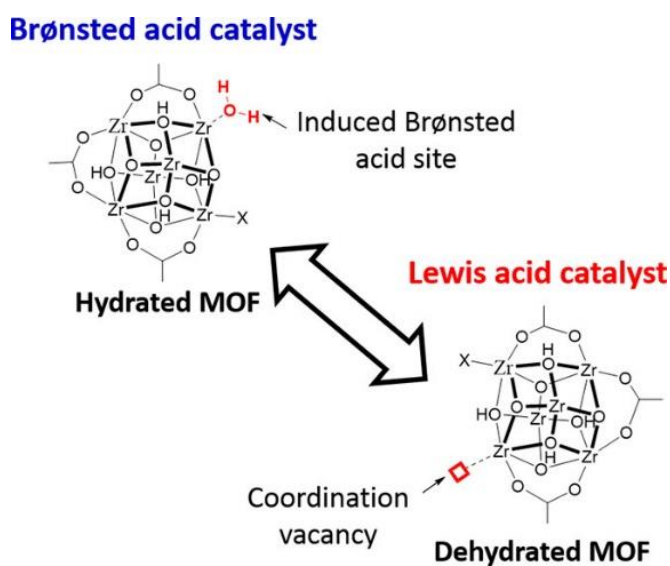


Figure 1.11 Tuning defect sites for catalytic properties in UiO-66 [36]

The defect site densities and, thus the catalytic activities of MOFs can be engineered for desired applications by temperature modulation [51] or using chemical

modulators (acids or bases) [53]. It was observed that the catalytic activity of UiO-66 increased with the increase in defect sites, with the cost of a reduction in thermal stability [36]. The positive aspects of having defects in MOFs are increased catalytic activity, surface area, and gas adsorption capacity, with the negative aspect of reduced thermal stability [36], [51], [54]. Thus, these points need to be evaluated while designing MOFs for specific applications.

The main drawback of MOFs is their low thermal stability which is also the main hindrance in their practical applications. TGA analysis shows that most MOFs tend to decompose near 300°C, and their framework collapses at around 300-350°C. The weak components of the MOF structure are the organic linkers and their weak bondings with metal nodes [13]. Before employing MOFs for any industrial application in the future, the problem of thermal stability must be addressed.

In this study, three types of MOFs were synthesized, i.e., UiO-66, MIL-125, and MIL-47. Among these MOFs, UiO-66 is of particular importance due to its high thermal stability compared to other MOFs. UiO-66 is thermal stable up to 500°C in the air, making it the most stable MOF. Above 500°C the framework of UiO-66 completely collapses due to the decomposition of the organic linker (H₂bdc) [13], [54]. UiO-66 owes its thermal stability to the strong interaction between the inorganic metal nodes and oxygen atoms of the carboxylate group of organic linkers. Moreover, inorganic clusters in UiO-66 have the highest coordination number (12 organic linkers connected to each metal node) reported for MOFs forming a close-packed cubic structure [13].

The functionalization of MOFs is attaching chemical species or a functional group to the framework's organic linker or metal nodes, as shown in Figure 1.12.

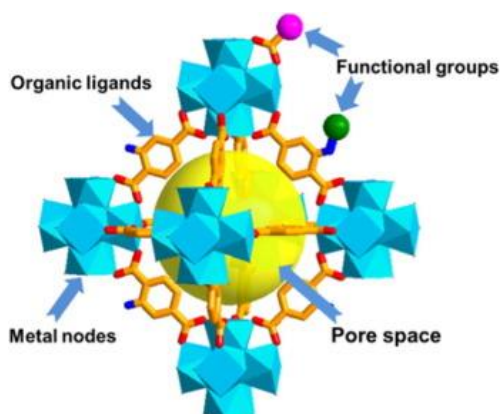


Figure 1.12 Functionalization of MOF [55].

Functionalization of MOFs can have tremendous effect on their catalytic [25],[42], adsorption [22], [25], [56] and electronic properties [57]. Introducing the $-NH_2$ group to the organic linker of MIL-47 has been shown to increase its adsorption capacity for methane and carbon dioxide, which can potentially help to store these gases for different applications [22]. Catalytic activities of MOFs can be increased by simply functionalizing either the organic linkers or metal nodes [42]. MOFs are generally insulators, but functionalization can change their electronic properties and bandgap [57]. For example, the bandgap of pristine MIL-125 is 3.60 eV which could be reduced to 2.60 eV just by functionalizing the organic linker with the amine ($-NH_2$) group [26]. Some researchers have been able to obtain conductive MOFs by filling pores with conductive polymers [58] or doping metal atoms onto the metal nodes [59]. Functionalization can also alter MOF's hydrophilic and hydrophobic nature [26].

1.1.5 Nucleation and crystal growth of MOFs

Over the years, many different methods have been developed for the synthesis of MOFs. Among them, solvothermal synthesis is a widely used method for MOFs synthesis [60] (MOFs synthesis is explained in Chapter 3). Solvothermal is a

relatively straightforward synthesis route with a high throughput of MOFs compared to other routes [60]. In this method, the precursors, i.e., metal salt, and organic linker, are dissolved in a high boiling point solvent like DMF (or DEF or water) in a glass vial or any other sealed container. The ingredients of the sealed container are left to react in an oven at a specific temperature and reaction time (ranging from a few hours to days). The evolution of MOFs into 3D networks (frameworks) in precursor solutions is still unclear. The formation of SBUs and the subsequent propagation of the MOF framework is still a debated topic among the MOF researchers [61], [62]. So, it is difficult to say which course is followed in solution during pre-nucleation, nucleation, and subsequent crystal growth of MOF particles. The already established model for nucleation and growth of crystals, from LaMar [63] and Johnson-Mehl-Avrami [64] models to the newer approach of pre-nucleation cluster formation and orientations [65], cannot properly explain the formation of MOFs in their mother solutions [61]. There are few studies [61], [62], [66] focused on the understanding of the nucleation and growth processes in the formation of UiO-66, a zirconium-based MOF. Using Pair Distribution Function (PDF) analysis, Xu et. al., [61] studied the evolution of SBUs of UiO-66 in precursor solution during solvothermal synthesis. This study has given some interesting insights into how nucleation and growth of UiO-66 crystals proceed in the precursor solution. Based on an in-situ PDF analysis of UiO-66 precursor solution during solvothermal synthesis reaction, Xu et al., [61] have proposed a theory about the evolution of the UiO-66 crystalline framework. According to this theory, the formation process of UiO-66 MOF in solution follows the following four steps.

1. The Hexa-nuclear Zr clusters (SBUs) are formed at room temperature as soon as the metal salt ($ZrCl_4$) is dissolved in the solvent (DMF).
2. When terephthalic acid (organic linker) is added to the solution of step 1, the Hexa-nuclear Zr clusters (SBUs) connect through organic linkers and arrange themselves into multinuclear clusters.
3. When this solution (of step 2) is heated to desired reaction temperature, the multinuclear clusters start to aggregate.

- The aggregation of these multinuclear clusters results in the 3D framework of UiO-66

The above four steps of UiO-66 framework evolution are schematically shown in Figure 1.13.

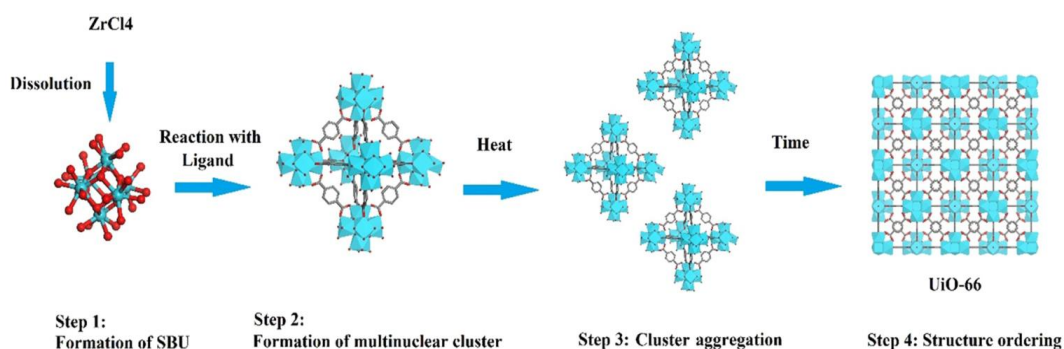


Figure 1.13 Step-by-step evolution of UiO-66 SBUs into the 3D framework in precursor solution [61]

Some studies have shown that an intermediate product also has an active role in the nucleation of UiO-66 MOF. Taddei et. al., [62] have reported the role of an intermediate species in the crystallization of UiO-66 MOF. In this study, an intermediate ($[ZrCl(OH)_2(DMF)_2]Cl$) product was observed when the precursor solution was aged for a few hours before the addition of an organic linker (terephthalic acid). After the addition of the organic linker to the solution, the intermediate active chemical species ($[ZrCl(OH)_2(DMF)_2]Cl$) then rearranges itself to form the UiO-66 MOF as shown in Figure 1.14.

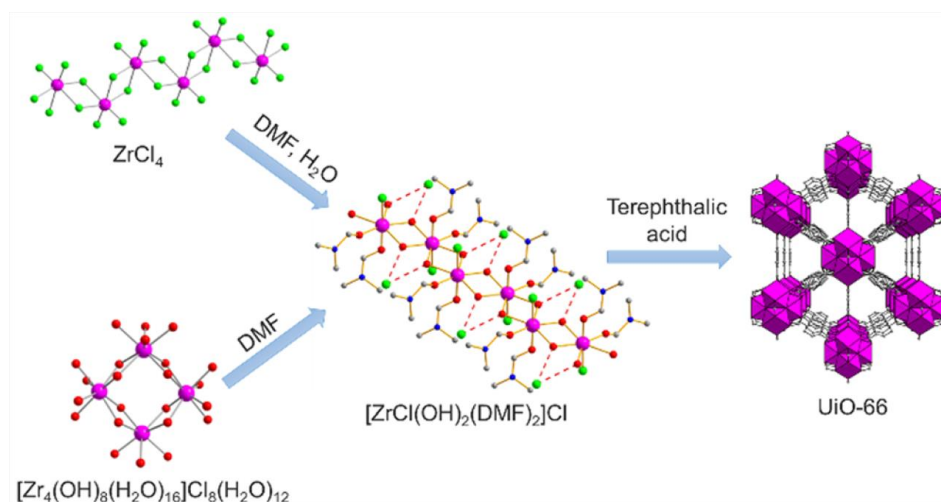


Figure 1.14 Formation of intermediate ($[ZrCl(OH)_2(DMF)_2]Cl$) and subsequent conversion into UiO-66 MOFs in the synthesis solution by using $ZrCl_4$ and $ZrOCl_2 \cdot 8H_2O$ as metal sources [62].

The intermediate product was successfully extracted and then used as a precursor for UiO-66 synthesis, which showed that this intermediate chemical species has an active role in forming the UiO-66 framework. So, it was concluded that the formation of intermediate species ($[ZrCl(OH)_2(DMF)_2]Cl$) in aged metal salt solution influences the thermodynamics and kinetics of crystallization, which can be a rate-determining step in the nucleation of UiO-66 framework [62].

Another study by Goesten et al. [67] of UiO-66 synthesis suggests the formation of multinuclear clusters after the dissolution of metal salt and organic linker in the solvent. These multinuclear clusters then condense into larger metastable clusters following an unknown path. The metastable clusters then rearranged themselves to form the stable framework of UiO-66. Goesten et al. observed that the protons (H^+) play the role of an autocatalyst in the formation of the UiO-66 framework from the metastable multinuclear clusters in the final step [67].

CHAPTER 2

LITERATURE REVIEW

2.1 Metal-Organic Frameworks: history and background

Tomic, E. A., (1965) synthesized coordinated polymers by linking di-, tri-, and tetravalent metals using di-, and tetra-topic carboxylic acid linkers [68]. This study investigated the correlation between valency of metals, coordination sites, and thermal stability of the polymers. After 25 years of this work, Hoskins and Robson proposed a variety of porous low-density infinite 3D frameworks and scaffolding-like materials based on the previous knowledge of coordination polymer chemistry [69]. These materials were predicted to show high thermal and chemical stability with the promise of other potentially useful properties and applications. The study of these 3D scaffolding-type frameworks and the coordinated polymers eventually paved the way for the discovery of Metal-Organic Frameworks (MOFs). The term MOF was first coined by Yaghi et al., in 1995 [5] but there is still confusion in the definition of MOFs and it is still debated among MOF researchers [6], [7]. MOFs are sometimes called ‘coordination polymers’ and are defined as “coordination polymers (or coordination networks) with open framework having voids”. But some researchers disagree with this definition because according to the IUPAC definition, ‘coordination polymers’ include only straight-chain polymers and not 2D or 3D chains [6]. Generally, researchers agree on the definition that “MOFs are crystalline materials consisting of metal-atom-centered clusters of atoms (metal nodes or SBUs) connected by organic linkers to form 2D or 3D structures based on ‘building block’ approach” [1], [6], [7].

MOF-5 (zinc-based MOF), reported by Yaghi et al. in 1999 [11], was the first MOF to show permanent porosity and structural integrity even after removing the guest molecule from its framework. Later on, with the help of computational power, better

and stable MOFs structures having very high surface areas and porosities, were predicted and subsequently synthesized in laboratories [2], [10], [12]. Since the discovery of MOF-5 thousands of new MOFs has been reported in CSD [7]. The reason for a large number of MOFs reported in the literature is that a nearly infinite number of different structural frameworks of MOFs can be designed due to the availability of a wide range of inorganic nodes (i.e. metal clusters or nodes) and organic linkers (ligand) [66]. Since the 1990s, tremendous attention has been given to the field of MOF research. Since then, a lot of work has been carried out in the areas of synthesis, chemistry, nucleation, and applications of MOFs [10], [12], [32], [49], [66], [70], [71]. As of 2016, more than 70,000 MOFs were reported in CSD, but this number swelled up to almost 100,000 in August 2019, corresponding to around 1000 new structures per month between that time [1], [7].

One of the main reasons why MOFs have attracted so much attention is their ultrahigh surface area and porosity. MOFs can have a BET surface area of up to $\sim 7000 \text{ m}^2/\text{g}$ (e.g. NU-110, a Cu-based MOF) with up to 90% of the free volume and very low density [2], [72]. The theoretical prediction for MOFs surface area is as high as $\sim 14600 \text{ m}^2/\text{g}$, which is far greater than the previously predicted ceiling value of $\sim 10500 \text{ m}^2/\text{g}$ [72]. The progress in synthesizing ultrahigh surface area MOFs over the years is compared with some of the conventional porous materials in Figure 2.1.

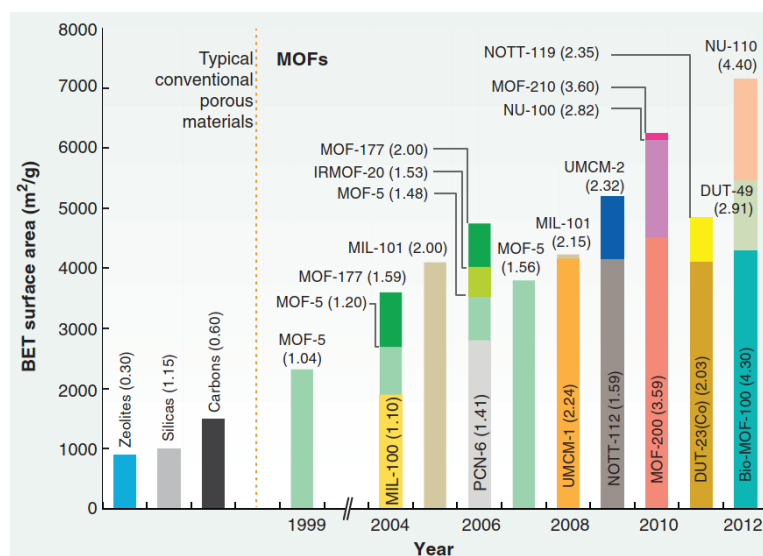


Figure 2.1. BET surface areas of some MOFs with ultrahigh porosity compared with other conventional materials available in the porous material market. The values in parenthesis are pore volumes (cm³/g) of respective materials [10].

Figure 2.2 shows different areas which have been the focus of research related to MOFs in the literature for the previous couple of decades.

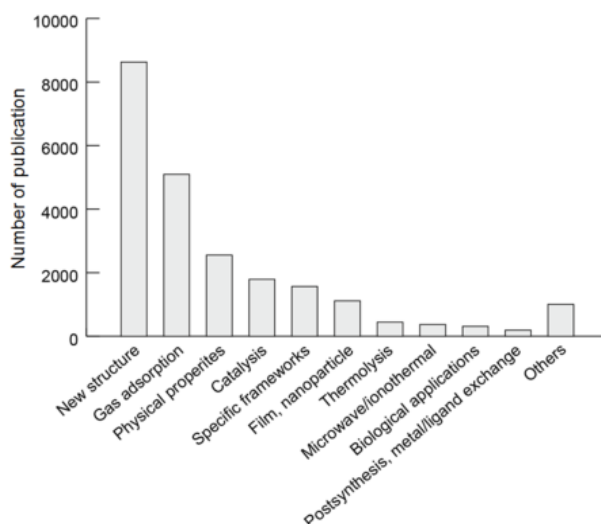


Figure 2.2 Number of publications in different research areas related to MOFs [73].

As shown in Figure 2.2, most of the research related to MOFs is carried out to design new MOF structures and their applications for gas adsorption and separation. Considerable research was also carried out to study the physical properties of MOFs, e.g. magnetism, electron conductivities, luminescence, etc, and MOFs as catalysts for reactions.

Figure 2.3 compares the ratio of publications in different research domains for Zeolites and MOFs. Accordingly, for zeolites, most of the previous research is focused on their properties and applications, but for MOFs, most focus is still on their synthesis [73].

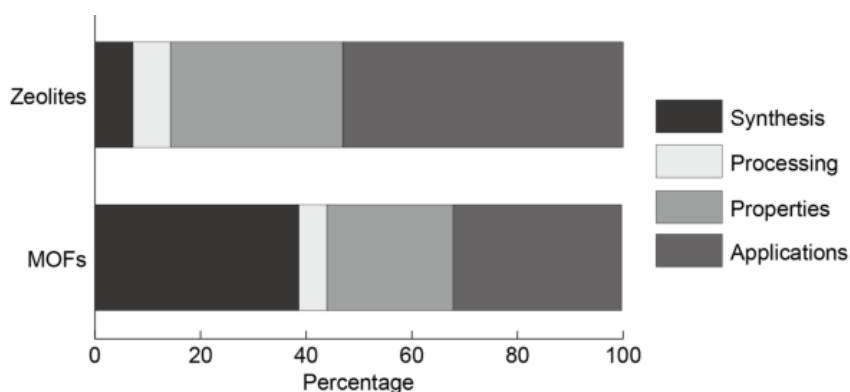


Figure 2.3 Comparison of the ratio of publications in different research domains for Zeolites and MOFs [73].

2.2 Synthesis of MOFs

The first MOFs were synthesized by the solvothermal method, but over the years, new synthesis routes were developed. Presently, MOFs can be synthesized by different methods, e.g., conventional solvothermal synthesis, microwave-assisted solvothermal synthesis, sonochemical synthesis, electrochemical and mechanochemical synthesis [2] [60]. Solvothermal is the method of choice for MOFs

synthesis, which is explained in detail in Chapter 3. In the solvothermal method, the synthesis is usually carried out in a solvent near or above the boiling point of the solvent in a sealed container or reactor [74]. The synthesis of MOFs is a very delicate process because slight variations in the experimental parameters can drastically affect the structure and properties of MOF products. MOFs synthesis is very sensitive to even the small variations in conditions, e.g., the concentration of reagents, nature of reactants, pH, and even type of solvent [2], [75]. Conditions for MOFs synthesis should be chosen in a way so that metal cluster-ligand bonds are dynamic, which is important for structure propagation in ordered and crystalline materials. The dynamic bonding in MOFs means that the metal-ligand bonds are continuously formed, broken, and then reformed during synthesis to allow the 3D framework to propagate [2].

The first crystalline MOF ever reported to have permanent porosity, and stable framework structure was MOF-5 in 1999 by Yaghi and his coworkers [11]. MOF-5 was synthesized by a hydrothermal process and the synthesis was based on the principles of metal-carboxylate cluster chemistry. MOF-5 can maintain its porosity and crystallinity up to 300°C and remains stable after dissolution in a variety of solvents. The framework of MOF-5 consists of Zn_4O tetrahedrons bonded to the CO_2 group forming metal-atom-centered clusters, and these clusters are linked together by 1,4-benzodicyclohexane (H_2bdc) linkers to form a 3D network of MOF-5 (Figure 2.4).

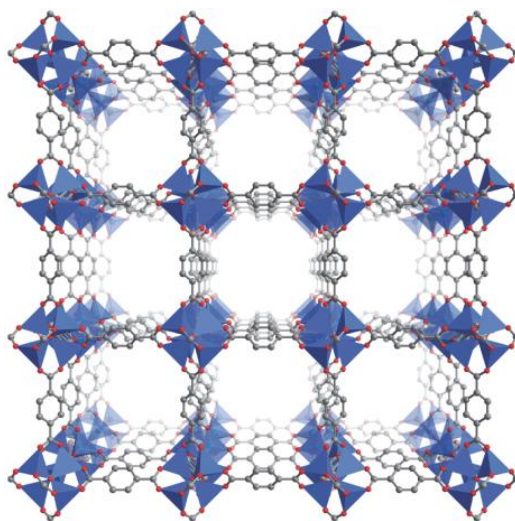


Figure 2.4 Schematic of MOF-5: The first MOF reported to have permanent porosity and stable framework structure [76].

The framework of MOF-5 has 80% free volume with two types of cavities, lined with C atoms and H atoms, which can accommodate guest molecules with Van der Waals radii of 11.0 Å and 15.1Å, respectively, and the aperture between the two cavities is 8Å. Authors showed that 55-61% of the free volume is accessible to guest molecules. Nitrogen adsorption analysis showed type-I isotherm with no hysteresis, which is typical for microporous materials [11].

The literature review and progress in various research areas related to the three MOFs, i.e., UiO-66, MIL-125, and MIL-47, synthesized in this study are discussed below. The frameworks of these MOFs contain the same organic linker (i.e. H₂bdc) but different metal clusters. The structures of these three MOFs are discussed in detail in Chapter 1.

2.2.1 UiO-66

After the seminal contributions from Tomic [68], Hoskins and Robson [69], and Yaghi [5], [77] in the field of MOFs, a steady streak of MOFs discoveries started in

the late 1990s. One such discovery was made in 2008 by the Lillerud group from the University of Oslo (UiO). They reported a new class of zirconium-based MOFs, i.e., UiO-66 and UiO-67, with remarkable stability. The chemical formula of UiO-66 is $Zr_6O_4(OH)_4(H_2bdc)$. UiO-66 is considered a benchmark of thermal stability for MOFs. Most of the MOFs decompose above 350°C, thus losing the 3D framework structure but zirconium metal-based MOFs reported by the Lillerud group have thermal stability up to 500°C. The stability of Zr-MOFs is due to the strong interaction of Zr atoms with surrounding oxygen atoms in the metal cluster and the oxygen atoms of the carboxylate group in organic linkers. Metal cluster in the UiO-66 framework ($Zr_6O_4(OH)_4(CO_2)_{12}$) has the highest coordination (12-coordinated) for any MOFs reported, making a cubic close-packed structure. Zr-based MOFs containing linkers with one benzene ring (i.e., H_2bdc) and two benzene rings (i.e., BPDC) were named UiO-66 and UiO-67, respectively. It was observed that increasing the length of linkers from one benzene ring to two rings did not affect the stability of the Zr-MOFs, but it increased the surface area and pore size of the framework. Zr-MOFs also showed enhanced stability in a variety of solvents as well as under high mechanical pressure without losing their crystallinity [13].

After the discovery of Zr-MOFs, their structures, chemistry, and synthesis were extensively studied to optimize their synthesis procedures and crystal morphologies [36], [54], [78], [79]. Katz et al., [15] investigated the role of HCl in synthesizing UiO-66, UiO-77, and their derivatives. They found that HCl significantly speeds up the synthesis of Zr-based MOFs and their derivatives. Precipitation of the final product was observed within two hours, which usually takes a couple of days. It was observed that the solubility of $ZrCl_4$ precursor in DMF solution was increased with the addition of HCl. According to this study, the synthesis of Zr-MOFs in the presence of HCl was successful at all temperatures, i.e., 60 °C, 80 °C, and 120 °C. Keeping the synthesis temperature at 80°C, it was noted that increasing the concentration of HCl in the precursor solution increases the surface area and pore volume of the final product and vice versa. In this study, defective (missing linkers) MOFs were obtained which was the reason for the increased specific surface areas

as defects in MOF provide more open sites in clusters for gas molecules to adsorb. The increase in surface area of Zr-MOFs is consistent with the works in literature [78], [79]. IR spectra showed that the defective sites on metal nodes were occupied by hydroxide (-OH) ions which can play a crucial role in catalysis [36]. Authors demonstrated that a 50-fold scale-up is possible without losing the crystallinity and porosity using this strategy of rapid synthesis of Zr-MOFs belonging to the UiO-66 framework [15].

Acid or base modulated synthesis of MOFs has been observed to have significantly decreased the time of reaction and, at the same time, increased the yield of MOFs [15], [53]. Zhao et al., [53] employed an acid-base co-modulation synthesis route for producing monodispersed and size-tunable octahedral crystals of UiO-66 MOF. The authors claim to have used the organic base as modulators for the first time for the synthesis of UiO-66. Acetic acid and triethylamine (TEA) base were used as modulators in UiO-66 synthesis. Acetic acid helped to tune the shape of the crystal, and TEA controlled the nucleation and size of crystals. It was observed that introducing TEA in reaction solution has increased the rate of nucleation, and discrete crystals were formed in narrow size distribution. When the TEA concentration in the reaction mixture was slowly increased from 0.5 to 8 mM, the size of the UiO-66 octahedral crystals decreased gradually from 1949 nm to 583 nm. At high TEA concentrations, intergrown crystals were observed in SEM images. Missing linkers in the UiO-66 framework were quantified from TGA results following the method of Lillerud and his coworkers [80]. It was observed that the use of TEA had reduced the number of missing linker defects in the framework of UiO-66, and the lowest number of defects was observed when 4 mM TEA was used in the reacting solution. BET surface area of MOF UiO-66 was also reduced when the acid-base co-modulation synthesis route was followed, which is understandable as the reduction of defects means a reduction in specific surface area, as shown in previous studies [54], [79].

The temperature during the synthesis reaction of MOF can also affect the density of defects. Destefano and coworkers studied the thermal modulated synthesis of UiO-

66 MOF for controlling defect densities in the frameworks [51]. They also claim to have synthesized UiO-66 for the first time at room temperature. They used two steps synthesis, first synthesizing metal cluster (SBU) intermediates at high temperature and then reacting these clusters with the organic linker at room temperature. The intermediate SBUs were synthesized by reacting zirconium propoxide $[\text{Zr}(\text{OnPr})_4]$ with methacrylic acid at 130°C and then adding the linker to the solution at room temperature to obtain UiO-66. The authors were also successful in synthesizing functionalized UiO-66 using the same method. It was observed that as the temperature in the second step of the synthesis increases, the defects (missing linkers) in the UiO-66 framework decrease. Nitrogen adsorption analysis showed that as the defects in the framework decrease, the surface area and total pore volume UiO-66 MOF framework decreases, which is consistent with observations in previous studies [79], [81]. PXRD patterns showed that temperature in the second step of the synthesis did not have a drastic effect on the crystallinity of UiO-66. Missing linkers (defects) were quantified using the acid-base titration technique. The sample synthesized at 45°C showed the highest number of missing linkers, i.e., 2.6 linkers per SBU, and the one synthesized at 130°C showed the lowest number of missing linkers, i.e., 0.3 linkers per SBU. A strong correlation between titration results and BET surface areas of the samples was observed [51]. Defect engineering of MOFs is a whole new research topic, and a lot of work is now also focused on this area [42], [52], [80], [82]. Defects in MOFs are not necessarily unwanted because defects can improve the catalytic and gas adsorption activities of MOFs [42], [80], [81].

The role of solvent in MOFs synthesis is still not a very well understood topic, but certain solvents have proven to be crucial for MOFs synthesis, e.g., DMF and DEF. Though toxic, DMF is the solvent of choice for a variety of MOF syntheses, including UiO-66. Venturi et al. studied the role of solvent in UiO-66 synthesis, and in this study, the aim was to perform green synthesis of UiO-66 by testing various solvents. The idea was to select green solvents that are safer, cleaner, and non-toxic and those that comply with European REACH 1907/200 standard regulations for

industrial solvents. The quality of solvents is analyzed based on the crystallinity, porosity, surface area, and yield of the final product (UiO-66) and also the non-toxicity and reusability of the solvent for synthesis. UiO-66 was successfully synthesized in twelve different solvents, but two solvents (γ -valerolactone (GVL) and propylene carbonate (PC)) were found to have produced a better product at the same time, complying with the above-mentioned EU criterion. DMF solvent gives the best MOF product but does not conform with EU standards due to its high toxicity. Nonetheless, most of the MOF syntheses employ DMF as a solvent. Generally, it was observed that solvents with high boiling points ($>100^{\circ}\text{C}$) are good for synthesizing UiO-66. When GVL and PC were used as solvents, octahedral nanocrystals with an average size of 200 nm with high crystallinity were obtained. GVL and PC are non-toxic, non-carcinogenic, recyclable, and green solvents that can potentially be employed for the industrial synthesis of MOFs [83].

2.2.2 MIL-47

Another MOF that was synthesized in this study is MIL-47 ($\text{V}^{\text{IV}}\text{O}(\text{O}_2\text{C}-\text{C}_6\text{H}_4-\text{CO}_2)$), which is vanadium metal-based (V-MOF). The literature work about MIL-47 is very obscure and not much research work has been carried out related to MIL-47 MOF, specifically when it comes to its synthesis. The previous studies on MIL-47 are mainly focused on its functionalization and applications [22], [57], [84]. Barthelet et al. [19] synthesized MIL-47 for the first time by the hydrothermal method in 2001. In this study, VCl_3 was used as a vanadium source, and deionized water as a solvent. The mixture of VCl_3 and organic linker (H_2bdc) was dissolved in deionized water and the reaction was carried out at 200°C in a Teflon-lined stainless-steel autoclave. MIL-47 is a 3D framework with channel-style (1D) long pores and framework flexibility (flexibility here means that the dimensions of the framework change with guest molecules adsorbed in it). The MIL-47 and MIL-53 MOFs both have this unique property of framework flexibility, i.e., the dimensions of the pores change when there are guest molecules in the framework, this phenomenon is also

sometimes called the ‘breathing effect’ [19], [21], [22]. Flexibility (breathing effect) in the MIL-47 framework depends upon the oxidation state of the V atom of metal clusters [19], [22], [23]. MIL-47 is observed to have shown the breathing effect when the vanadium atom is in V^{+III} oxidation state rather than the V^{+IV} oxidation state for which the framework is rigid (no flexibility) [19], [22], [23]. The oxidation state of the V atom in the MIL-47 framework depends on guest molecules inside the framework. When the MIL-47 framework has guest molecules such as DMF or unreacted organic linker, the vanadium atom is in V^{+III} oxidation (MIL-47as), and when the framework is free of occluded molecules (activated MIL-47) the vanadium atom is in a V^{+IV} oxidation state [19], [23], [56]. The oxidation state of the V atom and flexibility of the MIL-47 framework can affect the XRD patterns of MIL-47 and can slightly change the positions of its characteristic crystalline peaks [19], [23].

The structure of MIL-47 consists of vanadium-centered octahedral metal clusters (SBUs) linked by H_2bdc linkers. Single-crystal XRD of evacuated MIL-47 and guest molecule (unreacted H_2bdc) containing MIL-47 showed 3D orthorhombic framework with large tunnel-like large pores in [100] orientation. The pore dimensions of the MIL-47 framework change with and without guest molecules. TGA results showed two distinct weight loss steps, i.e., first due to the desorption of the H_2bdc linker trapped inside the framework and the second one at $420^\circ C$ due to the decomposition of the linkers in the framework of MIL-47. This was also confirmed in nitrogen sorption isotherm results which showed no nitrogen was absorbed in MIL-47 with guest molecules (unreacted H_2bdc) in the framework. The nitrogen adsorption of the evacuated MIL-47 framework showed a Type-I isotherm with a BET surface area of $930\text{ m}^2/\text{g}$. MIL-47 MOF could retain its crystallinity and framework flexibility after dissolution in solvents [19].

Yan et al., [84] synthesized MIL-47 by the solvothermal method using $VOSO_4 \cdot nH_2O$ as a vanadium source, H_2bdc as an organic linker, and DMF as a solvent. The reaction was carried out at $160^\circ C$ in a Teflon-lined stainless steel autoclave for 72 hours. Needle-like crystals were observed for MIL-47. The synthesized MIL-47 was employed for supercapacitor application. MIL-47-based capacitors showed superior

electrochemical properties with high specific capacitance, high energy density, and excellent cycle stability.

MOFs with amine (-NH₂) group functionalization are of particular interest to researchers for carbon dioxide adsorption due to their high affinity for CO₂ molecules. Leus et al., [22] for the first time investigated the adsorption properties of MIL-47 and its isorecticular MOF NH₂-MIL-47 (-NH₂ group attached to the organic linker). VCl₃ and deionized water were used as a vanadium source and as a solvent, respectively. For NH₂-MIL-47 synthesis, 2-aminoterephthalic acid (NH₂-H₂bdc) was used as an organic linker. The reaction was carried out in an autoclave at 150°C for 4 days. Adsorption of CO₂ and CH₄ on MIL-47 and NH₂-MIL-47 MOFs was probed in this study. It is previously observed that MIL series MOFs exhibit some framework flexibility (breathing effect) which can be engineered to increase the adsorption capacities of these MOFs [23][85]. MIL-47 is observed to have shown the 'breathing effect' when the vanadium atom is in V^{+III} oxidation state and the framework is rigid when in V^{+IV} oxidation state [23]. EPR analysis showed that when NH₂-MIL-47 is not activated (DMF solvent trapped inside framework pores) the vanadium in the metal node is in V^{+III} oxidation state and the possible reason could be the interaction of DMF with vanadium atoms [23]. IR spectra have confirmed the presence of DMF in non-activated NH₂-MIL-47 [22]. Biswas et al., [56] also reported that the oxidation state of MIL-47 (as-synthesized) changed from V^{+III} to V^{+IV} when the guest or the trapped DMF solvent molecules were removed from the framework by activation. For the adsorption of gases the MOF framework needs to be activated (heat treatment under vacuum to remove solvent from the framework) and optimum conditions for activation of MIL-47 were found to be heating at 125°C for 90 minutes [22].

2.2.3 MIL-125

The titanium metal-based MOFs are notorious for their difficulty in synthesis because of the extremely reactive nature of titanium sources. Particular care is

needed in synthesizing Ti-MOFs since the titanium sources readily react with the moisture and oxygen in the air, which could interfere with the synthesis reaction [86], [87]. Due to the reactivity of titanium sources, insoluble metal oxides could be formed in the reacting solution, which can hinder the process of crystallization of MOF [88]. MOFs are usually based on transition metal atoms, but among them, Ti is unique due to its photocatalytic activity, low toxicity, and redox activity. Ti-MOFs have attracted a lot of attention mainly due to their photoactive nature, which is a useful property for a variety of applications [24] [86].

Titanium metal-based MOF (MIL-125) was first synthesized by the Ferey group [24] in 2009. MIL-125 was the first MOF in the Ti-MOF family with a carboxylate linker [24]. In this work, MIL-125 ($\text{Ti}_8\text{O}_8(\text{OH})_4(\text{O}_2\text{C}-\text{C}_6\text{H}_5-\text{CO}_2)_6$) was synthesized via the conventional solvothermal method by dissolving titanium tetra-isopropoxide in a solvent mixture of DMF and methanol then reacting it in autoclaves at 150°C. The occluded solvent molecules in the framework structure can be removed from MIL-125, when it is calcined at 200°C. The Ferey group [24] found from X-ray thermogravimetry analysis that the removal of solvent guest molecules at below 200°C does not decrease the crystallinity of the material. There was some phase transition in the material between 290-350°C, which resulted in the decrease of crystallinity, and after that, a complete collapse of the framework happened at 360°C. The phase transition around 300°C may be due to the removal of the hydroxo group from the framework. N_2 adsorption-desorption analysis of MIL-125 showed the BET surface area and pore volume of 1550 m^2/g and 0.65 cm^3/g , respectively [24].

Zlotea et al., [89] used the same method and precursors as the Ferey group [24] for MIL-125 synthesis but instead of an autoclave, a Teflon-lined PAAR digestion bomb was as a reaction vessel. Reaction time and temperature were kept at 15 hours and 150°C, respectively. Amine ($-\text{NH}_2$) and CF_3 functionalized MIL-125 were also synthesized in this study for hydrogen sorption application. Kim et al. tried another type of reaction vessel for MIL-125 and NH_2 -MIL-125 synthesis. They successfully obtained disc-shaped crystals of MIL-125 at 150°C in 16 hours. In this study, NH_2 -MIL-125 was successfully synthesized in just one hour at 150°C using microwave-

assisted heating. The synthesized MOFs were then tested for catalytic and CO₂ adsorption properties.

Usually, the synthesis of MIL-125 MOF is carried out in small batches with a total reaction solution volume of about 15-20ml. Huang et al., [87] successfully synthesized MIL-125 and its derivative in relatively bigger batches with a total reaction solution volume of above 62 ml. Titanium isopropoxide and terephthalic acid were dissolved in 62 ml of DMF and methanol solution (9:1 v/v, respectively). The reaction was carried out in stainless steel (Teflon-lined) autoclaves at 150°C for 48 hours.

The bottleneck in the synthesis of MIL-125 and titanium MOFs, in general, is the handling of titanium sources. In the literature, a variety of titanium sources have been used for Ti-MOFs to tailor their properties for various applications as well as increase the efficiency of synthesis. Some of these Ti sources are titanium isopropoxide, tetra-n-butyl titanate, and titanium tetrachloride [86].

Usually, for MIL-125, disc-shaped crystal morphologies have been observed in the literature [86], [87], [90] but some studies reported circular plate and even octahedron crystal morphologies for functionalized MIL-125 [38]. Hu et al., reported a unique behavior of MOFs crystals that was never observed before for MOFs [38]. In this study, NH₂-MIL-125 crystals with a circular plate to octahedral morphologies were synthesized by keeping all the reaction parameters the same except concentrations of the reactants. XRD, IR, and UV Raman spectra confirmed that all crystal morphologies were indeed NH₂-MIL-125. Circular plate, truncated pyramid, octahedron, and tetragonal plate-shaped crystals were observed in SEM images. In-situ, XRD results showed that NH₂-MIL-125 MOFs could retain their crystallinity until 290°C after which the crystallinity decreased and no crystalline peaks were observed above 300°C. In situ XRD results were consistent with TGA analysis. Synthesizing different morphologies with this method may be preferable because no extra chemical like surfactants and capping agents are needed thus no extra impurities [38].

2.3 Chemistry, nucleation, and functionalization of MOFs

2.3.1 UiO-66

The formation of SBUs, crystallization, and the subsequent propagation of the MOF into a 3D framework are still debated [61], [62]. The classical nucleation and crystallization theories, from LaMar [63] and Johnson-Mehl-Avrami [64] models to the newer approach of pre-nucleation cluster formation and orientations [65], could not completely explain the MOFs crystallization and subsequent growth. Various studies have put forward theories about the evolution of MOF in the precursor solution [61], [62]. These studies give some clues and insights into the world of MOFs nucleation and crystal growth. Xu et al. [61] used Pair Distribution Function (PDF) analysis and studied the evolution of SBUs of UiO-66 in solution. This study has given some interesting insights into the mechanism by which UiO-66 MOF is formed in the precursor solution. Xu et al., [61] proposed a four steps process for the formation of UiO-66 in solution (illustration shown in Figure 1.13).

Step 1. Formation of hexa-nuclear Zr clusters (SBUs) at room temperature by dissolving metal salt ($ZrCl_4$) in the solvent.

Step 2. Hexa-nuclear Zr clusters (SBUs) are bridged by organic linkers and are arranged into multinuclear clusters after the addition of terephthalic acid (organic linker) to the metal salt solution

Step 3. The multinuclear clusters start to aggregate by heating the solution (of step 2) to the reaction temperature,

Step 4. Finally, the multinuclear cluster aggregation results in UiO-66 MOF.

The unique observation according to this study is the formation of hexa-nuclear clusters at room temperature, which has never been reported before.

Another study [62] found the formation of an intermediate in the precursor solution during UiO-66 synthesis before the addition of an organic linker. The effect of aging

the precursor solution (metal salt solution), the role of water, and an intermediate was studied by Taddie et al. [62]. In this study, an intermediate ($[\text{ZrCl}(\text{OH})_2(\text{DMF})_2]\text{Cl}$) product was observed when the precursor solution was aged for a few hours before the addition of the organic linker (terephthalic acid). This intermediate specie was observed even after using two different types of metal salt precursors i.e. ZrCl_4 and $\text{ZrOCl}_2 \cdot 8\text{H}_2\text{O}$ (zirconium oxychloride octahydrate) with very different atomic structures. The intermediate product was successfully extracted and then also used as a precursor for UiO-66 synthesis. In this study aging time was used as a modulator for UiO-66 MOFs synthesis. Small crystallite sizes of UiO-66 were obtained, as deduced from consistent broadening of (111) peak in PXRD patterns, when the metal salt solution was aged for 2 hours at 60°C . TEM images showed no definite crystal morphology when $[\text{ZrCl}(\text{OH})_2(\text{DMF})_2]\text{Cl}$ was used as precursor or when the metal salt solutions were aged. Spherical crystals were observed when ZrCl_4 salt was used without the aging process. The role of water in UiO-66 synthesis came to light in this work. According to this study, water plays an important role in the aging process and crystallization of UiO-66 as it provides the hydroxide (-OH) and oxide (-O) groups to be incorporated in hexa-nuclear zirconium clusters (nodes) [91].

Taddie et al., [62] concluded two possible scenarios for UiO-66 crystallization in the precursor solution.

1. $[\text{ZrCl}(\text{OH})_2(\text{DMF})_2]\text{Cl}$ acts as an intermediate chemical specie that is actively involved in the crystallization of UiO-66.
2. When terephthalic acid (organic linker) was present in the precursor solution from the start, $[\text{ZrCl}(\text{OH})_2(\text{DMF})_2]\text{Cl}$ intermediate was not observed and the crystallization of UiO-66 possibly followed a different route.

The authors of this study deduced that it is possible that the aging of solution influences the thermodynamics and kinetics of crystallization, and the formation of intermediate species ($[\text{ZrCl}(\text{OH})_2(\text{DMF})_2]\text{Cl}$) acts as a rate-determining step [62].

The synthesis of MOFs in the presence of acid or base modulators has been extensively investigated by researchers in recent years [15], [18], [53]. Modulated synthesis of MOFs has few advantages over non-modulated synthesis as it can significantly reduce the reaction time and prevents early precipitation of amorphous material. Modulators are particularly important for synthesis when the metal cluster-linker bonds are very strong in MOFs. Modulated synthesis of MOFs, as previous studies [18], [53] claimed, gives us greater control over crystal shapes, sizes as well as the rate of nucleation and crystal growth. Han et al., [18] carried out modulated solvothermal synthesis of UiO-66 crystals with different shapes and sizes using hydrofluoric acid (HF) as a modulator. Cubic and Cubo octahedral crystal morphologies were observed with variation in reactants and modulator concentrations. It was observed that when HF modulator concentration increases the crystal size of UiO-66 also increases but the rate of nucleation decreases. Keeping reactants concentration constant, at low HF concentration cubic crystals with a size range of 150 nm-650 nm were observed. As the HF/ZrCl₄ molar ratio was increased to 3, large (up to 7 μm) Cubo octahedral crystals were formed. Agglomerated crystals with no specific shape and morphology were obtained when the precursor (ZrCl₄) concentration was increased from 18.2 mM to 27.2 mM. Moreover, a fast rate of nucleation and crystal growth was observed as the reactant concentration increased. In this study, it was observed that due to the strong electronegativity of fluorine (F), F ions were adsorbed on the open metal Zr metal sites left open due to missing linker defects in the framework of UiO-66. The adsorbed F ions did not affect the crystallinity, and F ion adsorbed UiO-66 samples were thermally more stable, as shown by XRD and TGA results. Argon adsorption isotherms showed an increase in surface area and pore volume with the increase in modulator concentration [18].

Greig C. Shearer et al. [54] carried out a comprehensive study to synthesize ideal UiO-66 MOF free of defects or missing linkers. UiO-66 MOFs were synthesized at different temperatures and organic linker to metal salt ratios. They found that the most ideal defect-free and thermally stable UiO-66 MOF was obtained at a synthesis temperature of 220°C and the organic linker (H₂bdc) to metal salt (ZrCl₄) ratio of

2:1. UiO-66 synthesized at 220°C retained its crystallinity even when the sample was heated in air at 400°C for 12 hours. Keeping the linker to metal salt ratio constant (2:1), the samples synthesized at 100°C and 160°C lost their crystallinity when treated in the air for 12 hours at 300°C and 350°C, respectively. In samples where linkers were missing (defects), small peaks were observed in XRD patterns at low 2θ angles, while these peaks were missing in defect-free samples. The authors argued that missing linkers could also be confirmed from TGA curves using molecular weights of UiO-66 and ZrO₂, which is the final product obtained when the UiO-66 framework is destroyed after decomposition. TGA results showed that thermally most stable UiO-66 was obtained at 220°C (L: M ratio 2:1), indicating a perfect defect-free UiO-66 framework. TGA curves also showed some trapped H₂bdc molecules in the framework of UiO-66 due to using excess linker during synthesis. From nitrogen adsorption isotherms, it was observed that samples with missing linkers exhibit higher BET surface area compared to defect-free UiO-66 MOFs, which is also observed in some other previous studies [15], [78], [79].

According to some studies [92], the quantification of missing linkers (defects) from the TGA curve (data) can be imprecise and misleading as it is very difficult to pinpoint the start of the decomposition of organic linkers in the MOF structure.

For MOFs to be used in catalytic applications understanding their surface chemistry is very important. Cirujano F.G., and Llabreśi Xamena, F. X., did a comprehensive study [36] of Brønsted and Lewis acid sites in UiO-66 MOF. They showed that the catalytic activity of defective UiO-66 can be tuned for the desired application. The catalytic performance of UiO-66 was also evaluated in reactions catalyzed by Brønsted and Lewis acid sites. In the UiO-66 framework when the organic linker is missing it leaves unsaturated Zr⁴⁺ sites on which water molecules adsorb forming Brønsted acid sites and by desorbing the water molecules Lewis acid sites are generated. Thus, the hydrated UiO-66 contains Brønsted acid sites, and just by thermal dehydration of UiO-66 MOF, these sites can be switched to Lewis acid sites. The catalytic activity of Brønsted acid sites containing UiO-66 was tested for

esterification levulinic acid and it was observed that for hydrated UiO-66 the catalytic activity increases with the increase in the concentration of defects in the framework. The same trend was observed for dehydrated Lewis acid sites containing the UiO-66 framework in the isomerization reaction of citronellal to isopulegol. FTIR spectroscopy of CO adsorbed defective UiO-66 MOF showed the presence of Brønsted and Lewis acid sites in hydrated and dehydrated samples, respectively. The potentiometric acid-base titration method was employed to find the concentration of Brønsted acid sites in the UiO-66 framework and the results were consistent with the FTIR analysis. It was observed that the concentration of Brønsted and Lewis acid sites in the UiO-66 framework increased with the increase in the number of defects which is consistent with the previous studies [78], [79], [93]. Defective UiO-66 MOF was more hydrophilic than an ideal defect-free UiO-66, consequently, more sites for water molecules to adsorb and induce Brønsted acid sites in the framework. The authors also found that amino group (-NH₂) functionalized defective UiO-66 is catalytically more active than pristine (defective) UiO-66 [36].

The nature of defects in the framework of UiO-66 has been in discussion among researchers. It is very hard to precisely figure out the chemical nature of defects in UiO-66 MOF at the molecular level. A lot of studies have been done on the chemical structure of the UiO-66 framework (287 articles from 2008 to 2014) but for the first time, Yaghi and his coworker [3] have definitively determined the nature of defects in the UiO-66 framework using state of the art techniques. One of the main hindrances in studying the defects, using different characterization methods like SXRD, is the small size of UiO-66 crystals [94]. To overcome this difficulty researchers in this study have devised a new synthesis method for the synthesis of UiO-66 MOF and obtained big micron-sized single crystals. Defects in UiO-66 arise due to missing linker (H₂bdc) substituted by other chemical species like water, hydroxide, chloride, modulators, and DMF solvent [36], [62], [94]. According to Yaghi et al., the defect sites in the UiO-66 framework are usually substituted by water molecules and the hydrogen bonding between hydroxide counterion and μ_3 -OH group of Zr metal clusters balances the charge [3].

Temperature-induced distortions in metal clusters of zirconium-based MOFs were investigated by Hupp et al., using X-ray pair distribution (PDF) data and density functional theory (DFT) [95]. At elevated temperatures distortions have been observed in the metal nodes of these MOFs which needs to be understood before any widespread potential application of these MOFs. In this study, it was observed that transitions in metal clusters of UiO-66 happen when heated to around 120-130°C and the change was specifically observed between Zr-Zr bond distances which can result in distortions of the octahedral structure of nodes. But these distortions did not have any effect on the overall symmetry of the framework and no change was observed in the powder XRD patterns after these transitions. After distortion in the nodes, it became metastable and did not converge immediately to their original symmetry upon cooling. After several weeks in ambient conditions the metal nodes of UiO-66 returned to their original symmetry [95].

One possible use of MOFs can be in electronics applications but MOFs usually have high bandgaps [57]. For MOFs to be used in electronic applications their bandgap needed to be tuned. Taddei et al., [82] focused their study on tuning electronic properties of defective Zr-based MOF (UiO-66) by functionalization of defective sites. Engineering defects in MOFs is a recent phenomenon to tune the chemical, physical and electronic properties. For this purpose, Zr-based MOFs are particularly interesting due to their ability to maintain structural integrity despite having defects (missing linkers) in the framework [54], [96]. In this study, amino-functionalized benzoic acid was attached to the defective sites of the UiO-66 framework using the post-synthetic defect exchange (PSDE) approach. It was observed that the bandgap of MOF decreases (from 4.1 to 3.3 eV) and the decrease is probably achieved by the upward shift of the valence band due to the functionalization of metal nodes. The number and position of amino groups on benzoic acid were observed to have also affected the bandgap of UiO-66. Defective MOFs could potentially provide more flexibility for chemical activity compared to organic linker functionalized MOFs [57].

2.3.2 MIL-47

Biswas et al. [56] studied the synthesis, characterization, and structure of non-functionalized MIL-47 and functionalized particular MIL-47-X (X= -Cl, -Br, -CH₃, -CF₃, -OH, -OCH₃) MOFs. Furthermore, carbon dioxide adsorption capacities of pristine and functionalized MIL-47 were compared. It was observed that in as-synthesized (occluded guest molecules) MIL-47 vanadium atoms were in V^{+III} oxidation state. The activated MIL-47 (no guest molecules) and functionalized MIL-47-X MOFs vanadium atoms were V^{+IV} oxidation states which is consistent with the previous studies [22], [23]. The occluded molecules in the framework of as-synthesized MIL-47-X were mostly functionalized linkers (H₂bdc-X) or the solvent. DRIFT and Raman analysis showed that the trapped guest molecules were significantly removed during the thermal activation process. XRD patterns of all as-synthesized and functionalized MIL-47-X MOFs were the same as pristine activated MIL-47. XRD confirms that all MOF samples have the same framework topology (isoreticular frameworks) with orthorhombic orientations. From TGA results, it was observed that all functionalized samples were thermally stable between the temperature range of 330-385°C, which is slightly lower than pristine MIL-47 (400°C). The -CH₃ group functionalized MIL-47 showed the highest BET surface area (897 m²/g), while the -Br functionalized sample had the lowest surface area (305 m²/g).

Besides their structural and chemical properties, MOF's electronic properties can also be altered by the functionalization of organic linkers. MOFs are generally insulators or large bandgap semiconductors but functionalization can change the bandgap of MOFs. Vanpoucke D.E.P., [57] carried out a computational study of the change in electronic properties of vanadium MOF (MIL-47) after functionalization by different chemical functional groups. Vanpoucke found that functionalization changes the bandgap of MIL-47 (V-MOF), the same effect was previously observed for UiO-66 (Zr-MOF) [97] and MIL-125(Ti) [98]. It was concluded that functionalization of the organic linker not just decreased the pore size but also

induced slight rotation in the linker and the rotation angle gets bigger with a heavier functional group.

2.3.3 MIL-125

Synthesis of Ti-based MOFs is very difficult due to the high reactivity of Ti sources. The high reactivity of titanium sources leads to complex association and dissociation of Titanium-organic linker bonds thus resulting in poor quality or sometimes even amorphous products. Insoluble metal oxides are formed due to the reactive Ti sources which disrupt the process of Ti-MOF crystals growth [88]. In Ti sources the coordination number of Ti is usually 4 which makes them unstable, thus Ti-sources readily hydrolyze in humid conditions to form a stable TiO_2 compound in which the Ti atom has a coordination number of 6 [26]. The hydrolysis of Ti-sources into TiO_2 has a significant negative effect on the crystallization of Ti-MOFs. Moreover, Ti-sources can react with the carboxylate group in the organic linker forming strong Ti-O bonds which effectively hinders the dissociation and association process of bonding between metal clusters and linkers. The dissociation and association process of bonding (dynamic bondings) between metal clusters and linkers is necessary for the propagation of MOF structures [2], [26], [88].

MIL-125 was the first MOF to have octamer metal clusters. In MIL-125, octahedral titanium metal clusters are connected from corners to form circular (cyclic) octamers. Organic linkers (H_2bdc) connect these octamers to twelve (12) other octamers to form a 3D framework of MIL-125 [27]. The octamers in MIL-125 are oriented along the [001] plane [24]. The fast photochromatic effect observed by the Ferey group [24] when MIL-125 was irradiated by light (UV-visible excitation) the color of the material changed from white to purple-gray-blue. The photochromatic effect was observed when alcohols (methanol, ethanol, etc.) were adsorbed in the MOF. The photochromatic phenomenon is an indication of the possible use of MIL-125 in a photocatalytic application.

Kim et al., [25] functionalized MIL-125 with Amine (-NH₂) group and compared its performance for carbon dioxide adsorption. The results showed that NH₂-MIL-125 had a better affinity for CO₂ than pristine MIL-125 thus more adsorption capacity. Clausius-Claperyon plots showed that the heat of adsorption for CO₂ was higher on NH₂-MIL125 compared to MIL-125 which means that energetically CO₂ prefers to adsorb on functionalized NH₂-MIL-125. Temperature programmed desorption (TPD) results indicated the presence of Lewis acid and base active sites on both MIL-125 and NH₂-MIL-125 MOFs, though, more Lewis base active sites were observed on functionalized MOF.

Esra et al., [27] studied the catalytic performance of pristine and sulfated MIL-125 in the esterification of acetic acid. Both sulfated (sulfonyl group) and non-sulfated MIL-125 showed catalytic activity in the esterification reaction of acetic acid but the performance of sulfated MIL-125 was superior. With sulfated MIL-125 used as a catalyst, the conversion of acetic acid was 62.3% and 75.2% at 80°C and 90°C, respectively. Conversion of acetic acid was 55.74% and 18% with pristine MIL-125 used as a catalyst and without any catalyst, respectively. So, the presence of MOFs as a catalyst has significantly increased the esterification of acetic acid. Both catalysts showed the same performance when reused in the reaction. Nitrogen adsorption results showed that BET surface area and pore volume decreased in the sulfated MIL-125 sample due to the induction of the sulfonyl group in the framework. It was interesting to see that thermal stability did not change as both pristine and sulfated MIL-125 were stable until 400°C in air.

Some studies have shown that using different concentrations of reagents and modulators the sizes and morphologies of MIL-125 crystals can be controlled. Hu et al. obtained circular plates, truncated pyramids, octahedrons, and tetragonal plates shaped morphologies for NH₂-MIL-125 just by changing the concentrations (w.r.t the volume of solvent) of the precursor reagents [38]. The use of monocarboxylic acids as modulators has a tremendous effect on the morphologies and sizes of the amine-functionalized MIL-125. Hu et al., [99] reported that using small molecular monocarboxylic acid like acetic or thioglycolic acid can drastically affect the

morphology of NH₂-MIL125 crystals. When acetic acid was used circular plate-like crystals were observed but when thioglycolic acid was used as a modulator, ultrathin-truncated octahedrons shaped crystals were observed. The small molecular acids (acetic and thioglycolic) attach themselves to certain facets of the MOF crystals thus hindering the growth of crystals in that particular direction that is the reason why different crystal shapes were observed for different modulators. Benzoic acid as a modulator controlled the crystal sizes when used in different concentrations in the reacting solution. The relation between the concentration of benzoic acid and the size of the crystal was observed to be non-linear.

2.4 Properties and applications of MOFs

The synthesis of MOFs needs to be improved to use in practical applications. MOF researcher groups are carrying out intense research to find a viable, practical, easy, and cost-effective synthesis method for MOF synthesis.

MOFs have attracted considerable attention in the last couple of decades due to their exceptional properties. The potential applications of MOFs can be unlimited, which could include catalysis [42] to gas adsorption and storage [47], [56], fuel cells [50], electronics [84] and solar energy [28], and so on. Here, some studies will be discussed that deal mainly with the applications side of MOFs particularly UiO-66, MIL-47, and MIL-125.

2.4.1 UiO-66

Jodlowski et al. [52] designed a drug delivery system based on defective UiO-66 (Zr-MOF), which could potentially be used in curing heart diseases. Defective MOF was used because of its high surface area and pore volume, which can accommodate sufficient drug to be delivered to the target location and slowly release. The stability in the solvent environment, low toxicity, high biodegradability, and biocompatibility of Zr-MOFs make them perfect candidates for drug delivery systems. To achieve

controlled defects in the UiO-66 framework HCl modulated route was employed for synthesis. The reaction was carried out in a small continuous flow microreactor with the flexibility of changing residence time for the reactants. Increasing the concentration of HCl increased the number of defects in the framework of UiO-66 [15]. It was observed that a sample with a high ratio of defects has a high surface area resulting in higher drug capacities. Chloroquine diphosphate (CQ) drug was loaded using the solution mixing method. CQ loading in the UiO-66 framework was confirmed from UV-vis, ATR-FTIR, and Raman spectra. Drug loading of up to 21.2 wt% in UiO-66 MOF was achieved in this work. In vivo and in vitro testing of this drug delivery system showed promising results and the author argued that this method could possibly be employed for curing COVID-19 related complications. It was further elaborated that this method could mitigate the potential detrimental effects to human health pose by direct use of the CQ drug [52].

Defects in the UiO-66 framework induce catalytic active sites (Lewis and Brønsted acid) in MOF [36]. It is observed that the density of catalytic sites increases with the increase of defects in the UiO-66 framework [100]. Defects decrease thermal stability but at the same time increase the catalytic and adsorption activities. So, in designing or synthesizing MOF it should be kept in mind that it is always a trade-off between stability and catalytic or adsorption capacities of MOF [54]. Defected UiO-66 has shown catalytic activity in carboxylic acids esterification, the cycloaddition of CO₂ to epoxides, isomerization of carbonyl-ene to isopulegol, and many more reactions [42]. Catalytic active sites can also be introduced in UiO-66 by functionalization of the organic linker (H₂bdc) with different chemical species e.g. Amine (-NH₂) or sulfonic acid (-SO₃H) groups [42].

Successful photocatalytic reduction of carbon dioxide to carbon monoxide was performed by Taddei et al. [82] using the functionalized defective UiO-66 and the photocatalytic performance rivals that of P25 (TiO₂).

The high surface areas of MOFs are very good for gas adsorption and storage. UiO-66 has shown a reasonable capacity for carbon dioxide storage and separation.

Pristine UiO-66 can store up to 7.9 wt% CO₂ while hydroxy group functionalized UiO-66 can adsorb up to 17.9 wt% CO₂ [34]. UiO-66 incorporated polymer-based membrane has shown to be very successful in separating CO₂ from different gaseous mixtures [101]. Moreover, UiO-66 based catalysts can be potentially useful in the conversion of CO₂ into useful chemicals like Methanol at lower temperatures [102]. The storage of natural gas (a clean fuel) in UiO-66 has recently been investigated for the design of fuel systems that can be used in transport vehicles in the near future [103]. BASF chemicals have recently tested a prototype technology for natural gas fuel systems based on MOFs for heavy-duty trucks and showed great promise for future fuel storage technologies [47].

Recently highly porous MOFs have been used as a stationary solid phase in packed columns of High-Performance Liquid Chromatography (HPLC) [104]. UiO-66-silica composite incorporated into the packed column for HPLC successfully separated ethylbenzene and styrene [105]. UiO-66 as a stationary phase is also effective in capillary gas chromatographic separation of hexane isomers and benzene homologs [106].

2.4.2 MIL-47

Methane is one of the main components of fossil fuels. For a while, researchers are in a quest for new catalysts that can convert methane into useful products like acetic acid (AA). For this purpose, it is desired to catalytically oxidize methane to AA at low temperature and a catalyst is required which has a superior activity to a homogeneous catalyst and is easy to use like a heterogeneous catalyst. Due to their highly porous structure and flexibility of design, MOFs can be promising candidates for this type of catalyst. Phan et. al. [21] evaluated the catalytic activities of MIL-47 and a new MOF-48 (isoreticular structure of MIL-47 with a methyl group in an organic linker pointing inwards in pore channels) for the oxidation of methane to acetic acid. In the presence of K₂S₂O₈ oxidant, MIL-47 catalyst converted methane into acetic acid at 80°C with yield and selectivity of 70% and 80%, respectively. The

new MOF-48 showed superior performance when CO was used in the reaction mixture and resulted in the increase of selectivity to 100% towards acetic acid at the same temperature (80°C). These MOFs showed better performance than heterogeneous catalysts and were comparable to homogenous catalysts. The MOFs were reusable and showed structural stability even after a few cycles of reactions. The performance of these MOF catalysts can be improved with a variety of functionalization.

MIL-47 is observed to have considerable CO₂ and CH₄ adsorption capacities. CO₂ and CH₄ adsorption capacities for MIL-47 were found to be 7.7 and 4.1 mmol/g, respectively. It was interesting that the CO₂ and CH₄ capacities for NH₂-MIL-47 were found to be 20% and 10%, respectively, which is less compared to the pristine MIL-47. The decrease may be due to the lack of breathing effect (flexibility) and the protruding amino group inside the pores of MOF. Pulse chromatography results showed that the adsorption enthalpies in MIL-47 for both gases (CO₂, CH₄) were slightly lower than NH₂-MIL-47. So, there was a slight increase in affinity for adsorbates in the case of NH₂-MIL-47. NH₂-MIL-47 was thermally less stable and TGA results showed that the framework is destroyed completely at 280°C [22].

Carbon dioxide adsorption capacities of pristine and functionalized MIL-47-X (X= -Cl, -Br, -CH₃, -CF₃, -OH, -OCH₃) were compared by Biswas et al. [56]. It was found that CO₂ adsorption capacities (at 0°C, 1bar) were different for functionalized MOFs suggesting varied interaction of carbon dioxide molecules with different functionalized linkers (H₂bdc-X). Despite the decrease in pore sizes of functionalized MOFs their CO₂ uptake increased pointing to the strong interaction of CO₂ molecules in these groups.

MOFs are generally insulators or large bandgap semiconductors but it recently came to light that the bandgap can be altered either by playing with metal nodes or by functionalization of organic linkers [57]. This new insight may pave the way for MOF's electronics applications. Some researchers are trying to design MOFs with

conducting properties by filling the 1-D pores of MIL-47 with conducting polymers [58] or doping metal atoms onto the metal nodes [59].

Vanadium-based materials have long been used as electrodes in capacitors but Yan et al. [84] were the first to investigate the performance of vanadium-MOF (MIL-47) electrodes in supercapacitors. The high density of valence electrons in the V atom is one of the reasons vanadium-based compounds are used as capacitors. Different MOFs have shown potential to be used in supercapacitors [107] but this is the first time V-MOF is used for this purpose. The needle-like crystals of MIL-47 have a high surface-to-volume ratio, thus a high active surface which is good for a supercapacitor electrode. When needle-like crystals of MIL-47 were used as an electrode in a typical three-electrode capacitor, a specific capacity of 572.1 F/g with a current density of 0.5 A/g (in 1.0 M Na₂SO₄ solution) was obtained. No decay was noticed in the capacitance even after 10,000 cycles at the current density of 1 A/g. A solid-state asymmetric supercapacitor was also designed using activated carbon and V-MOF (MIL-47) as negative and positive electrodes, respectively. The solid-state capacitor showed superior performance regarding capacity, cycles, and energy density [84].

2.4.3 MIL-125

MIL-125 MOF is also reported to have catalytic and photocatalytic properties. Esra et al. [27] tested the catalytic activity of pristine and sulfated MIL-125 in the esterification of acetic acid. Both sulfated and non-sulfated MOFs showed catalytic activity in the esterification reaction of acetic acid but the performance of MIL-125 (sulfated) was superior. With MIL-125 (sulfated) used as a catalyst, the conversion of acetic acid was 62.3% and 75.2% at 80°C and 90°C, respectively. Conversion of acetic acid was 55.74% and 18% with pristine MIL-125 used as a catalyst and without any catalyst, respectively [27].

MIL-125 is observed to have tremendous UV adsorption capacity thus having potential for outstanding photocatalytic activities and applications [86]. Composite

catalysts based on MIL-125 MOFs are observed to have better photocatalytic activities than normal MIL-125 [87], [90]. Zhao et al. [90] tested reduced graphene oxide incorporated NH₂-MIL-125 composite catalyst (rGO@NH₂-MIL-125) for photocatalytic conversion of CO₂ into methyl formate. Composite catalyst (rGO@NH₂-MIL-125) showed better performance in photocatalytic reduction of CO₂ than pristine MIL-125. The separation of photo-induced charge carriers (electron and holes) was far better in rGO@NH₂-MIL-125 catalyst which was attributed to the synergistic effect due to amino group (-NH₂) and incorporated rGO. Moreover, rGO incorporation in NH₂-MIL-125 significantly reduced the agglomeration of MOF particles.

The synergistic effect of the amine group and TiO₂ particles in a composite catalyst based on MIL-125 MOF was also investigated in another study [87]. In this study, TiO₂ incorporated NH₂-MIL-125 composite catalyst was successful in photocatalytic degradation of formaldehyde pollutants. Theoretical studies showed that the bandgap of MIL-125 can be altered by the functionalization of the organic linker with different functional groups which can be useful for the widespread application of MIL-125 in photocatalytic and electronics applications [98].

Titanium-based MOF (MIL-125) and its isostructural amine-functionalized MOF (NH₂-MIL-125) were tested in catalytic reactions and CO₂ adsorption by Kim et al [25]. MOFs were synthesized by conventional solvothermal and microwave heating routes. Smaller particles were obtained due to the rapid heating of microwaves, which provided a way for quick nucleation, and shorter reaction times limiting particle growth. The BET surface areas of amine-functionalized samples were up to 40 m²/g less than the pristine MOF sample (1510 m²/g) which is obvious due to the presence of the -NH₂ group in the functionalized samples. The amine-functionalized MOF showed better affinity and capacity for CO₂ adsorption compared to pristine MOF at different temperatures (0°C-30°C). Due to better van der Waals interaction in its small micropores, the CO₂ adsorption capacity of the NH₂-MIL-125 sample was better. The presence of both Lewis acid and base sites was observed for both pristine and functionalized samples in TPD analysis. Lewis base sites were

considerably more in functionalized samples. NH₂-MIL-125 showed better catalytic performance in CO₂ cycloaddition to epichlorohydrin reaction while non-functionalized MOF was better as catalysts in desulphurization of dibenzothiophene reaction [25].

Some types of MOFs have been tested in a very unique application area of airconditioning systems in buildings. Traditional cooling systems for buildings consume a lot of energy on dehumidifying (latent cooling) the ambient air. About 30% of the total energy consumed by air conditioning systems goes to the latent cooling of ambient air. By designing MOFs-based systems 30% to 40% of air conditioning energy consumption can be reduced [32]. In a study report in 2018 [32], authors used highly porous MOF (MIL-100) for dehumidifying the ambient air before cooling it down to the desired temperature in a building air conditioning system. MOFs with exceptional water adsorption capacity, amphiphilic nature, non-toxic, and producible on a large scale at low cost are needed for this purpose. Keeping in mind these requirements the authors selected MIL-100(Fe) for this purpose. The MOF (MIL-100(Fe)) was coated onto the heat exchanger of the air conditioning system which worked in both adsorption (dehumidification of ambient air) and desorption (removal of adsorbed water) modes. For desorption mode, no extra energy was consumed but the heat extracted from the ambient air (that is cooled) by the condenser was used for the desorption of water from the coated MOF. With this design, the authors managed to eliminate the latent cooling step and reduce the energy consumption of the air conditioning system by up to 36% [32].

2.5 Goals and Objective

- Synthesis of UiO-66 (zirconium MOF), MIL-125 (titanium MOF), and MIL-47 (vanadium MOF) via the solvothermal method,
- Studying the effect of experimental parameters e.g. temperature, time, concentrations, and addition of modulators on the synthesis of the above three MOFs,

- Characterization of UiO-66, MIL-125, and, MIL-47,
- Concluding the best synthesis protocols for all three MOFs studied in this work,
- Conducting preliminary water adsorption and uptake studies for UiO-66.

CHAPTER 3

EXPERIMENTAL SECTION

3.1 Synthesis of MOFs

Traditionally, MOFs are synthesized by conventional solvothermal process (Figure 3.1), but some new methods have also been developed over the years, for example, microwave-assisted solvothermal synthesis, sonochemical, electrochemical, and mechanochemical synthesis methods.

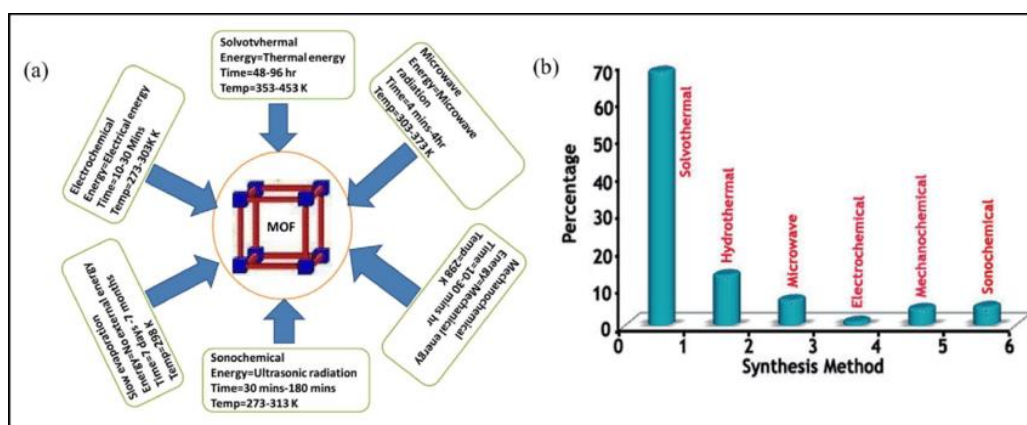


Figure 3.1 Synthesis of MOFs by different methods [108]

The timeline of patented synthetic routes for MOFs is shown in Figure 3.2. The main difference between these methods is the source of energy used e.g. in solvothermal electrical heating is used while in the sonochemical method ultrasonic waves are used as an energy source. Recently some new non-conventional avenues for MOFs synthesis have been explored like microfluidic synthesis, Ionic liquid synthesis, and dry-gel conversion synthesis [60].

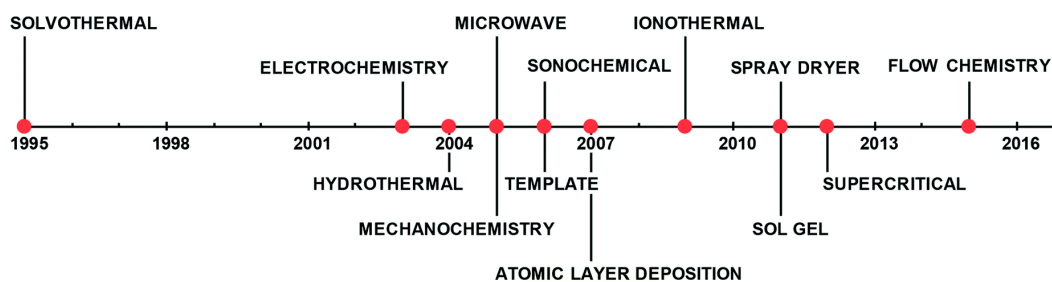


Figure 3.2 Timeline of patented synthetic routes for MOFs [109].

3.1.1 Solvothermal synthesis of MOFs

Solvothermal is a relatively straightforward synthesis route with a high throughput of MOFs compared to other routes [60]. In this method, the precursors, metal salt, and organic linker are dissolved in high boiling point solvents like DMF (or DEF or water) in a glass vial or any other sealed container. The ingredients of the sealed container are left to react in an oven at a specific temperature for a few hours or a few days. If the reaction temperature is high, the ingredients are transferred to Teflon lining stainless steel autoclaves for reaction. The as-synthesized MOF is washed with DMF a few times and then washed (or soaked) with any other low boiling point solvent, like methanol, for solvent exchange. Solvent exchange is a necessary step to remove the occluded DMF molecules from the porous framework of MOF as the high surface tension of DMF can damage the framework in the drying (or activation) step [2]. After the solvent exchange step, the as-synthesized MOF is dried and activated by heating directly or under the vacuum to remove all the solvent molecules trapped in its framework. The general schematic of the solvothermal process is shown in Figure 3.3.

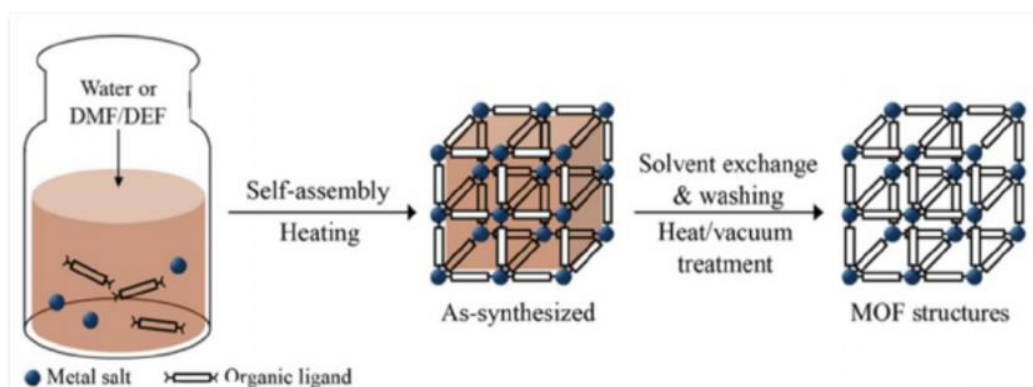


Figure 3.3 Solvothermal synthesis of MOFs [60].

In the following pages, the solvothermal synthesis procedure of the MOFs synthesized in this study will be explained in detail.

3.1.1.1 Solvothermal synthesis of UiO-66

In this study, UiO-66 was synthesized following the general procedure mentioned by Cavka et al,[13] and Howarth et al. [2] with some modifications for various batches. In solvothermal synthesis for UiO-66, a Zirconium metal-based MOF, the metal salts ($ZrCl_4$) and organic linker (terephthalic acid, H_2bdc) were dissolved separately in N, N-dimethylformamide (DMF) by sonication or stirring (20 minutes) in 250 ml sealed HDPE bottles. The two solutions were then mixed in a single HDPE bottle and sonicated again for 20 minutes. After the complete dissolution of precursors (metal salt and organic linker) in DMF solvent, the final solution was left for reaction in an oven at a specific temperature. The temperatures and time of reaction range from $80^\circ C$ to $120^\circ C$ and a few hours to a few days, respectively. For reaction temperatures higher than $120^\circ C$, the syntheses were carried out in sealed Teflon-lined stainless-steel autoclaves instead of HDPE bottles. After completion of the reaction the solution containing precipitated MOF (white precipitate) was transferred to the centrifuge tube for removal of supernatant liquid, washing, and recovering the MOFs by centrifugation. Washing of MOF with DMF using

centrifugation was repeated 2 to 3 times and then the recovered as-synthesized MOF was soaked in ethanol (or methanol or acetone) for 24 hours. The next day UiO-66 MOF was washed again 2 to 3 times with ethanol in a centrifuge tube. Every time after centrifugation, the supernatant ethanol was removed and fresh ethanol was added to the tube. The purpose of soaking and washing MOF in ethanol is to replace the trapped DMF solvent and unreacted precursors from the pores in the framework [2]. This step is called solvent exchange. To take advantage of the high surface area and porosity of MOF, ethanol should also be removed from the pores in the framework, in other words, it needs to be activated by heat drying or under vacuum. Finally, the as-synthesized UiO-66 MOF was dried at 70°C for 24 hours. The drying temperature for MOFs should be slightly higher than the boiling point of the exchange solvent, which was chosen to be ethanol (or methanol) [2]. The flowchart of the solvothermal synthesis of UiO-66 MOF is shown in Figure 3.4.

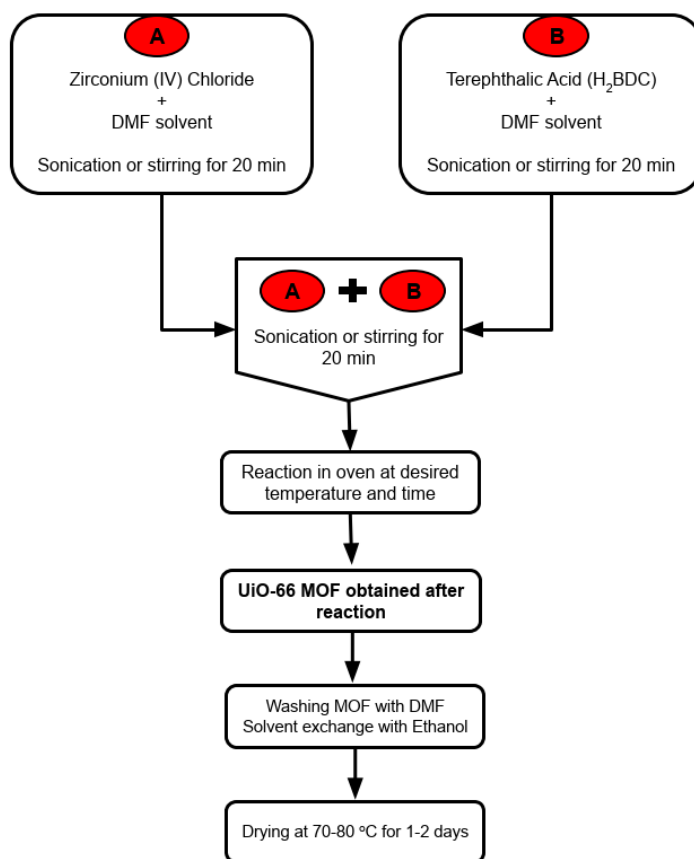


Figure 3.4 Step-by-step solvothermal synthesis of UiO-66 MOF

Sample codes and notations of various UiO-66 samples synthesized in this study are shown in Table 3-1. C1 and C2 refer to the two different concentrations in mM of precursors used during synthesis. C1 refers to 8.66 of ZrCl₄ and 8.66 of H₂bdc; while C2 refers to 19.16 of ZrCl₄ and 39.11 of H₂bdc. Accordingly, the sample codes used in this work for naming and identifying different UiO-66 MOF samples can be interpreted as follow. The sample code ‘U66-80-C1’, refers to UiO-66 synthesized at 80°C, using the concentrations of precursors mentioned for C1.

Table 3-1 Sample codes and experimental conditions for the solvothermal synthesis of UiO-66

Sample code	Reaction conditions			
	Temperature (°C)	Concentration (mM)		Time (days)
		ZrCl ₄	H ₂ bdc	
U66-80-C1	80	8.66	8.66	5-10
U66-100-C1	100	8.66	8.66	2-3
U66-120-C1	120	8.66	8.66	1
U66-80-C2	80	19.16	36.11	5-10
U66-100-C2	100	19.16	36.11	2-3
U66-120-C2	120	19.16	36.11	1

3.1.1.1.1 Modulated solvothermal synthesis of UiO-66

For HCl modulated synthesis of UiO-66, the general procedure is the same as discussed above in section 3.1.1.1 but the only difference was that the HCl was added to the zirconium salt solution (see Figure 3.4). For acetic acid-TEA co-modulation synthesis of UiO-66, the procedure was slightly different. First, the organic linker and TEA were added to the DMF solvent, and the solution was sonicated for 20 minutes. After sonication, acetic acid and ZrCl₄ salt were added to the same solution and sonicated again for 20 minutes. The final solution was then transferred to the oven for reaction at 120°C for 6 hours. The washing, solvent exchange, and drying steps were the same as discussed in section 3.1.1.1. The general schematic of acid-base co-modulation synthesis is shown in Figure 3.5.

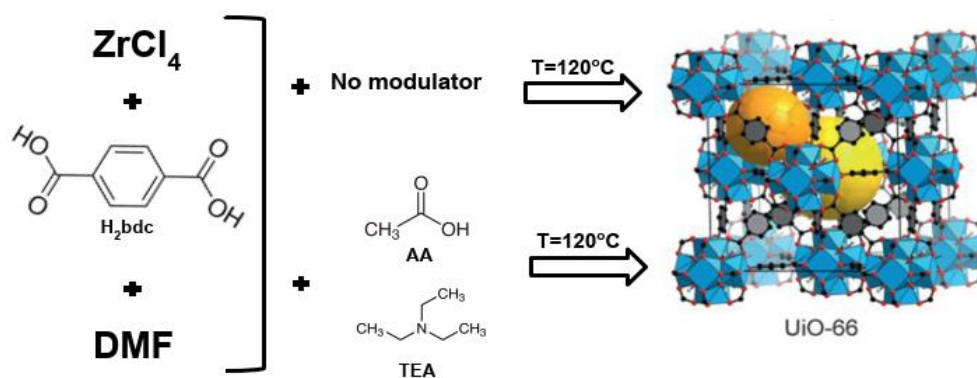


Figure 3.5 A general schematic of the acid-base co-modulates solvothermal synthesis of UiO-66 [3]

Table 3-2 shows the sample codes for the AA-TEA co-modulation synthesis of UiO-66 at 120°C with precursor concentration C2.

Table 3-2 Sample codes for the AA-TEA co-modulation synthesis of UiO-66 at 120°C with precursor concentration C2 (sample U66-120-C2)

Samples code	Modulator concentration		Time of reaction (hours)
	AA (M)	TEA (mM)	
U66-S1	2.4	2	6
U66-S2	2.4	4	6
U66-S3	2.4	8	6
U66-S4	2.4	12	6
U66-S5	2.4	16	6
U66-S6	2.4	19	6
U66-S7	2.4	-	6
U66-120-C2	-	-	24

3.1.1.2 Solvothermal synthesis of MIL-47

Vanadium metal-based MOF, MIL-47, was also synthesized using the solvothermal method. Vanadium (IV) oxide sulfate hydrate ($\text{VO}_2\text{SO}_4 \cdot n\text{H}_2\text{O}$) and terephthalic acid (H_2bdc) were separately dissolved in DMF by sonication for 20 minutes. The two solutions were then mixed and sonicated again for 20 minutes in an HDPE bottle. The final solution was then transferred to Teflon-lined stainless-steel autoclaves and sealed tightly. The autoclaves were then kept for reaction in an air-forced lab scale oven at a specific temperature. The temperatures and the time of reaction range from 160°C to 220°C and 24 hours to 5 days, respectively. After completion of the reaction, the solution containing precipitated MOF (brown color precipitate) was transferred to the centrifuge tube for washing and recovering the MOFs by centrifugation. Washing removes unreacted precursors from the pores of the MIL-47 framework. Washing of MOF with DMF using centrifugation was repeated 2 to 3 times, and then the recovered as-synthesized MOF was soaked in methanol (or ethanol) for 24 hours (solvent exchange). The next day MIL-47 MOF was washed 2 to 3 times again with methanol in the centrifuge. Every time after centrifugation, the supernatant methanol was removed, and fresh methanol was added to the tube. The as-synthesized MIL-47 MOF was then dried at 70°C for 24 hours to remove the trapped methanol from the framework. The flowchart of the solvothermal synthesis of MIL-47 MOF is shown in Figure 3.6.

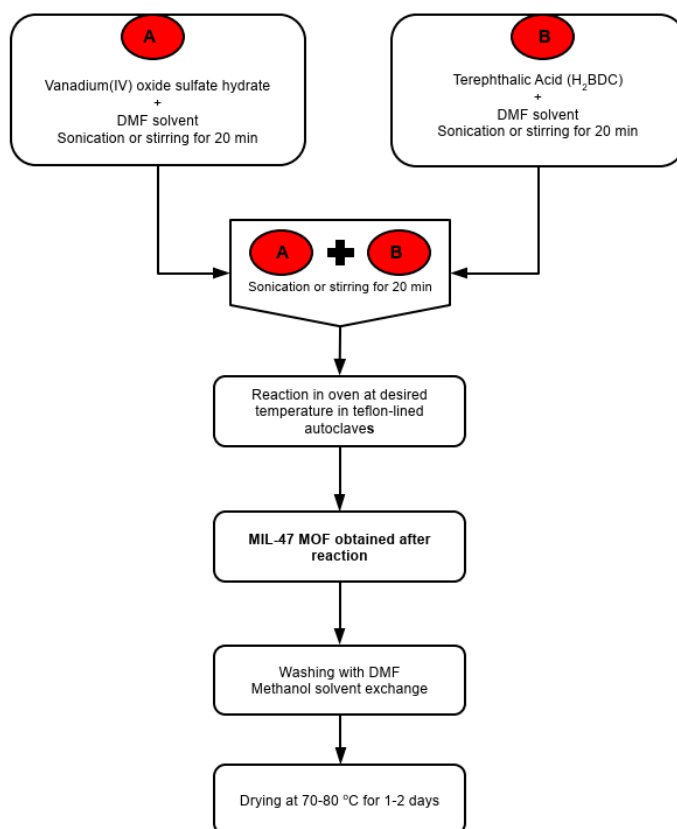


Figure 3.6 Step-by-step solvothermal synthesis of MIL-47 MOF

The general procedure of Yan et al. [84] was followed in this work with some modifications in the synthesis conditions, like temperature and precursor concentrations, for various batches of MIL-47. Sample codes and notations of various MIL-47 samples synthesized in this study are shown in Table 3-3. For the sample code ‘M47-160-5-C1’; ‘M47’ is used for MIL-47, ‘160’ for the synthesis temperature in °C, ‘5’ for the reaction time in days, and ‘C1’ denotes the precursor concentrations mentioned in Table 3-3.

Table 3-3 Sample codes and experimental conditions for the solvothermal synthesis of MIL-47

Sample code	Reaction conditions			
	Temperature (°C)	Concentration (mM) (solvent DMF)		Time (days)
		VOSO ₄ .nH ₂ O	H ₂ bdc	
M47-160-1-C1	160	148	108	1
M47-160-3-C1	160	148	108	3
M47-160-5-C1	160	148	108	5
M47-220-1-C1	220	148	108	1
M47-220-3-C1	220	148	108	3
M47-220-5-C1	220	148	108	5
M47-160-5-C2	160	74	54	5
M47-160-5-C3	160	296	216	5

3.1.1.3 Solvothermal synthesis of MIL-125

In this study, titanium metal-based MOF, MIL-125, was synthesized using the solvothermal method. The precursors required for MIL-125 are titanium isopropoxide (C₁₂H₂₈O₄Ti) and terephthalic acid (H₂bdc). First, titanium isopropoxide was dissolved in the solvent mixture of DMF and methanol (v/v ratio of 9:1, respectively) by magnetic stirring in a conical flask for 15-20 minutes. The solution gets muddy (white color) after a few minutes of stirring in the flask. Then the required amount of organic linker (H₂bdc) is added to the solution and again stirred for 15-20 minutes. Precursors were completely dissolved in the solvent and the final solution was a clear solution with slight yellowish color or colorless (like water). The final solution was then transferred to Teflon lining stainless steel autoclaves and was left to react for 48-72 hours at 100°C-160°C in the air-forced

laboratory oven. The final product was recovered from the reaction solution by centrifugation and washed with DMF 2 to 3 times to remove unreacted materials. After washing, the as-synthesized MIL-125 MOF was soaked in methanol (or ethanol) for 24 hours. The next day MIL-125 MOF was washed again 2 to 3 times with methanol in the centrifuge and dried at 80°C for 24 hours. The final MIL-125 product was white. The flowchart of the solvothermal synthesis of MIL-125 is shown in Figure 3.7.

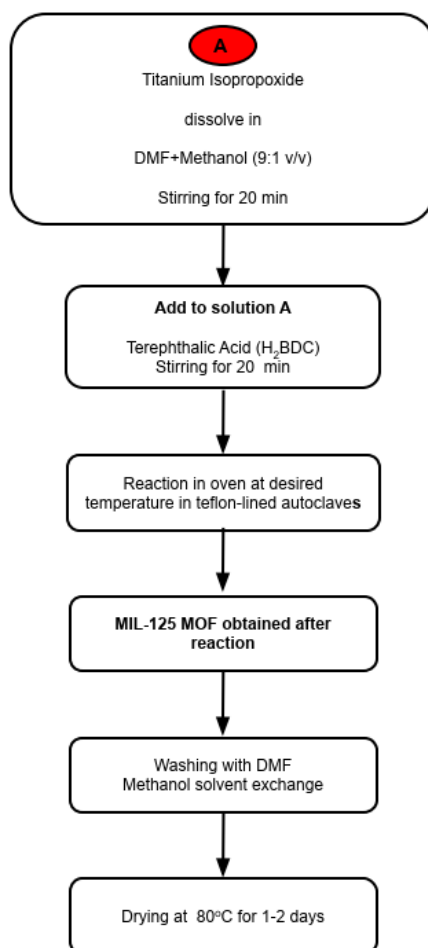


Figure 3.7 Step-by-step solvothermal synthesis of MIL-125 MOF

For MIL-125 synthesis a lot of recipes from different studies [24], [25], [87], [89] were followed in this study but none of them was successfully replicated to obtain crystalline MIL-125 product. The reasons could be those which are already mentioned in the literature review (chapter 2) for the difficulty of MIL-125 synthesis. One synthesis procedure by Huang et al. [87] was successful in repeated experiments and then this recipe was followed for MIL-125 synthesis for later experiments, albeit, with some modifications. Sample codes of various MIL-125 samples synthesized in this study are shown in Table 3-4. For example, the sample code ‘M125-150-3’ refers to MIL-125 MOF synthesized at 150°C in 3 days.

Table 3-4 Sample codes and experimental conditions for the solvothermal synthesis of MIL-125

Sample code	Reaction conditions			
	Temperature (°C)	Concentration (mM)		Time (days)
		Ti-isopropoxide	H ₂ bdc	
M125-150-1	150	87.72	293	1
M125-150-2	150	87.72	293	2
M125-150-3	150	87.72	293	3
M125-100-3	100	87.72	293	3
M125-130-3	130	87.72	293	3
M125-160-3	160	87.72	293	3
M125-150-5	150	87.72	293	5

3.1.2 Activation of MOFs

The as-synthesized MOFs usually have unreacted precursors or solvent molecules trapped inside their porous structure. For MOFs to be used in any application, they

must be activated to remove the trapped or occluded molecules from the framework. This removal of occluded species is called activation. The MOFs synthesized in this study were activated by heating them at 150°C for 3 hours under a vacuum (96-98%). The NUVE EV-018 vacuum oven was used for the activation of all the MOFs samples.

3.2 Characterization of MOFs

The three MOFs synthesized in this study were characterized using a variety of state-of-the-art techniques such as X-ray Diffraction (XRD), Scanning Electron Microscopy (SEM), and surface and pore characterization by nitrogen adsorption-desorption isotherms. All the characterization analyses were carried out in METU Central Laboratory.

3.2.1 X-Ray Diffraction

X-ray diffraction analyses were carried out using Rigaku-Ultima IV XRD equipment. For crystalline phase identification of MOFs, the samples were scanned between 2° and 50° with a scanning rate of 1°/min.

3.2.2 Field Emission Scanning Electron Microscopy

FE-SEM images of MOF crystals were obtained by using Hitachi S-4700 FE-SEM (accelerating voltage 30kV, beam current 10 μA). The MOFs samples were prepared on the FE-SEM sample stage and covered with a carbon tap for keeping the sample stick to the sample stage.

3.2.3 Nitrogen adsorption-desorption analysis

Surface and pore characterization of all MOFs was carried out by an instrument of Quantachrome Corporation, Autosorb-6. Before analysis, all the samples were degassed at 150°C for 3 hours to evaporate the moisture and solvents from the pores of the framework. The isotherms were obtained at liquid nitrogen (~77 K) conditions. The isotherms obtained were between relative pressure (P/P^0) values of 1×10^{-5} to 0.9.

3.2.4 Water adsorption studies

The water adsorption studies were carried out in the Sanyo Fitotron climate chamber. Besides the climate chamber's temperature and humidity sensors, an extra temperature and humidity sensor was fitted inside the climate chamber for the accuracy of the data. The dual temperature and %Rh external sensor installed in the climate chamber was Testo176HI AG Germany with temperature and %Rh ranges of -20°C-+70°C and 0-100%, respectively. The MOF sample was kept inside the chamber at each relative humidity (%Rh) and temperature values for a minimum of 12 hours to reach an equilibrium value for water adsorption.

CHAPTER 4

RESULTS AND DISCUSSION

4.1 UiO-66 (Zr-MOF)

UiO-66 is a zirconium-based MOF synthesized in this study. The structure and properties of UiO-66 were discussed in section 1.1.1 of Chapter 1. For the general synthesis procedure, please refer to chapter 3. The effect of reaction temperature, concentrations of precursors, and modulators (acids and bases) on the UiO-66 MOF product was investigated in this study. The results of synthesis experiments and the corresponding analysis of these results will be discussed below for every synthesis parameter. The codes used for naming and identifying different UiO-66 MOF samples are given in Table 3-1 of Chapter 3.

4.1.1 Effect of reaction temperature on the synthesis of UiO-66

UiO-66 MOF was synthesized at different reaction temperatures following the recipe from Cavka et al., [13] but with some modifications in the synthesis procedure. UiO-66 was synthesized with the same initial concentrations of precursors ($ZrCl_4$ and H_2bdc) in DMF solvent at three different reaction temperatures, i.e. 80°C, 100°C, and 120°C identified by notations U66-80-C1, U66-100-C1, and U66-120-C1, respectively (see Table 3-1). Figure 4.1 shows the PXRD patterns of UiO-66 samples synthesized at 80°C, 100°C, and 120°C.

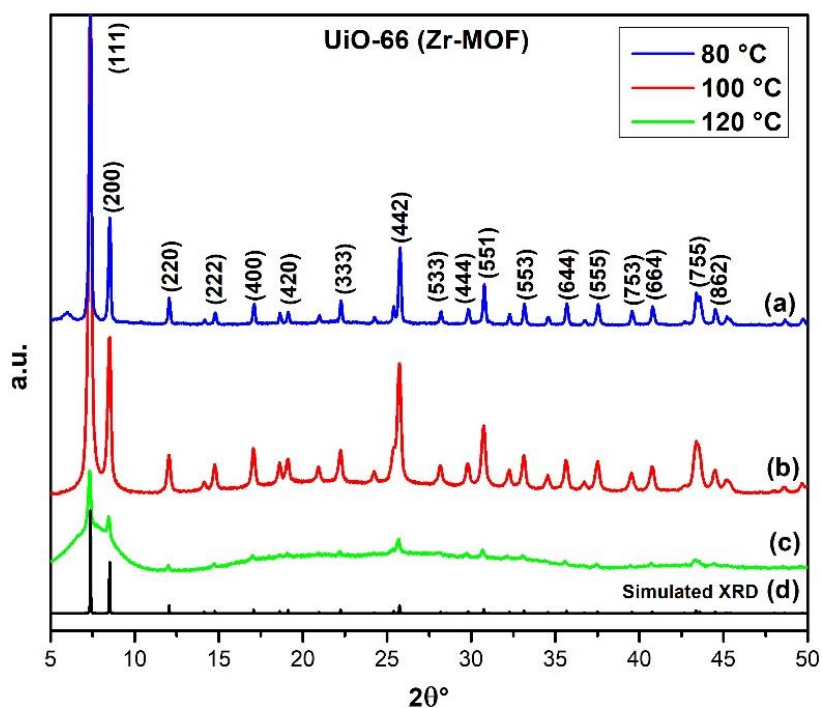


Figure 4.1 PXRD patterns of samples (a) U66-80-C1, (b) U66-100-C1, and (c) U66-120-C1 synthesized at 80°C, 100°C, 120°C, respectively, and (d) simulated XRD pattern of UiO-66 (COD ID 4512072)

The PXRD pattern in Figure 4.1a shows that highly crystalline UiO-66 MOF crystals with no impurities were obtained at 80°C (U66-80-C1). All the characteristic peaks were observed in UiO-66 MOF synthesized at 80°C. The main peaks were observed at 2θ angles of 7.4° , 8.5° , 12.0° , 14.8° , 17.0° , and 25.7° , which correspond to miller indices for planes (111), (200), (220), (222), (400), and (442), respectively as shown in Figure 4.1a. For reference, the simulated XRD pattern of UiO-66 (COD ID 4512072) is shown in Figure 4.1d. All the characteristic crystalline peaks can also be observed in the MOF sample synthesized at 100°C (U66-100-C1) as shown in Figure 4.1b. The crystalline peaks observed in U66-100-C1 were at the same 2θ angles as observed in sample U66-80-C1. The PXRD pattern of sample U66-120-C1 is shown in Figure 4.1c. The characteristic crystalline peaks for U66-120-C1 were

observed at 2θ angles of 7.4° , 8.5° , 12.0° , 25.7° , and 43.3° . PXRD patterns in Figure 4.1 suggest that UiO-66 was successfully synthesized at 80°C , 100°C , and 120°C at C1 concentrations (Table 3-1). The low intensities of the crystalline peaks for U66-120-C1 compared to the samples U66-80-C1 and U66-100-C1, and the amorphous hump-like peak between 2θ angles of 5° - 10° suggests the presence of amorphous phase in the sample. Goesten et al. had previously mentioned the formation of an amorphous metastable phase during the synthesis of the UiO-66 framework [67]. So, this could be the reason for the decrease in crystallinity of the U66-120-C1 sample. No impurity-related peaks were observed in any of the synthesized UiO-66 samples i.e. U66-80-C1, U66-100-C1, and U66-120-C. With significant crystallinity loss for synthesis conducted at 120°C .

FE-SEM images of UiO-66 samples U66-80-C1, U66-100-C1, and U66-120-C1, synthesized at 80°C , 100°C , and 120°C , respectively, are shown in Figure 4.2.

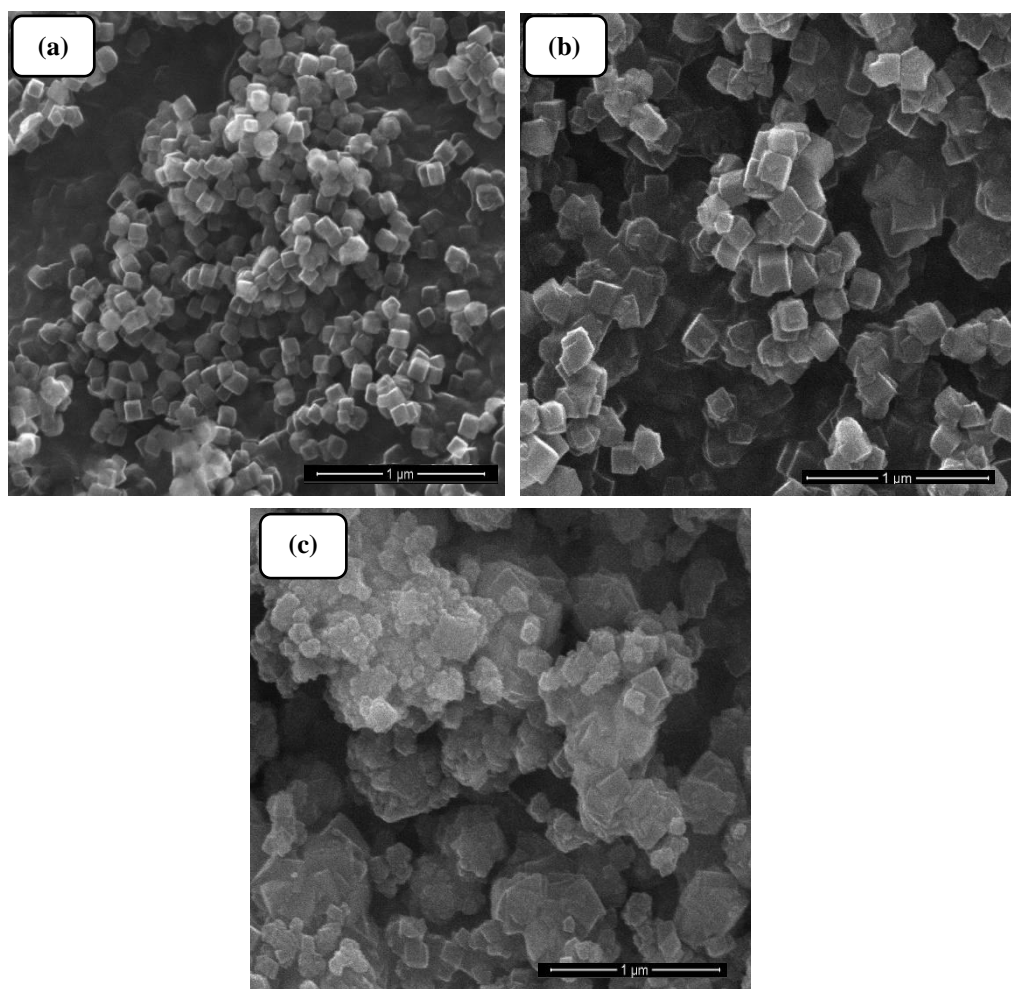


Figure 4.2 SEM images of samples (a) U66-80-C1, (b) U66-100-C1, and (c) U66-120-C1 synthesized at 80°C, 100°C, and 120°C, respectively

FE-SEM image in Figure 4.2a show that cubic crystals were obtained for UiO-66 MOF synthesized at 80°C (U66-80-C1). Intergrown, agglomerated as well as discrete cubic crystals were observed for UiO-66 obtained at 100°C (U66-100-C1) as can be seen in Figure 4.2b. On the other hand, for the U66-120-C1 sample, only agglomerated and intergrown crystals were observed, as shown in Figure 4.2c. The FE-SEM image of the U66-120-C1 sample (Figure 4.2c) also shows some lumpy solid with no specific morphology, which could be just the precipitated precursors

or other amorphous solids. It is worth noting that MOF crystals precipitated after five days of reaction with a clear supernatant solution for sample U66-80-C1. On the other hand, precipitation for U66-100-C1 and U66-120-C1 samples was observed after two days and one day, respectively. In other words, increasing the reaction temperature decreases the synthesis time for UiO-66 MOF. The higher temperature increases the solubility of reactants and also decreases the nucleation time, which results in a decrease in reaction time [110].

UiO-66 was also synthesized at different temperatures with higher precursor concentrations (C2) (see Table 3-1). In a previous research study, this recipe was used to synthesize a different MOF in the UiO MOF family, i.e. UiO-67 MOF, and in the presence of HCl or benzoic acid modulator with biphenyl-4,4-dicarboxylic acid (H₂bpdc) as organic linker [2]. In this work, the same recipe was examined for synthesizing UiO-66 without using acid modulators for the first time. H₂bpdc is the organic linker used for UiO-67, which differs from H₂bdc used for UiO-66 (see Figure 1.6). In this study, UiO-66 was successfully synthesized at different temperatures using this recipe.

Figure 4.3 shows the PXRD patterns of UiO-66 produced at 80°C, 100°C, and 120°C with C2 precursor concentrations. For reference, the simulated XRD pattern is also shown in Figure 4.3.

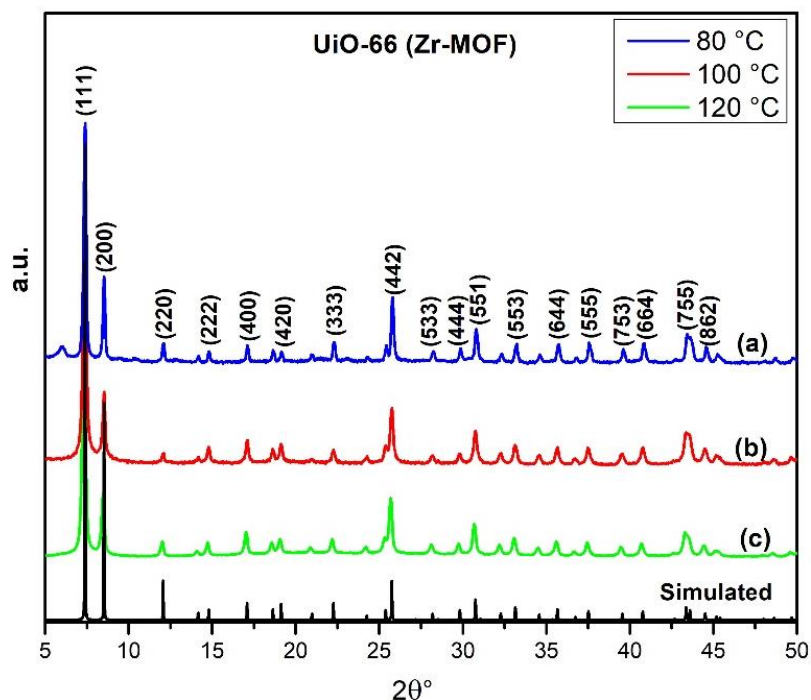


Figure 4.3 PXRD patterns of samples (a) U66-80-C2, (b) U66-100-C2, and (c) U66-120-C2 synthesized at 80°C, 100°C, and 120°C, respectively, and the simulated XRD pattern of UiO-66 (COD ID 4512072)

Figure 4.3 shows that crystalline UiO-66 MOF was obtained at all synthesis temperatures at C2 precursor concentrations (see Table 3-1). PXRD patterns for samples U66-80-C2, U66-100-C2, and U66-120-C2 are shown in Figure 4.3a, Figure 4.3b, and Figure 4.3c, respectively. Compared with the simulated XRD patterns (Figure 4.3d), it can be seen that all the characteristic diffraction peaks were observed for all three samples (U66-80-C2, U66-100-C2, and U66-120-C2). The main peaks were observed at 2θ angles of 7.4° , 8.5° , 12.0° , 14.8° , 17.1° and 25.8° , which correspond to miller indices for planes (111), (200), (220), (222), (400), and (442), respectively as shown in Figure 4.3. No impurity-related peaks were observed for any sample synthesized at high concentrations (C2).

FE-SEM images of U66-80-C2, U66-100-C2, and U66-120-C2 are shown in Figure 4.4a, Figure 4.4b, and Figure 4.4, respectively.

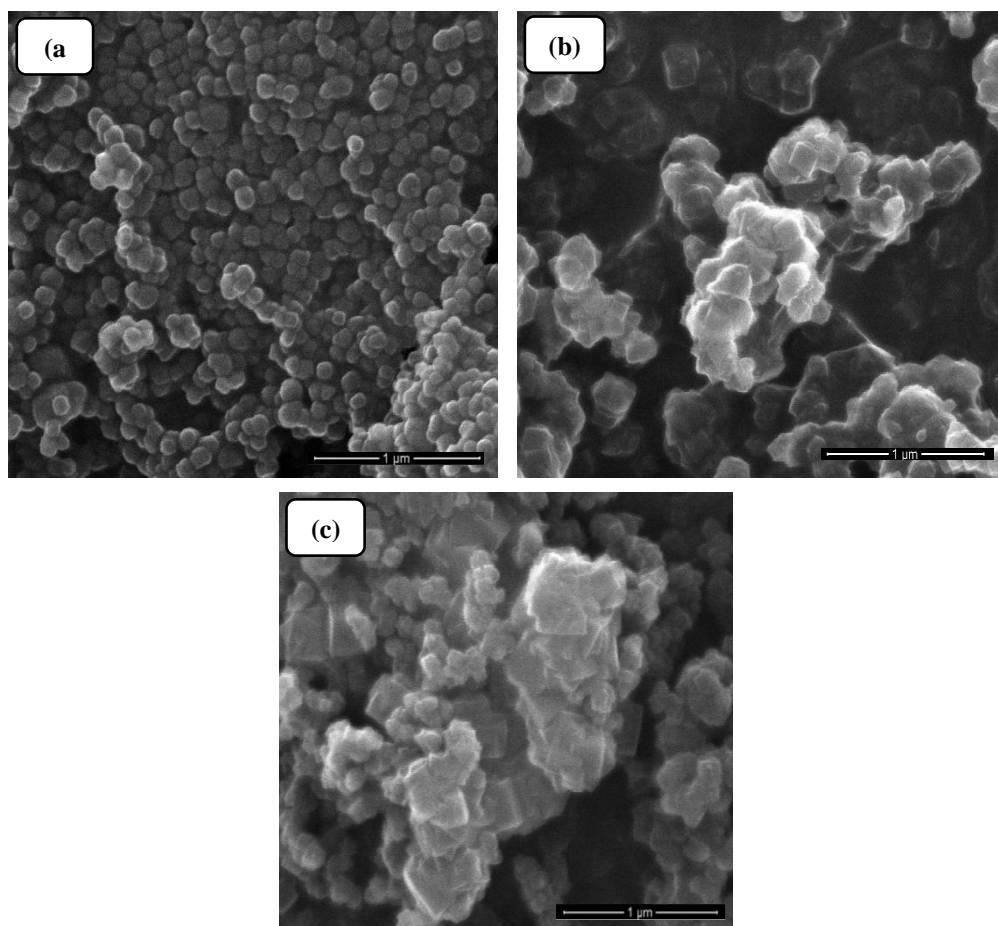


Figure 4.4 SEM images of samples (a) U66-80-C2, (b) U66-100-C2, and (c) U66-120-C2 synthesized at 80°C 100°C 120°C, respectively

Rounded edge cube-like crystals were obtained at 80°C for high concentration (C2) synthesis (sample U66-80-C2), as can be seen in Figure 4.4a. Figure 4.4b shows that sharp-edged and agglomerated cubic crystals were obtained for U66-100-C2. Intergrown sharp-edged and agglomerated cubic crystals were observed for sample U66-120-C2 as shown in Figure 4.4c

In general, for both C1 and C2 precursor concentrations, crystalline UiO-66 with definite crystal morphologies were successfully synthesized at all three reaction temperatures i.e. 80°C, 100°C, and 120°C. The agglomeration of the crystals was seen in the samples synthesized at 100°C and 120°C. It seems that agglomeration of the UiO-66 crystals increases with the increase in synthesis temperatures, as shown in Figure 4.2 and Figure 4.4. The possible reasons for the agglomeration of UiO-66 crystals with the increase in synthesis temperature will be discussed in the coming paragraphs.

In this study, the reaction or crystallization time decreased when the synthesis temperature for UiO-66 MOF was increased. When the synthesis was carried out at 80°C, it took 5-10 days to obtain the UiO-66 MOF product. However, it took only 2 days to synthesize UiO-66 at 100°C and 24 hours at 120°C. The increase in temperature increases the solubility of the reactants and decreases the nucleation time, thus decreasing the reaction time for MOF synthesis [110]. The increase in reaction temperature helps to overcome the kinetic and thermodynamic limitations leading to a lower nucleation time and consequently, lower crystallization or reaction time [62], [111]. Increase in temperature also increases the diffusion of precursors to the crystal surface in the solution, consequently, favoring the growth of the crystals (Ostwald ripening- a thermodynamically driven process [112]). These could possibly be the reasons for the increase in the mean crystal size with the increase in synthesis temperature, which was previously observed in some studies for MOFs synthesis [110], [113].

The agglomeration of crystals was observed with the increase in synthesis temperatures. At high temperatures, the nuclei formation speeds up, leading to rapid local density fluctuation in the reacting solution. This density fluctuation could force some of the formed nuclei or small crystals to collide and aggregate, resulting in crystal agglomeration. The increase in Brownian motion with an increase in temperature may also contribute to the collisions of nuclei and small crystals and, consequently, the agglomeration of crystals [114]. On the other hand, at low

temperatures, the slow nucleation and thus the reduced density fluctuation or Brownian motion could help reduce the collisions of nuclei or small crystals, which resulted in discrete crystals.

In this work, UiO-66 was successfully synthesized at various temperatures (i.e. 80°C, 100°C, and 120°C) for both C1 and C2 precursor concentrations, and similar products were obtained with some exceptions. Firstly, the high temperature synthesis was more successful at higher precursor concentrations of C2, suggesting that C1 could be falling behind the critical limit of supersaturation. This might have resulted in the dissolution of formed nuclei back into the solution at a higher level at higher reaction temperatures. Secondly, the agglomeration of UiO-66 crystals was relatively more for C2 than C1 precursor concentrations, as can be seen in Figure 4.2 and Figure 4.4. The difference in agglomeration was more visible in samples U66-100-C1 and U66-100-C2, as shown in Figure 4.2b and Figure 4.4b. The possible reason for the higher agglomeration at C2 could be the high rate of nucleation per unit area (or volume) in the solution due to high concentrations. The higher nucleation rate per unit area means the formation of more nuclei and the proximity of small crystals. These closely formed nuclei could collide or aggregate due to the slightest fluctuation in the local density (or concentration), which could increase the agglomeration of the crystals. Moreover, the mean crystal size for higher concentrations (C2) at the same temperature decreased compared to lower concentrations (C1). It is because at higher concentrations the nucleation is favored compared to the growth of the crystals. The aforementioned discussion about the agglomerations due to temperature and concentrations is hypothesized based on the discussion of the nucleation theories and observation of similar results in the literature [110], [113], [114]. From the above discussion, it is clear that the temperature and concentration of the precursors are both driving forces for the nucleation and growth of the MOF crystals.

PXRD patterns of some of the UiO-66 samples synthesized at 80°C showed an extra small peak at a 2θ angle of around 5.9° as can be seen in Figure 4.5.

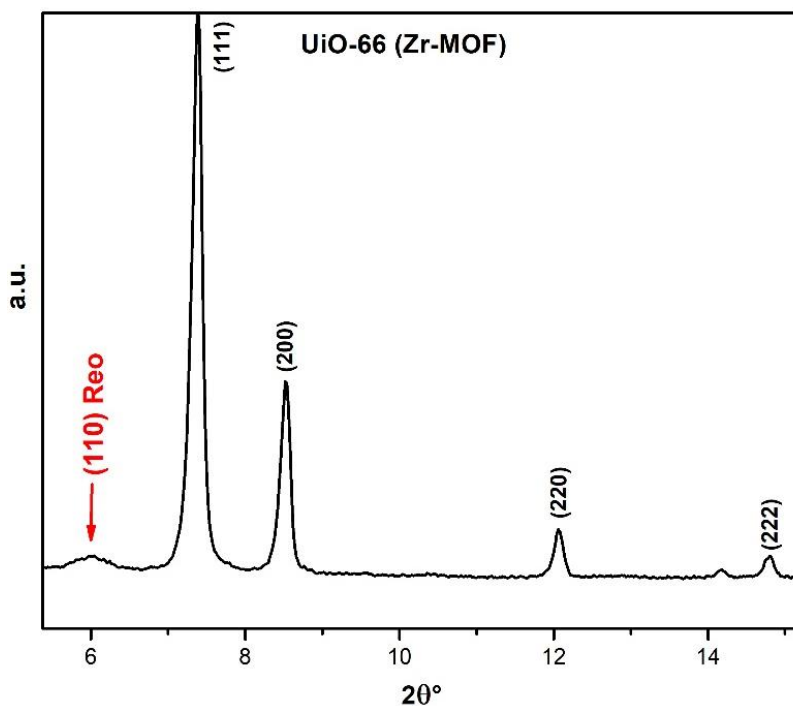


Figure 4.5 PXRD of UiO-66 MOF synthesized at 80°C (U66-80-C1) with reo-phase peak marked in red

The small peak in Figure 4.5 at around 5.9° has been previously reported in various studies [54], [115]. This peak is observed due to the so-called missing cluster defects. A missing cluster defect is created when the metal cluster and the associated organic linkers are missing in the framework, resulting in reo-topology or reo-phase. Shearer et al. also called these peaks the “symmetry forbidden reflections” [54]. The reo-phase is observed when there is water in the reaction mixture or the synthesis is carried out at a low temperature. The reo-phase can be eliminated by high-temperature synthesis of MOF, usually above 100°C [54], [115]. In this study, the peak related to the reo-phase was only observed in samples synthesized at 80°C (see Figure 4.1a and Figure 4.3a) and was not observed in the samples synthesized at 100°C or above or in the presence of AA-TEA modulators (see Figure 4.1b, Figure 4.3b and Figure 4.6). The reason for the absence of this peak at high-temperature synthesis (above 100°C) could be the evaporation of water from the reacting solution.

Evaporation of water from reacting solution can lead to its exclusion from taking part in the reaction. This is in correlation with the literature stating that water could be the reason for cluster defects [115]. Note that in our case, there was no water added as a reagent, but because of the hygroscopic nature of zirconium salt, a small amount of water may have entered the reaction system due to the ambient moisture absorption. Reo phase peak at 2θ angle of around 5.9° was assigned to (110) reflection as shown in Figure 4.5 [115].

4.1.2 Effect of modulators on the synthesis of UiO-66

The synthesis of MOFs in the presence of acid or base modulators has been extensively investigated by different research groups in recent years. Different acids and bases, e.g. HCl [2], HF [18], acetic acid (AA), and triethylamine (TEA) [53], have been used as modulators for UiO-66 MOF synthesis. The modulated synthesis approach is used to either speed up the synthesis reaction [15] or induce defects in the MOF framework [15], [80], or tailor the crystal morphology [53]. In this work, HCl and AA-TEA modulated synthesis of UiO-66 was studied for the first time for C1 and C2 concentrations, respectively.

4.1.2.1 Acid-base co-modulation of UiO-66

Acid or based modulated synthesis of MOFs has been shown to significantly affect the time of reaction and yield of MOFs [15], [53]. Zhao et al. [53] employed an acid-base co-modulation synthesis route to achieve UiO-66 MOF crystals with tunable size. In this study, the concept of acid-base co-modulation applied by Zhao et al. [53] was employed to engineer the crystal morphology and reaction time of UiO-66. AA and TEA were used as the acid and the base modulators, respectively. The schematic of the AA-TEA co-modulated synthesis of UiO-66 was shown in Figure 3.5. The reaction was carried out at 120°C with C2 precursor concentration. Sample with higher precursor concentrations was chosen due to relatively higher product yield

than lower precursor concentrations (C1) and owing to the need for a considerable amount of product for the characterization of samples (see Table 3-2 for experimental conditions and sample codes).

In this work, the effect of AA-TEA co-modulation on the morphology and size of the UiO-66 crystal was studied. For all the samples synthesized, AA concentration was kept constant at 2.4 M while TEA concentration was varied from 2 mM to 19 mM in the starting solution (see Table 3-2). PXRD patterns of UiO-66 MOF samples produced via an AA-TEA co-modulation route are shown in Figure 4.6.

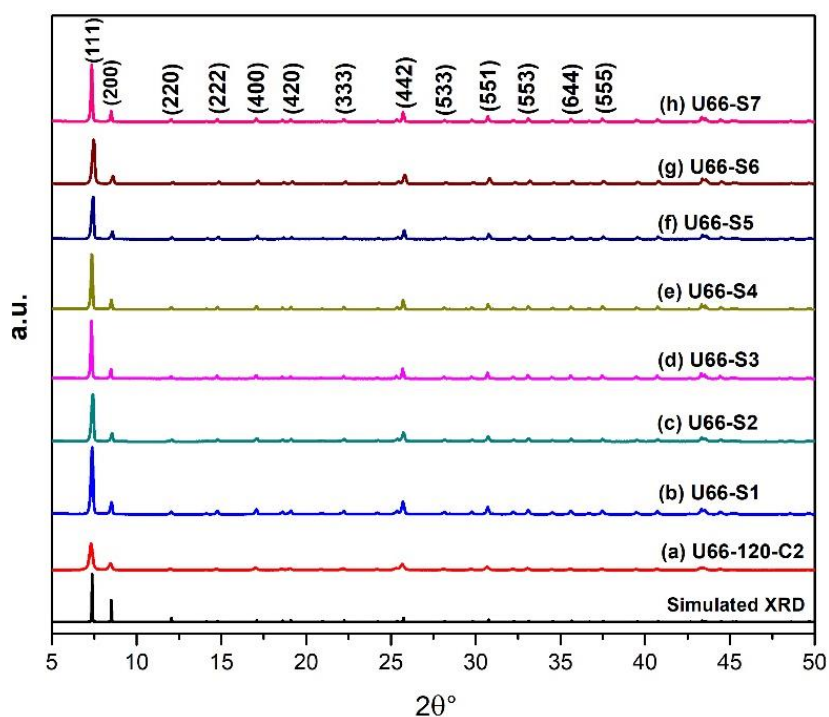


Figure 4.6 PXRD patterns of UiO-66 samples (a) U66-120-C2, (b) U66-S1, (c) U66-S2, (d) U66-S3, (e) U66-S4, (f) U66-S5, (g) U66-S6, and (h) U66-S7. Samples (b) to (g) were synthesized using AA-TEA co-modulation route at 120°C with TEA concentrations 2 mM, 4 mM, 8 mM, 12 mM, 16 mM and 19 mM, respectively. (h) The U66-S7 sample was synthesized with only AA as a modulator. A simulated XRD pattern of UiO-66 is also given (COD ID 4512072)

PXRD patterns in Figure 4.6 show that all the UiO-66 samples obtained via AA-TEA co-modulated synthesis were highly crystalline and all of them perfectly match the PXRD patterns reported in the literature [13], [15], [18] as well as with simulated XRD shown in Figure 4.6. No impurity peaks were observed in the PXRD pattern of any AA-TEA modulated UiO-66 MOF sample. The characteristic diffraction peaks for UiO-66 MOF were observed in all the samples synthesized with AA-TEA modulation (Figure 4.6b through Figure 4.6g). The peaks observed in all UiO-66 samples at around 2θ angles of 8.5° , 12.0° , 14.8° , 17.0° and 25.7° correspond to miller indices for planes (111), (200), (220), (222), (400), and (442), respectively (Figure 4.6). The PXRD pattern of the UiO-66 sample (U66-120-C2) synthesized without any modulator under the same experimental conditions is shown in Figure 4.3c and Figure 4.6a. It can be observed in Figure 4.6 that the crystallinity of AA-TEA modulated UiO-66 increased (judging from the relative intensities of main peaks) compared to the unmodulated sample (U66-120-C2), which is consistent with the observations in literature [116].

The FE-SEM images of the obtained crystals synthesized using six different concentrations of TEA and at an AA concentration of 2.4 M, are shown in Figure 4.7.

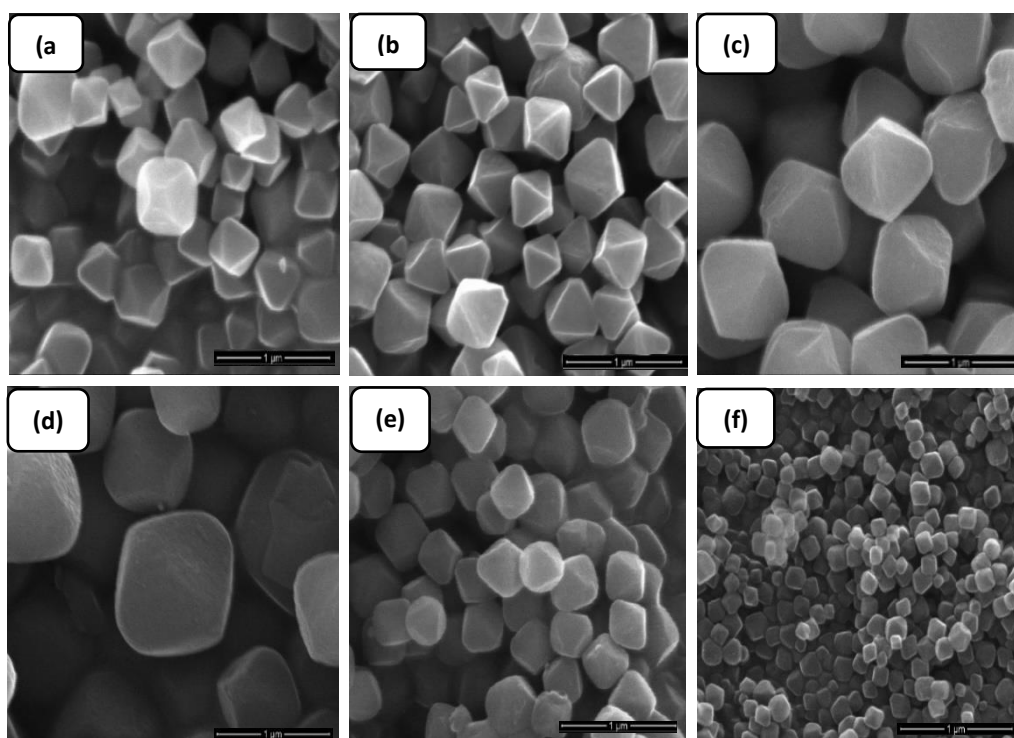


Figure 4.7 SEM images of samples (a) U66-S1, (b) U66-S2, (c) U66-S3, (d) U66-S4, (e) U66-S5 and (f) U66-S6 synthesized at 120°C using acid-base co-modulation route with TEA concentrations 2 mM, 4 mM, 8 mM, 12 mM, 16 mM and 19 mM, respectively

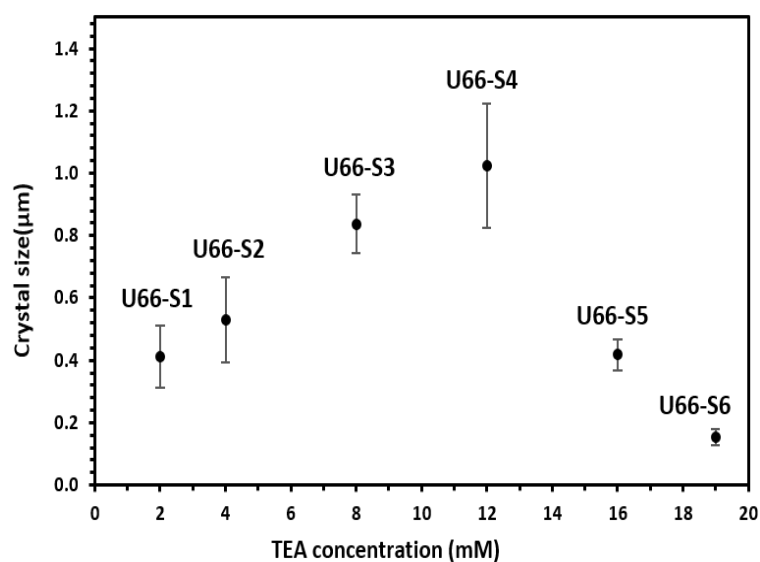


Figure 4.8 Evolution of UiO-66 mean crystal size with TEA concentration in the reacting solution

Table 4-1 Experimental parameters, the shape of crystals, and mean particle sizes for UiO-66 synthesized in the presence of acetic acid-TEA modulators at 120°C

Samples Name	Modulators		Time of reaction (hours)	Morphology of UiO-66 crystals	Mean crystal size (μm)
	AA (M)	TEA (mM)			
U66-S1	2.4	2	6	Octahedral	0.41
U66-S2	2.4	4	6	Octahedral	0.53
U66-S3	2.4	8	6	Octahedral	0.84
U66-S4	2.4	12	6	Octahedral	1.02
U66-S5	2.4	16	6	Octahedral	0.42
U66-S6	2.4	19	6	Octahedral	0.15
U66-S7	2.4	-	6	Octahedral	0.64
U66-120-C2	-	-	24	Cubic	0.12

The TEA concentrations in the reacting solution varied from 2 mM to 19 mM. It can be observed from FE-SEM images in Figure 4.7 that for all the UiO-66 samples synthesized at various TEA concentrations, discrete octahedral crystals were synthesized. The mean sizes of the UiO-66 crystals varied with a change in TEA concentrations as can be seen in FE-SEM images in Figure 4.7. The evolution of the UiO-66 mean crystal size with TEA concentration in the reacting solution is shown in Figure 4.8. The mean size of the obtained UiO-66 crystals, the concentrations of AA and TEA, and the experimental conditions for AA-TEA co-modulated synthesis are given in Table 4-1.

The mean crystal size of UiO-66 gradually increased from 0.41 μm at 2 mM TEA to 1.0 μm at 12 mM TEA. The mean crystal size of UiO-66 MOF increased with the increase in TEA concentrations from 2 mM to 12 mM in the starting solution. At 16 mM and 19 mM TEA in the starting solution, the mean crystal sizes observed were 0.42 μm and 0.15 μm , respectively. A decrease in mean crystal size was observed

when TEA concentration was further increased to 16 mM and 19 mM in the starting solution. The largest (1.02 μm) and smallest (0.15 μm) crystals of UiO-66 were obtained at 12 mM and 19 mM TEA concentrations, respectively. The mean size of the intergrown and agglomerated cubic crystals obtained for UiO-66 synthesized without the use of any modulator at the same conditions was 0.12 μm (see Figure 4.4c). Note that these mean crystal sizes were measured from FE-SEM images using ImageJ software [117]. From the above discussion, it can be concluded that the co-modulated UiO-66 synthesis in the presence of AA and TEA changed the crystal morphology to octahedral crystals from intergrown cubic crystals when synthesized without a modulator. However, the change in the concentration of TEA in the synthesis solution affected the mean size of the crystals (see Figure 4.7 and Figure 4.8).

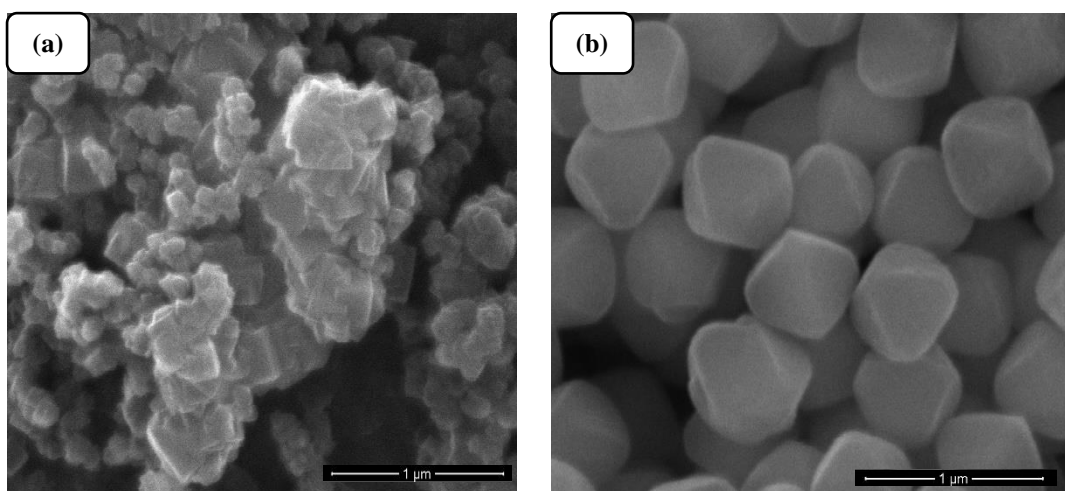


Figure 4.9 FE-SEM images of U66-120-C2 sample synthesize (a) without and (b) with only AA modulation

UiO-66 was also synthesized using only AA acid as a modulator (no TEA). The PXRD pattern of UiO-66 synthesized with only AA acid is shown in Figure 4.6h which shows that a perfectly crystalline UiO-66 sample, with all the characteristic crystalline peaks without any impurities, was obtained when compared with the simulated XRD pattern in Figure 4.6.

FE-SEM images of the U66-120-C2 sample synthesized without and with an AA modulator (U66-S7 sample in Table 4-1) are shown in Figure 4.9a and Figure 4.9b, respectively. Only AA modulated synthesis of UiO-66 also resulted in a change of morphology from intergrown agglomerated cube-like crystals to octahedral crystals with an increase in the mean particle size from 120 nm to 642 nm. From FE-SEM images in Figure 4.9, it is clear that AA is responsible for the octahedral shape of the UiO-66 crystal in modulated synthesis.

In the AA-TEA co-modulated synthesis of UiO-66, the role of AA is to engineer the shape of the UiO-66 crystals by selective adsorption onto specific crystallographic facets. It is previously stated in the literature that the adsorption was taking place specifically on the {111} planes of UiO-66 crystals, thus inhibiting the growth of crystals in that particular direction and allowing the crystal to grow in the [100] direction. Due to this role of AA, it can be stated that the octahedral UiO-66 crystals were obtained with {111} triangular facets [53], [118]. As a modulator, AA can also induce defects by competitive coordination with Zr^{+4} of the metal nodes, thus preventing organic linker (H_2bdc) from attaching to the metal nodes [53]. The competitive coordination of organic linkers with Zr^{+4} also helps in discouraging the formation of more nuclei during the nucleation stage and thus favors the growth of crystals, which could be one of the reasons for obtaining larger and discrete crystals with AA modulated synthesis [79].

The role of TEA is to decrease the nucleation time by producing more nucleation sites and promoting the growth of crystals. TEA promotes nucleation by deprotonation of linkers, thus making them more reactive to attach with metal nodes. This action can also result in countering defects in the framework [53]. Moreover, the product yield was more with AA-TEA modulated synthesis compared to only AA modulated synthesis. This could be because of the role of TEA in accelerating the nucleation process.

The increase of the mean crystal size with the increase in TEA concentration in the starting solution was seen to reach its highest point at 12 mM and then a decreasing

trend was observed with increased concentrations of TEA (see Figure 4.8). This trend is not consistent with the previous research works. It is not easy to come to a definitive conclusion on this behavior due to the peculiarities in MOF crystallization (which was discussed in detail in section 1.1.5). Based on the role of TEA in the synthesis of MOFs, it can be hypothesized that within a range of 2-12 mM of TEA concentration, TEA had a particular effect on both nucleation and crystal growth. On the other hand, in the range of 16-19 mM of higher concentrations of TEA, it could have a more significant role in increased nucleation compared to crystal growth. Accordingly, this could be the reason for smaller UiO-66 crystals and more monodisperse crystal size distribution at higher TEA concentrations.

From the aforementioned discussion, it is clear that the use of AA and TEA as modulators for Zr-UiO-66 synthesis was observed to have significantly affected the crystal morphology and reaction time of UiO-66 MOF. In AA-TEA modulated synthesis, it is clear that AA is responsible for the octahedral shape of the UiO-66 crystal while TEA significantly affects the mean size of the crystals as its concentration changes in the synthesis solution. Furthermore, discrete, well-defined octahedral crystals of UiO-66 were obtained with AA-TEA co-modulation and with only AA modulation. Additionally, the AA-TEA co-modulated and only AA modulated synthesis of UiO-66 reduced the crystallization time from 24 hours to just 6 hours.

4.1.2.2 HCl acid modulated synthesis of UiO-66

In this study, UiO-66 was also synthesized by employing HCl as an acid modulator. Discrete cubic crystals of UiO-66 were successfully obtained at synthesis conditions of 80°C and reactant concentration of C1 (U66-80-C1) without employing HCl as a modulator. Thus, the effect of the HCl modulator on UiO-66 was investigated using the synthesis conditions stated using U66-80-C1. It is important to note that the MOF synthesis was not successful at 80°C in the presence of AA-TEA modulators.

Accordingly, it was of special interest to try HCL as a modulator at 80°C in UiO-66 synthesis to decrease the synthesis temperature.

UiO-66 was successfully synthesized with different volumetric amounts of HCl (35 wt%) modulator added to the initial reacting solution. Figure 4.10 shows the PXRD patterns of UiO-66 samples synthesized with the HCl modulator, and for comparison, the PXRD pattern of UiO-66 synthesized without HCl modulators is shown in Figure 4.10c.

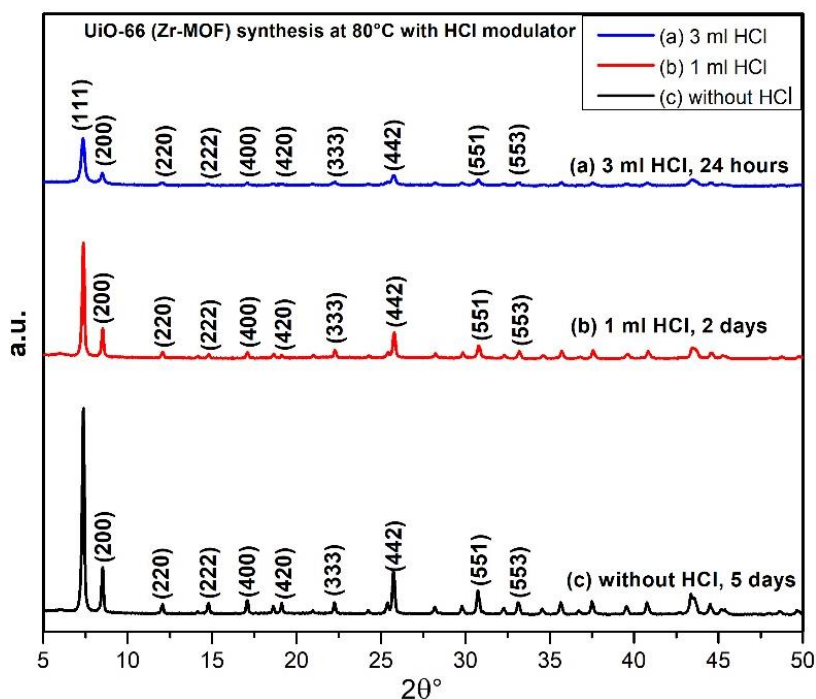


Figure 4.10 PXRD patterns of UiO-66 synthesized at 80°C (U66-80-C1) in the presence of HCl as a modulator. (a) 3 ml HCl (b) 1 ml HCl (c) without HCl

Crystalline UiO-66 MOF was obtained when HCl was used as a modulator in the synthesis solution. All the characteristic peaks for UiO-66 were observed in the PXRD patterns shown in Figure 4.10. By adding 1 ml HCl to the reagent solution, the reaction was completed in 2 days compared to 5 days without HCl as a modulator,

and when 3 ml HCl was added, the reaction time further decreased to 24 hours (Figure 4.10a and Figure 4.10b). The use of HCl as a modulator significantly decreased the reaction time for UiO-66 synthesis at C1 precursor concentrations (U66-80-C1).

The role of HCl in the reaction is twofold. Firstly, it increases the solubility of $ZrCl_4$ salt in the DMF solvent, and secondly, it speeds up the formation of metal clusters [15], [61]. One other role of HCl is also speculated that it neutralizes the basic impurities that may have formed due to the dissociation of DMF solvent [15]. Increasing the volumetric amount of HCl (or concentration) in the reacting solution further decreases the reaction time for UiO-66 synthesis. By adding 1 ml HCl to the reagent solution, the reaction was completed in 2 days compared to 5 days without HCl as a modulator. Moreover, increasing the HCl amount to 3 ml further decreased the reaction time to 24 hours (Figure 4.10a and Figure 4.10b).

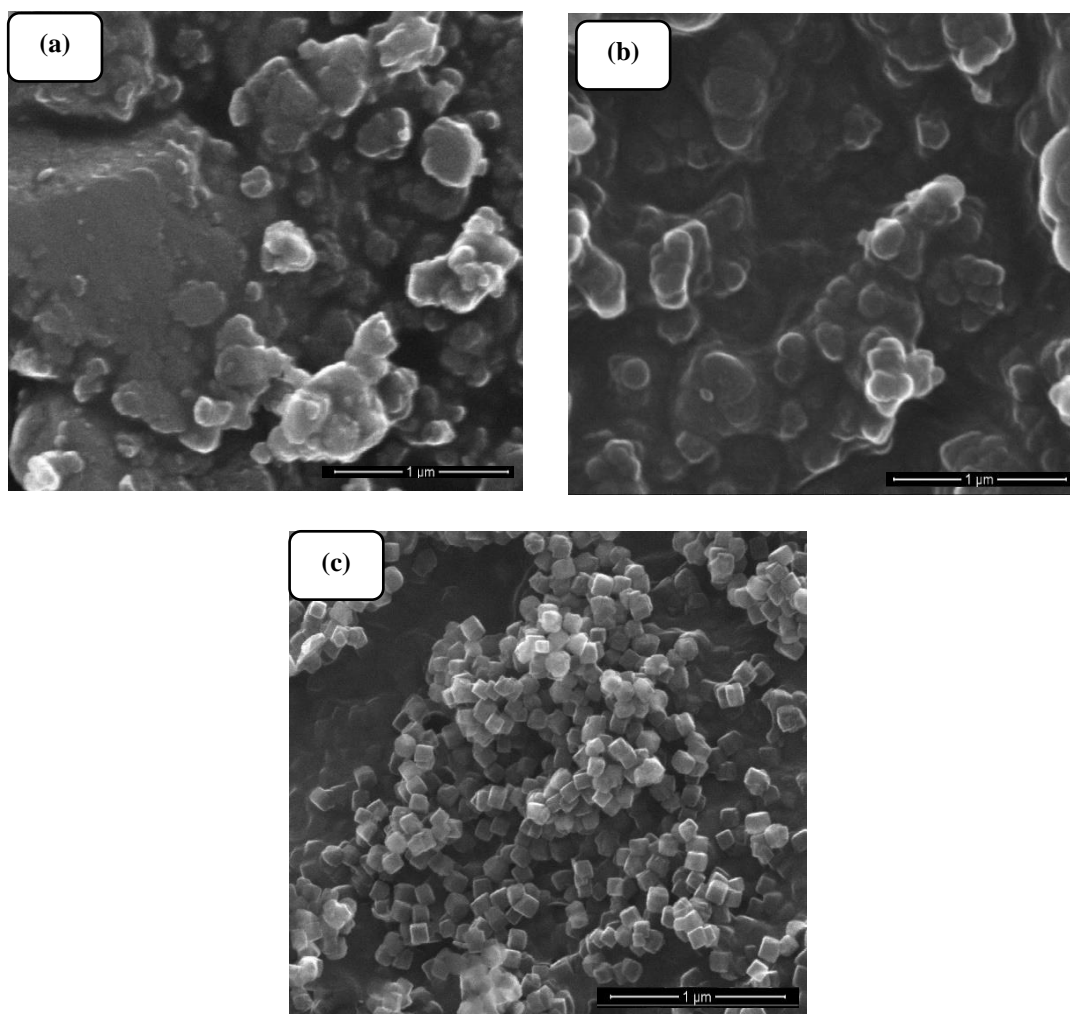


Figure 4.11 SEM images of UiO-66 synthesized at 80°C (U66-80-C1) in the presence of HCl modulator (a) 3m HCl (b) 1 ml HCl (c) without HCl

FE-SEM images of the U66-80-C1 sample synthesized in the presence of 3ml HCl, and 1ml HCl in the reacting solution are shown in Figure 4.11a, and Figure 4.11b, respectively. For comparison, the FE-SEM image of UiO-66 crystals synthesized without HCl at 80°C is also shown in Figure 4.11c. Analysis of FE-SEM images showed that no specific crystal morphology was obtained for UiO-66 MOF synthesized in the presence of HCl as a modulator. The possible reason for no morphology could be the fast nucleation (and secondary nucleation) in the presence of HCl which disfavored the growth of crystals into a specific morphology [15], [79].

In summary, HCl had a specific role in decreasing the reaction time of UiO-66 crystals with no particular enhancement in the particle morphology and size. It was also seen that, as reported in the literature [116], HCl resulted in a significant decrease in crystallinity of UiO-66 samples as observed by a gradual decrease in the PXRD intensities but an increase in product yield. Nevertheless, HCl as a modulator can further be investigated for controlling defects, tuning the surface area, and decreasing reaction time along with additional effects on the MOF crystallization process. Though, it can be stated that in the presence of HCl UiO-66 can be synthesized even at 80°C with a high product yield. On the other hand, UiO-66 synthesis was not successful at 80°C in the presence of AA-TEA.

4.2 MIL-125 (Ti-MOF)

MIL-125 was synthesized by following the experimental method of Huang et al., [87], albeit with modifications in the experimental parameters to study the effect of reaction temperature, reaction time, and Ti source concentration. Table 3-4 shows the MIL-125 sample codes and summarizes the experimental conditions for the synthesis of MIL-125 samples.

Figure 4.12 shows PXRD patterns of MIL-125 samples synthesized in two different batches at 150°C in 2 days (sample M125-150-2).

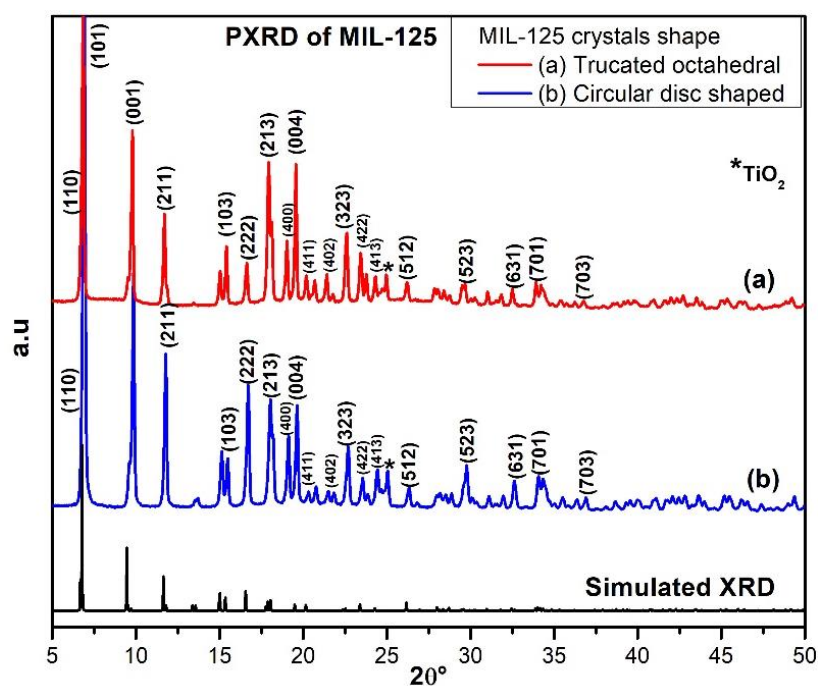


Figure 4.12 PXRD of MIL-125 MOF with (a) circular disc-shaped and (b) truncated octahedral crystals obtained at 150°C in 2 days (both samples are M125-150-2 synthesis in two different batches).

The PXRD patterns for both samples showed that indeed the product obtained was MIL-125 MOF. PXRD patterns showed that in both batches highly crystalline MIL-

MIL-125 MOF was obtained with all the characteristic peaks observed as shown in Figure 4.12. For reference, the simulated XRD pattern (COD ID 7211159) and PXRD pattern from the literature are shown in Figure 4.12c and Figure 4.13, respectively.

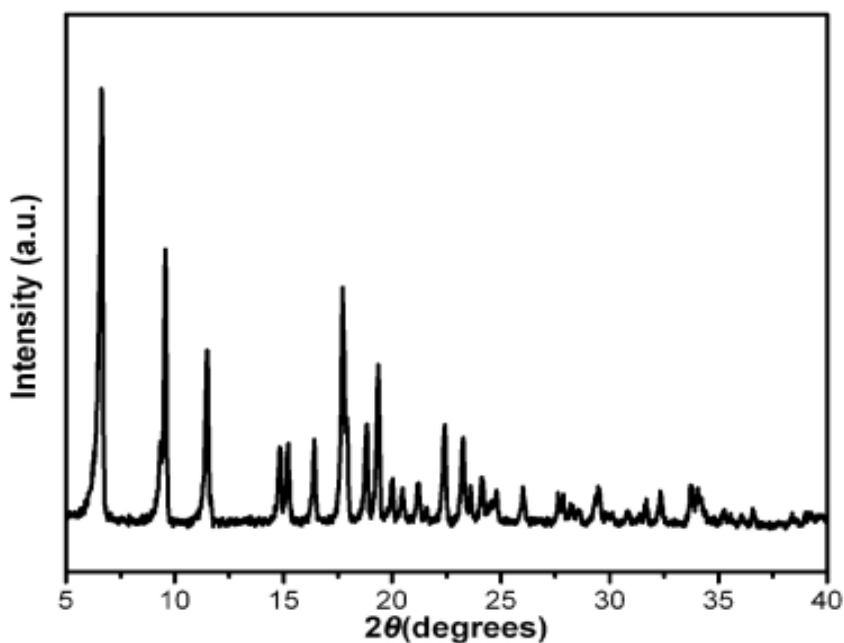


Figure 4.13 XRD pattern of MIL-125 (as-synthesized) from the literature [119]

Some of the main crystalline peaks were observed at 2θ angles of 6.68° , 6.90° , 9.84° , 11.78° , 16.70° , and 19.64° which corresponds to the plane reflections (110), (101), (001), (211), (222), and (004), respectively. A small peak in Figure 4.12a and Figure 4.12b was also observed at around a 2θ angle of 25° , which possibly belongs to TiO_2 impurities. The formation of TiO_2 impurities during solvothermal synthesis of MIL-125 was also reported in a previous study [24].

FE-SEM images of MIL-125 synthesized in two different batches at 150°C in 2 days (M125-150-2) are shown in Figure 4.14.

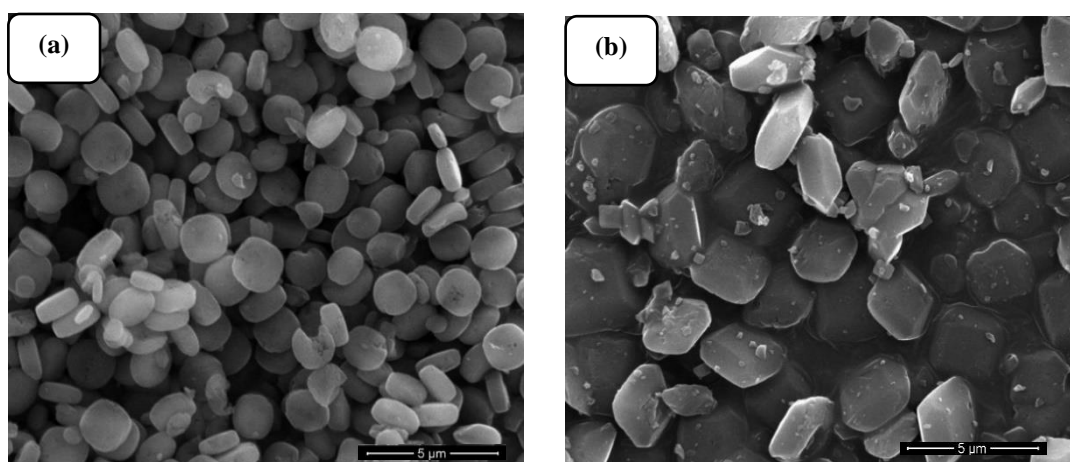


Figure 4.14 SEM image of (a) circular disc-shaped and (b) truncated octahedral MIL-125 MOF crystals obtained at 150°C in 48 hours (both samples are M125-150-2 synthesis in two different batches).

In MIL-125 synthesis, an interesting phenomenon was observed while synthesizing two different batches of MIL-125 MOF employing the Huang et al., [87] recipe. Despite following the same experimental parameters, MIL-125 obtained in two different batches were observed to have different shapes of crystals, i.e. circular disc-shaped and truncated octahedral, as can be seen in FE-SEM images in Figure 4.14. One possible reason for observing different crystal shapes could be the slight variations in precursor concentrations due to the reaction of titanium isopropoxide with air and moisture during the preparation of reacting solutions. The reaction of titanium isopropoxide with air and moisture is very difficult to control if the preparation of the reagent solution is carried out in ambient conditions, as was the case in this study. Generally, the synthesis solutions of Ti-based MOFs are prepared in a glove box under a dry inert environment (e.g. nitrogen or argon gas) to avoid the reaction of the Ti-source with moisture and air. In the literature, the change in the shape of the crystals due to the change in the concentration of the precursors has been previously observed for functionalized MIL-125 [38]. FE-SEM images show that discrete crystals were obtained for MIL-125 and no agglomeration was observed in any sample as can be seen in Figure 4.14.

It is clear from the above discussion that MIL-125 synthesized in different batches at the same experimental conditions could result in two different crystal morphologies. As mentioned earlier, the reason for observing this phenomenon could be the reactive nature of titanium sources which could perturb the synthesis solution concentrations and thus the final product. No studies in the literature have been observed to have addressed this problem in MIL-125 synthesis and further work is needed in this regard. Due to these difficulties in synthesis, special care is needed to handle the precursors while synthesizing MIL-125 or any other Ti-based MOF. That is why the preparation of Ti-MOFs synthesis solutions is usually carried out in a glove box under dry and inert conditions.

4.2.1 Effect of reaction temperature on the synthesis of MIL-125

MIL-125 synthesis was carried out at different reaction temperatures to study the effect of temperature on the synthesis of MIL-125. In the literature, most of the studies have synthesized MIL-125 at the reaction temperature of 150°C and the synthesis was usually unsuccessful at temperatures below 150°C [4], [24], [87], [89], [90].

In this study, MIL-125 MOF was synthesized at different reaction temperatures. MIL-125 was synthesized at 100°C, 130°C, 150°C and 160°C in 3 days (see Table 3-4). The PXRD patterns of MIL-125 synthesized at 100°C, 130°C, 150°C, and 160°C are shown in Figure 4.15a, Figure 4.15b, Figure 4.15c, and Figure 4.15d, respectively. For reference, the simulated XRD pattern (COD ID 7211159) of MIL-125 is also shown in Figure 4.15. Refer to Figure 4.13 for the MIL-125 PXRD pattern from the literature.

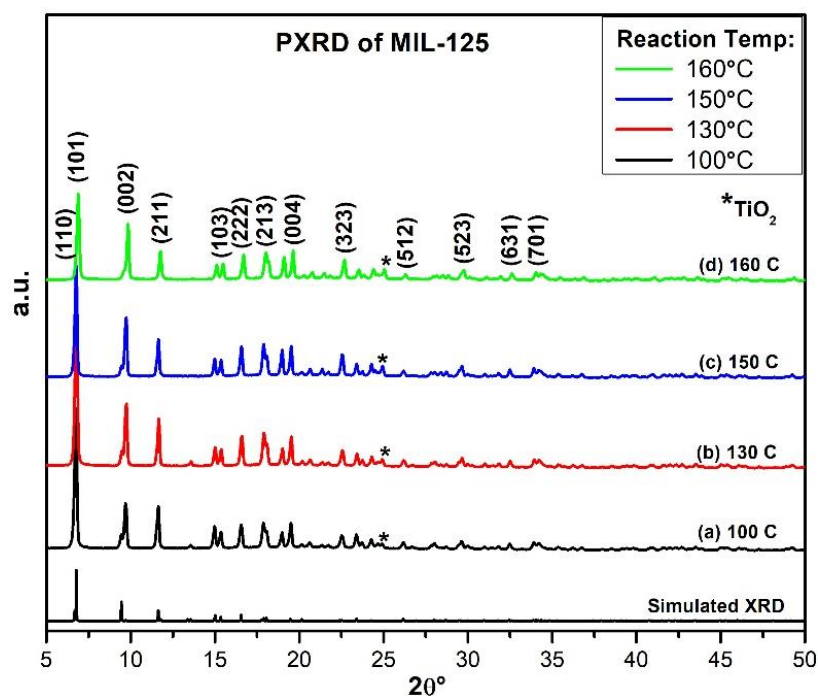


Figure 4.15 PXRD patterns of MIL-125 MOF obtained at (a) 100°C (M125-100-3), (b) 130°C (M125-130-3), (c) 150°C (M125-150-3), and (d) 160°C (M125-160-3).

The simulated PXRD pattern of MIL125 (COD ID 7211159)

The PXRD patterns shown in Figure 4.15 suggest that the MIL-125 powders obtained at all temperatures are perfectly crystalline. All the characteristic crystalline peaks were observed for MIL-125 synthesized at 100°C, 130°C, 150°C, and 160°C. The crystallinity of MIL-125 was not affected by the synthesis temperature judging from the relative intensities of the crystalline peaks in Figure 4.15. In this study, probably for the first time, MIL-125 was successfully synthesized via a solvothermal route at temperatures below 150°C (i.e. 100°C and 130°C) without using any acid or base modulators in synthesis. Studies regarding the synthesis of MIL-125 at mild conditions with a reaction temperature below 150°C are very rare. Those, who have successfully achieved the synthesis of MIL-125 at low temperatures, have employed different types of acid or base modulators [120].

The FE-SEM images of MIL-125 crystals synthesized at 100°C, 130°C, 150°C, and 160°C are shown in Figure 4.16a, Figure 4.16b, Figure 4.16c, and Figure 4.16d, respectively.

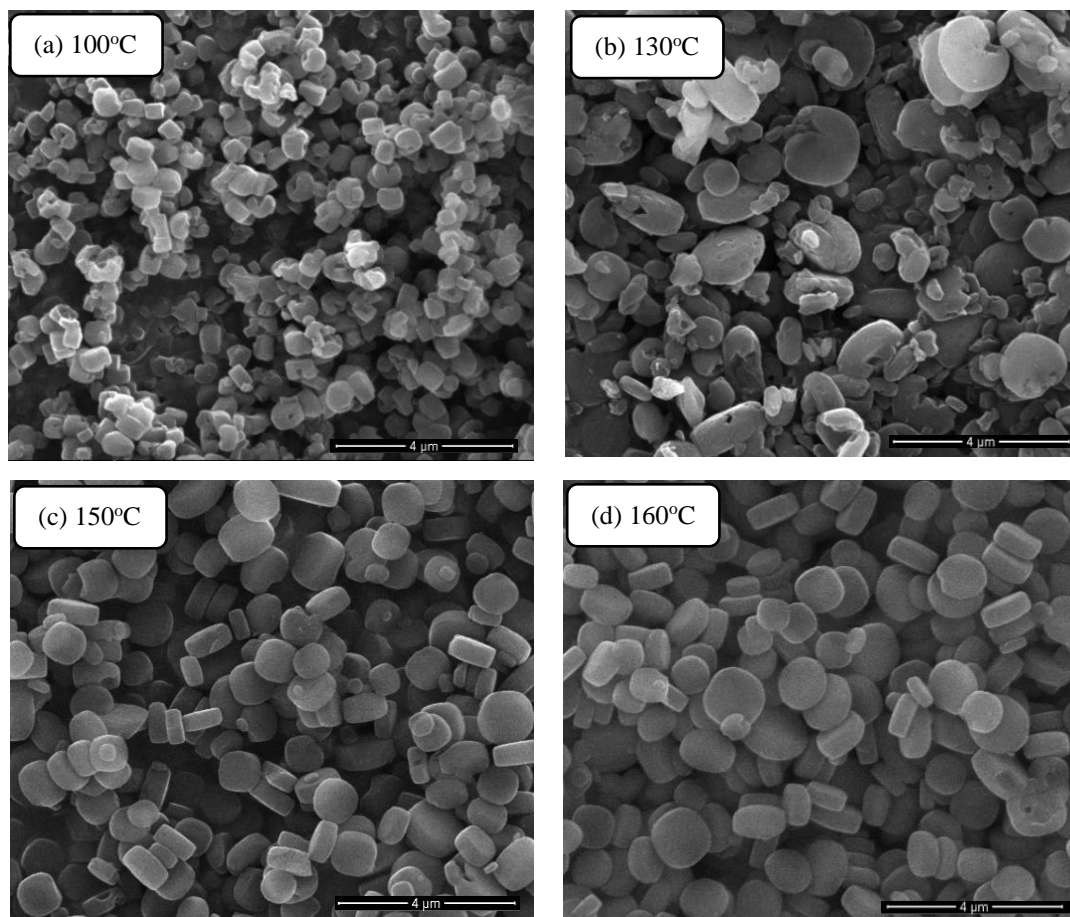


Figure 4.16 FE-SEM images of MIL-125 MOF obtained at (a) 100°C (M125-100-3), (b) 130°C (M125-130-3), (c) 150°C (M125-150-3), and (d) 160°C (M125-160-3).

The FE-SEM images in Figure 4.16 show that disc-shaped crystals were obtained for MIL-125 synthesized at all temperatures i.e. 100°C, 130°C, 150°C, and 160°C. It was observed that the mean size of the MIL-125 crystals progressively increased from 0.62 μm at 100° C, and 1.1 μm at 130°C to 2 μm at 160°C with the increase in MOF

synthesis temperature. The mean sizes of MIL-125 crystals obtained at 130°C (Figure 4.16b) were very diverse compared to other samples and varied between 0.7 μm to 1.9 μm . The mean crystal sizes were measured from SEM images by ImageJ software [117]. The fully formed disc-shaped crystals were obtained at 150°C and 160°C which is a typical crystal morphology observed for MIL-125 in the previous studies [90], [121]. The MIL-125 crystals obtained at 100°C and 130°C were fragmented disc-shaped crystals, which indicates that at low reaction temperatures (100°C and 130°C) the crystallization was not complete (Figure 4.16a and Figure 4.16b). Some agglomeration of MIL-125 crystals was observed at 100°C (Figure 4.16a) probably due to the favoring of nucleation compared to the growth of crystals at low temperatures during synthesis. Moreover, it is probably the first time that nanometer-scale MIL-125 crystals (Figure 4.16a) were obtained only by temperature modulation without the use of any acid or base modulators.

From the discussion of the temperature effect on MIL-125 synthesis, it was observed that the synthesis temperature affected the morphology of MIL-125 crystals. Though crystalline MIL-125 MOF was obtained at all temperatures, as the reaction temperature was increased, discrete disc-shaped MIL-125 crystals were observed, which is the signature morphology for MIL-125 MOF. It should be noted that due to the difficulties in the synthesis of MIL-125 as discussed earlier, the mean size of Ti-MOF crystals can vary from batch to batch even if they are carefully synthesized under the same experimental conditions. A slight variation in precursor concentrations due to impurities, like titanium oxide formation, is known to affect the synthesis of MIL-125 dramatically [38]. Nevertheless, the literature lacks studies regarding the effect of temperature on the synthesis of MIL-125 via the solvothermal route, and most of the studies referred to in the literature review (chapter 2) of this work are focused on the applications of MIL-125 MOF.

4.2.2 Effect of reaction time on the synthesis of MIL-125

The effect of reaction time on the shape of MIL-125 crystals was also investigated. For this purpose, all the experimental parameters were kept constant except the time of reaction for MIL-125 synthesis. MIL-125 MOF was synthesized at 150°C for 2 days and 3 days denoted by samples codes M125-150-2 and M125-150-3, respectively (see Table 3-4). PXRD patterns of MIL-125 obtained in 2 days and 3 days are shown in Figure 4.17a and Figure 4.17b. For reference, the simulated XRD pattern (COD ID 7211159) of MIL-125 is also shown in Figure 4.17.

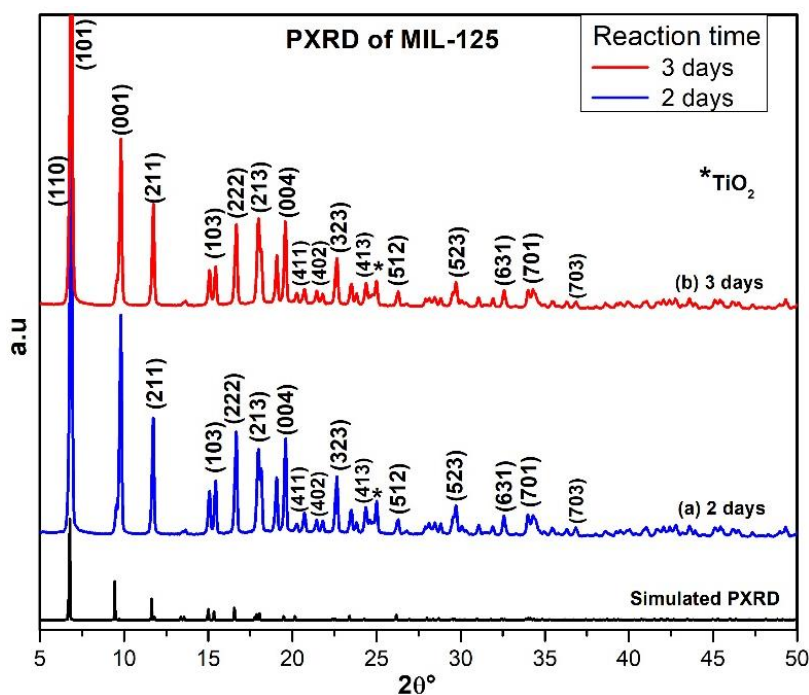


Figure 4.17 PXRD patterns of MIL-125 MOF synthesized at 150°C in (a) 2 days (M125-150-2), and (b) 3 days (M125-150-3). The simulated PXRD pattern of MIL125 (COD ID 7211159)

PXRD pattern suggests that MIL-125 was successfully synthesized in 2 days and 3 days at 150°C. PXRD patterns of the synthesized MIL-125 show all the characteristic crystalline peaks when compared with the simulated XRD in Figure 4.17. TiO₂ peak was observed in both samples synthesized in 2 days and 3 days at 150°C, which signals the formation of impurities during synthesis.

FE-SEM images of MIL-125 synthesized in 2 days (M125-150-2) and 3 days (M125-150-3) at 150°C are shown in Figure 4.18a and Figure 4.18b, respectively.

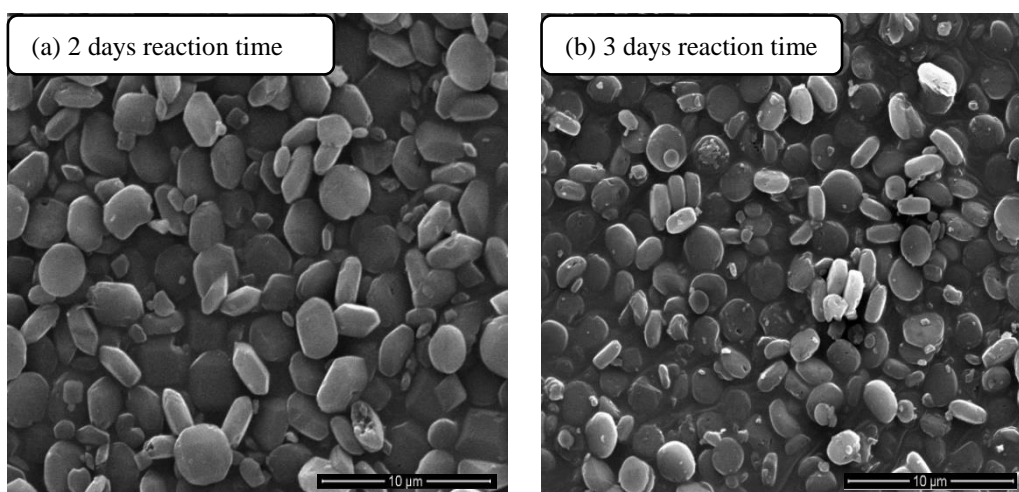


Figure 4.18 SEM images of MIL-125 MOF synthesized at 150°C in (a) 2 days (M125-150-2), and (b) 3 days (M125-150-3).

According to Figure 4.18a, it seems that the morphology of crystals was truncated octahedral crystals with some disc-shaped crystals for MIL-125 obtained in 2 days. However, upon increasing the reaction time to 72 hours, it was seen that all the crystals of MIL-125 obtained were disc-shaped (Figure 4.18b). Thus, it can be concluded that allowing more time for reaction led to the full development of MIL-125 crystals into disc-shaped morphology. The discussion on the effect of reaction (or synthesis) time suggests that the truncated octahedral MIL-125 crystals are probably the incomplete form of disc-shaped crystals. So, when sufficient time is

given to the reaction the truncated octahedral crystals develop into disc-shaped crystals.

4.2.3 Effect of concentration of titanium-source on the crystal shape of MIL-125

As mentioned earlier that the MIL-125 synthesis is very sensitive to even a slight perturbation in the experimental conditions and in section 2.2.3 it was explained in detail why slight changes in the experimental parameters can affect the final MIL-125 product. In a previous study, the effect of precursor concentrations on the morphology of functionalized MIL-125 crystals was studied [38]. In the current study, MIL-125 synthesis was tried for a variety of precursor concentrations but the synthesis was unsuccessful. The effect of a slight change in the concentration of titanium source was also investigated. M125-150-2 (Table 3-4) was synthesized by increasing the concentration of titanium isopropoxide (Ti source) from 87.72 mM to 98.62 mM in the starting solution while keeping the rest of the experimental parameters constant. PXRD pattern of MIL-125 synthesized with titanium isopropoxide concentrations 87.72 mM and 98.62 mM are shown in Figure 4.19a and Figure 4.19b. For reference, the simulated XRD pattern (COD ID 7211159) of MIL-125 is also shown in Figure 4.19.

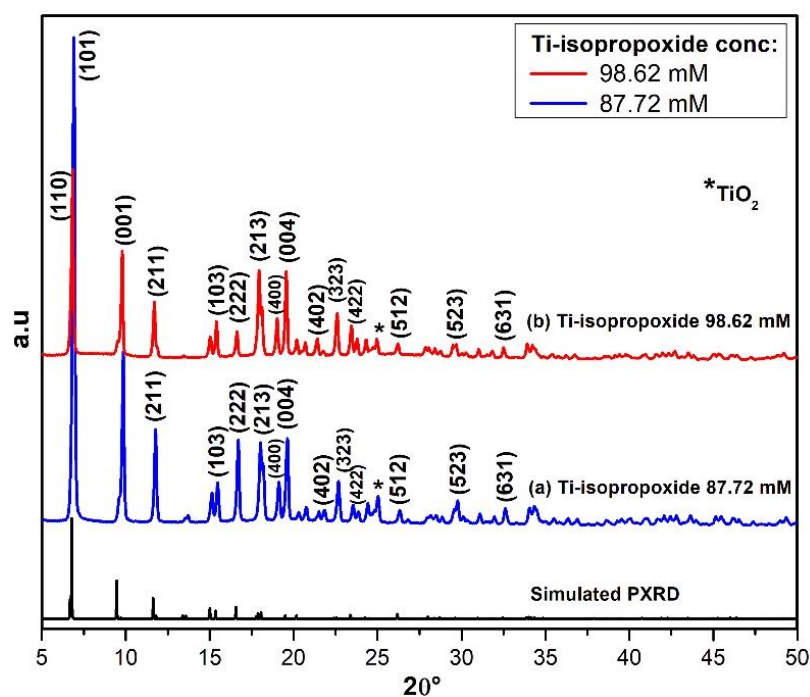


Figure 4.19 PXRD of MIL-125 MOF synthesized at 150°C in 2 days (M125-150-2) with (a) 87.72 and (b) 98.62 mM concentration of titanium isopropoxide in the reagent solution. The simulated PXRD pattern of MIL125 (COD ID 7211159)

PXRD patterns in Figure 4.19 show that MIL-125 was successfully synthesized at titanium isopropoxide concentrations of 87.72 mM and 98.62 mM and all the characteristic crystalline peaks were observed in both MIL-125 samples. The peak related to TiO_2 impurity was also observed in both samples as shown in Figure 4.19. The relative intensities of the crystalline peaks decreased as the concentration of titanium isopropoxide increased in the reacting solution.

FE-SEM images of MIL-125 synthesized with titanium isopropoxide concentrations 87.72 mM and 98.62 mM are shown in Figure 4.20a and Figure 4.20b.

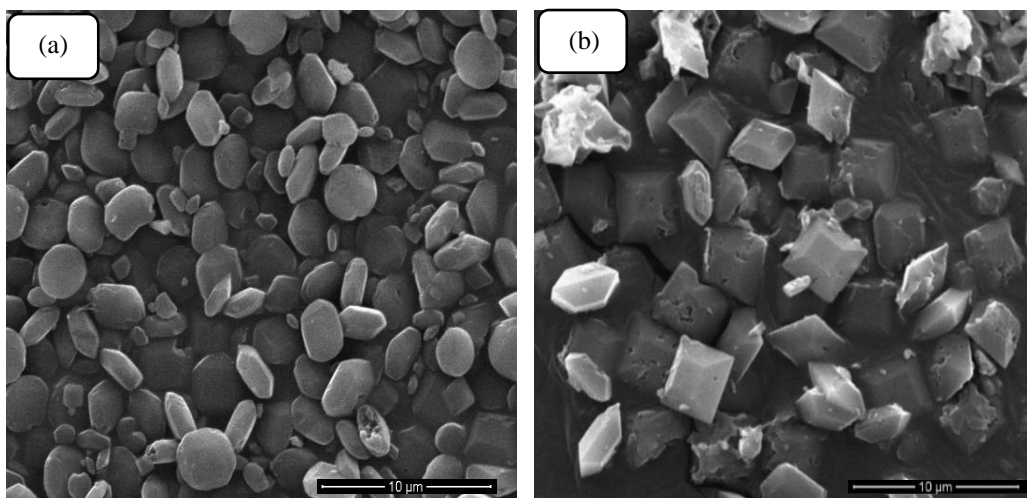


Figure 4.20 SEM image of MIL-125 MOF synthesized at 150°C in 2 days (M125-150-2) with (a) 87.72 mM and (b) 98.62 mM concentration of titanium isopropoxide in the reagent solution.

It can be seen in the FE-SEM image in Figure 4.19a that both disc-shaped and truncated octahedral crystals were obtained for MIL-125 with a titanium isopropoxide concentration of 87.72 mM. On the other hand, only sharp edged truncated octahedral crystals were obtained at 98.62 mM titanium isopropoxide concentration as shown in Figure 4.20b. The change in crystal morphology with change in the concentrations of precursors was previously observed for functionalized MIL-125 [38]. According to Hu et al., [121] the two dominant facets in MIL-125 disc-shaped crystal are {001} and in truncated octahedral crystals there are two {001} facets and eight {101} facets.

BFDH (Bravais, Friedel, Donnay, and Harker) law of crystal growth postulates that the shape of the crystal is determined by the rate of the relative growth of specific facets of the crystal [121]. Based on the BFDH law, it can be hypothesized that in the case of disc-shaped MIL-125 crystal the rate of the relative growth of {001} facets is slow so the dominant facets are {001}. In the case of a truncated octahedral crystal, the relative growth is slowest for {101} facets and that is why dominant

facets are {101} in a truncated octahedral crystal. Thus, low Ti-source concentration favors disc-shaped crystals (slow growth of {001} facets relative to {101} facets) while high concentration of Ti-source favors truncated octahedral crystals (slow growth of {101} facets relative to {001} facets).

BFDH law of crystal growth can also be extended to the effect of reaction time on MIL-125 crystal morphology discussed in section 4.2.2. At the same experimental conditions when reaction time is increased from 2 days to 3 days the shape of the crystal changes from truncated octahedral to disc-shaped. It means when given enough time to the slow-growing {101} facets of octahedral crystals, the shape of the crystals changed to disc-shaped crystals.

The above discussion suggests that the morphology of the MIL-125 can be changed either by changing the reaction time or the concentration of the reactants. As discussed in section 1.1.5, the crystallization of MOFs is not easily explained based on the traditional theories of nucleation and crystal growth. So, more theoretical studies are needed to understand the nucleation and crystal growth of MOFs.

In this study, the preparation of the synthesis solution for MIL-125 was carried out under ambient conditions. MIL-125 starting solution is prepared in a gloves box under an inert environment like nitrogen or argon. So, problems were encountered during the MIL-125 synthesis due to the reactivity of Ti sources, as explained earlier. The reproducibility of MIL-125 MOF in small batches was very low. When the volume of a single batch for the MIL-125 synthesis experiment was increased six-fold (i.e. the quantities of precursors and the DMF solvent increased), the reproducibility of MIL-125 increased, and considerable success was achieved. The possible reason could be that the impurities formed during the experiment were not affecting the larger volume synthesis as much. The formation of impurities like TiO_2 [13] may have affected the reactant concentration and reaction mechanism more significantly in the smaller batches. These points could also be further investigated by synthesizing Ti-MOFs in a tightly controlled environment of a glove box so that

the interference of moisture and air with the synthesis reaction can be avoided. This is still an open question for future studies.

4.3 MIL-47 (V-MOF)

In this work, the effect of temperature, reaction time, and precursor concentrations on the MIL-47 MOF was studied. The sample codes and experimental conditions are given in Table 3-3.

4.3.1 Effect of reaction temperature on synthesis of MIL-47

MIL-47(V) was synthesized at two different temperatures (i.e. 160°C and 220°C) while keeping all other experimental parameters constant. For sample codes and experimental conditions see Table 3-3. PXRD patterns of MIL-47 MOF synthesized at 160°C and 220°C are shown in Figure 4.21a and Figure 4.21b.

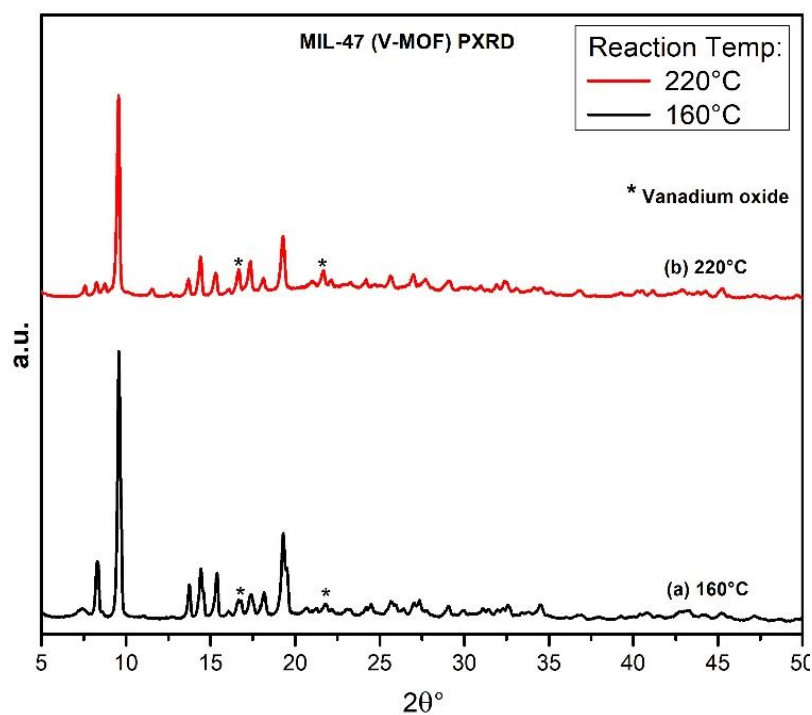


Figure 4.21 PXRD of MIL-47 MOF obtained at different temperatures (a) 160°C (M47-160-5) (b) 220°C (M47-220-5)

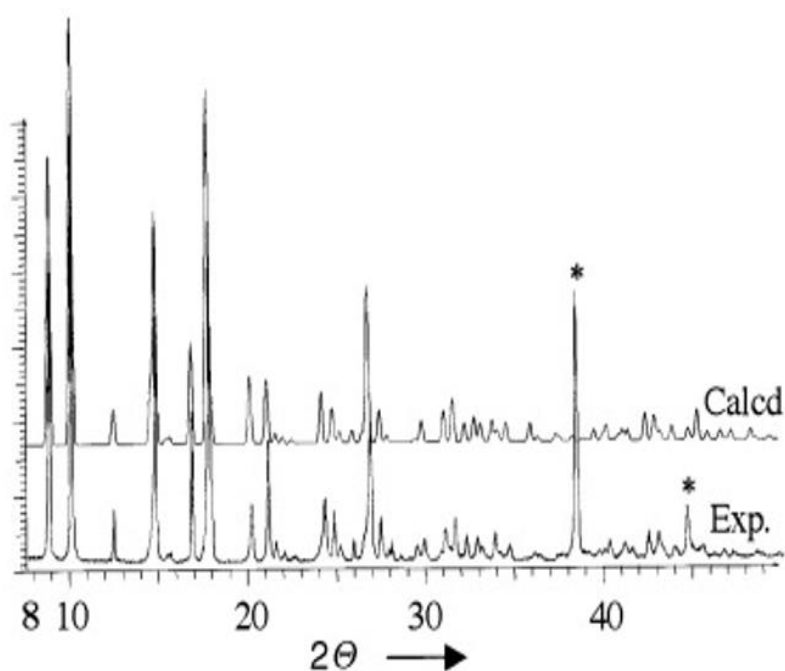


Figure 4.22 PXRD pattern of MIL-47as calculated (Calcd) and experimental (Exp) from Barthelet et al. (*peaks belong to aluminum sample holder) [19]

Accordingly, the observed peak patterns are characteristic of MIL-47(V), all the characteristic diffraction peaks for MIL-47 were observed in PXRD patterns in Figure 4.21. The pattern shows typical major diffraction peaks at around 2θ angles of 9.6° , 14.4° , 15.3° , 17.7° , and 19.3° as reported in the literature [19]. For reference, the XRD pattern of MIL-47 from the literature is shown in Figure 4.22 [19]. Figure 4.22 shows the PXRD pattern of MIL-47as calculated (Calcd) and experimental (Exp) from the work of Barthelet et al., [19]. X-ray diffraction results showed that MIL-47 MOF was successfully synthesized at both temperatures. The diffraction peaks of vanadium oxide were observed in PXRD of MIL-47 at both temperatures as can be seen in Figure 4.21, indicating the presence of residual oxide formation in a minor amount. Hence, the adopted synthesis solvothermal technique was found to be successful.

FE-SEM images of the MIL-47 crystals obtained at reaction temperatures of 160°C and 220°C are shown in Figure 4.23a and Figure 4.23b, respectively.

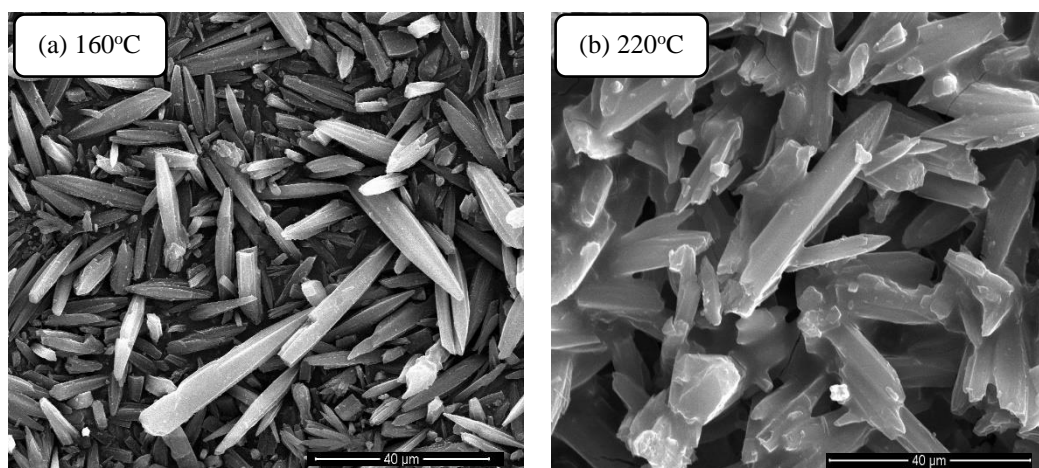


Figure 4.23 SEM images of MIL-47 MOF synthesized at (a) 160°C (M47-160-5)
(b) 220°C (M47-220-5)

According to Figure 4.23a, at 160°C discrete spindle-shaped (or needle-like) crystals were obtained in a variety of sizes. Some crystals obtained at 160°C were as big as 50 μm in length. On the other hand, the MIL-47 crystals synthesized at 220°C were fused and discrete needle-like (and rod-shaped) crystals, as shown in Figure 4.23b. Crystals up to 40 μm in length were observed at 220°C in FE-SEM images. Needle-like and rod-like crystals were also observed in some of the previous studies on MIL-47 like Yan et al., [84] and Zorainy et al. [122].

4.3.2 Effect of reaction time on MIL-47 at synthesis temperature of 160°C

The effect of reaction time on MIL-47 MOF was investigated at the synthesis temperature of 160°C and by keeping all other experimental parameters constant.

PXRD patterns of MIL-47 synthesized in 1 day, 3 days, and 5 days at 160°C are shown in Figure 4.24a, Figure 4.24b, and Figure 4.24c.

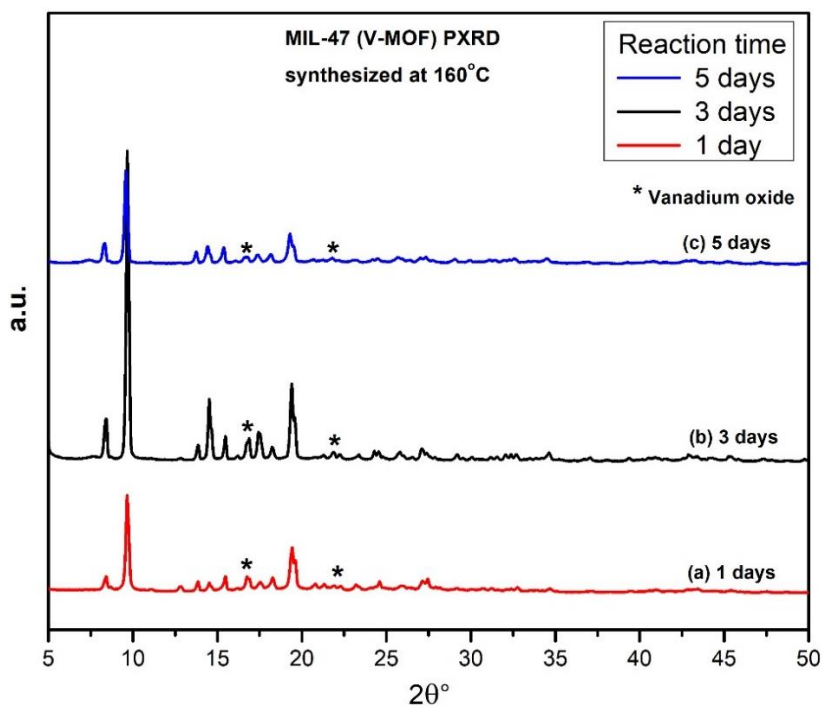


Figure 4.24 PXRD patterns of MIL-47 MOF obtained at 160°C in (a) 1 day (M47-160-1), (b) 3 days (M47-160-3), and (c) 5 days (M47-160-5)

In PXRD patterns in Figure 4.24, the main diffraction peaks were observed for all the three MIL-47 MOF samples synthesized in 1 day, 2 days, and 3 days at 160°C, when compared with the MIL-47 XRD in the literature [19] (Figure 4.22). PXRD results showed that MIL-47 was successful at 160°C for all the reaction durations tested in this study.

FE-SEM images of MIL-47 MOF samples synthesized in 1 day, 2 days, and 3 days at 160°C are shown in Figure 4.25a, Figure 4.25b, and Figure 4.25c.

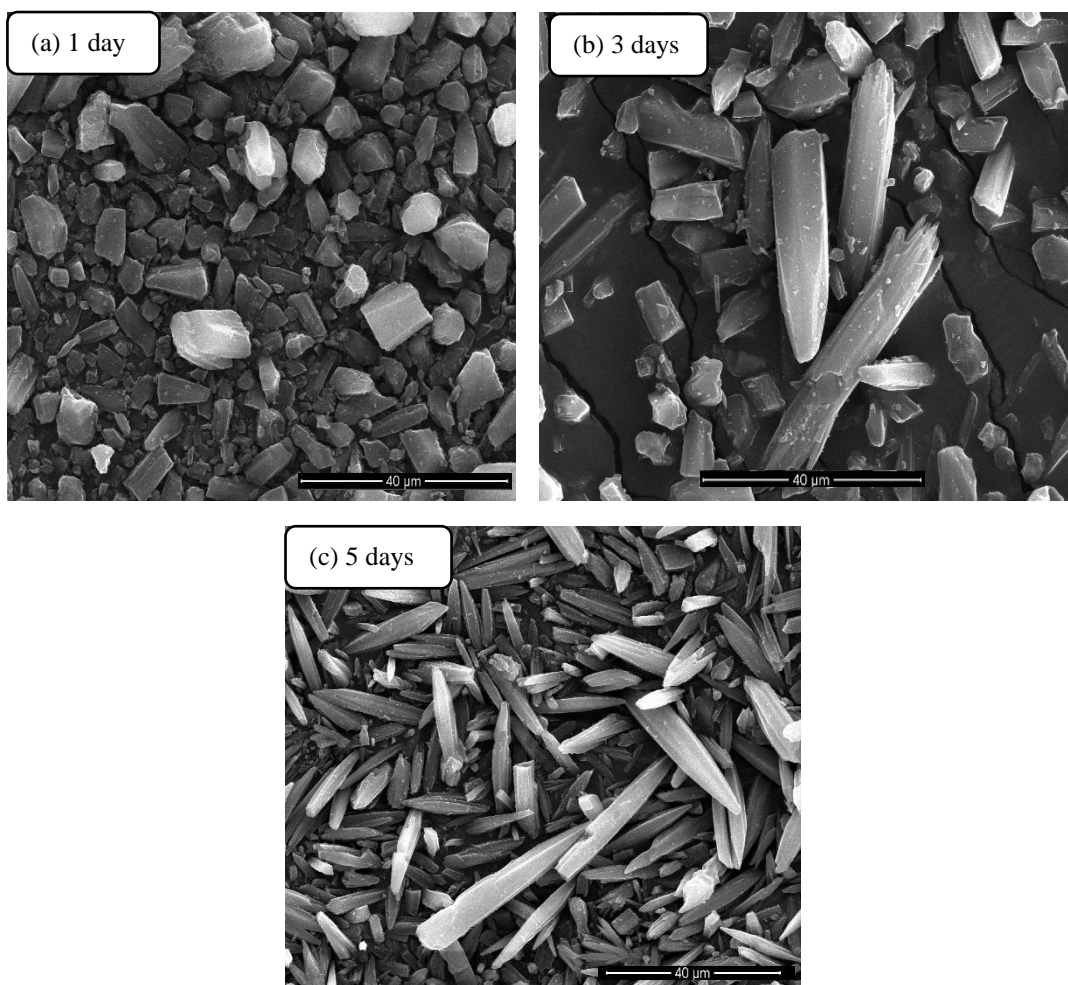


Figure 4.25 FE-SEM images of MIL-47 MOF obtained at 160°C at different reaction times (a) 1 day (M47-160-1), (b) 3 days (M47-160-3), and (c) 5 days (M47-160-5)

Figure 4.25a show that no specific crystal morphology was obtained when the MIL-47 synthesis reaction was carried out for 1 day at 160°C. The crystals formed at 160°C in 24 hours were of various morphologies and sizes with some crystals looking half-grown needle-type or spindle-shaped (see Figure 4.25a). Some full-grown spindle-shaped (and rod-shaped) crystals were observed when MIL-47 MOF was synthesized in 3 days at 160°C as can be seen in Figure 4.25b. It can be inferred by analyzing the FE-SEM images (in Figure 4.25a and Figure 4.25b) of both MIL-47 samples synthesized in 1 day and 3 days that for some crystals, nucleation started;

however, the crystals could not fully grow into spindle or needle shape morphology. So, one day and three days of reaction times at 160°C were not enough to overcome the thermodynamic limitations for crystals to grow into a full-size regime. This situation was different when MIL-47 synthesis was carried out for 5 days at 160°C. The SEM images show that fully grown spindle-shaped (or needle-like) crystals were obtained for the MIL-47 sample synthesized at 160°C in 5 days as can be seen in Figure 4.25c.

These synthesis results highlighted that although MIL-47 can be synthesized at 160°C in 24 hours to 5 days but the fully developed needle-like (or spindle-shaped) crystals were only obtained after 5 days of reaction time (sample M47-160-5). To get fully-grown spindle-shaped or needle-like crystals, minimum of 5 days of synthesis time is required at 160°C.

4.3.3 Effect of reaction time on MIL-47 at synthesis temperature of 220°C

The effect of reaction time was also studied at a synthesis temperature of 220°C. MIL-47 was synthesized in 1 day and 5 days at 220°C. PXRD patterns of MIL-47 synthesized in 1 day, and 5 days at 220°C are shown in Figure 4.26a and Figure 4.26b.

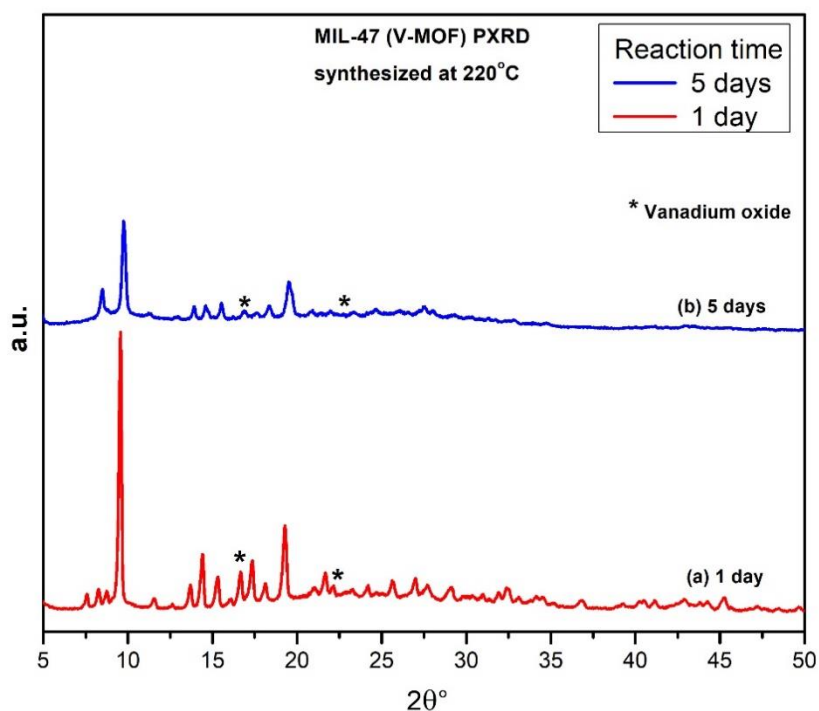


Figure 4.26 PXR D of MIL-47 MOF obtained at 220°C in (a) 1 day (M47-220-1)
(b) 5 days (M47-220-5)

PXR D patterns in Figure 4.26 show that crystalline MIL-47 MOF was synthesized in 1 day and 5 days at 220°C. All the main crystalline peaks were observed in PXR D patterns for both MIL-47 samples, which suggests that both samples were MIL-47 MOF. Vanadium oxide formation was also observed in the PXR D patterns in Figure 4.26. The intensities of diffraction peaks decreased with an increase in reaction time. The reason for this decrease in crystallinity of MIL-47 with an increase in time is not clear.

FE-SEM images of MIL-47 MOF samples synthesized in 1 day and 5 days at 220°C are shown in Figure 4.27a and Figure 4.27b, respectively.

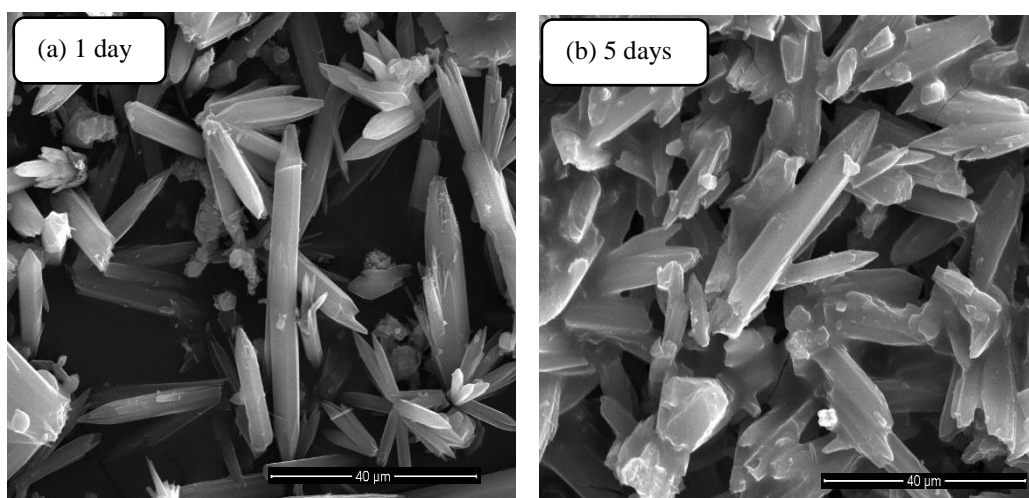


Figure 4.27 FE-SEM images of MIL-47 MOF obtained at 220°C in (a) 1 day (M47-220-1) (b) 5 days (M47-220-5)

FE-SEM images show that fully-grown needle-like (or rod-shaped) MIL-47 MOF crystals (see Figure 4.27a) were obtained just in 24 hours (M47-220-1) at 220°C which was not the case at 160°C (see Figure 4.25a). Another interesting phenomenon was seen in Figure 4.27a where many crystals sprouted out from the same nucleation point (dendrites) and grew into needle-like crystals, making flower-like structures, as seen in Figure 4.27a. The possible reason for dendritic crystals could be that the thermodynamic driving force for overcoming the free energy barrier for nucleation was relatively high at 220°C, which resulted in a faster crystal growth rate compared to nucleation. Moreover, the crystals were rod-like instead of spindle-shaped and some of the crystals were as big as 55μm in length. The MIL-47 MOF synthesized in 5 days at 220°C (M47-220-5) was observed to have fully grown but fused crystals as can be seen in Figure 4.27b. The fusion of crystals was not observed at 160°C. The longer reaction time at 220°C could have destabilized the crystals, and the crystals started to dissolve back into the DMF solution at high temperatures. Then during the cooling period, some of the dissolved solids recrystallized, possibly leading to the fusion of crystals. This could be the reason for the low diffraction peak

intensity for the sample obtained at 220°C in 5 days (M47-220-5), as shown in Figure 4.26b.

So, from the above observations, it seems that MIL-47 can be successfully synthesized even in 1 day at 220°C. MIL-47 was also successfully synthesized in 1 day at 160°C but the crystals were not fully grown into needle-like or rod-shaped. This also suggests that synthesis time decreases with an increase in reaction temperature. The effect of experimental parameters on the shape of the crystal could be further investigated in future studies as the morphology of MIL-47 crystals can affect their electronic and magnetic properties as observed in previous studies [57], [123].

4.3.4 Effect of concentration of precursors on the synthesis of MIL-47

MIL-47 MOF was synthesized at different reactant concentrations to understand the role of precursor concentration, keeping all other experimental parameters constant. The reaction temperature and time of 160°C and 5 days, respectively, were chosen to study the role of precursor concentrations on the synthesis of MIL-47 MOF. The concentrations of precursors i.e. $\text{VOSO}_4 \cdot n\text{H}_2\text{O}$ and H_2bdc , for all the synthesis till now in this work were kept at 148 mM and 108 mM (C1), respectively (see Table 3-3). The precursor concentrations were decreased to C2 (half of C1) and increased to C3 (two times C1) to study the effect of precursor concentrations.

PXRD patterns of MIL-47 synthesized at 160°C in 5 days with precursors concentrations C2 and C3 are shown in Figure 4.28a Figure 4.28b.

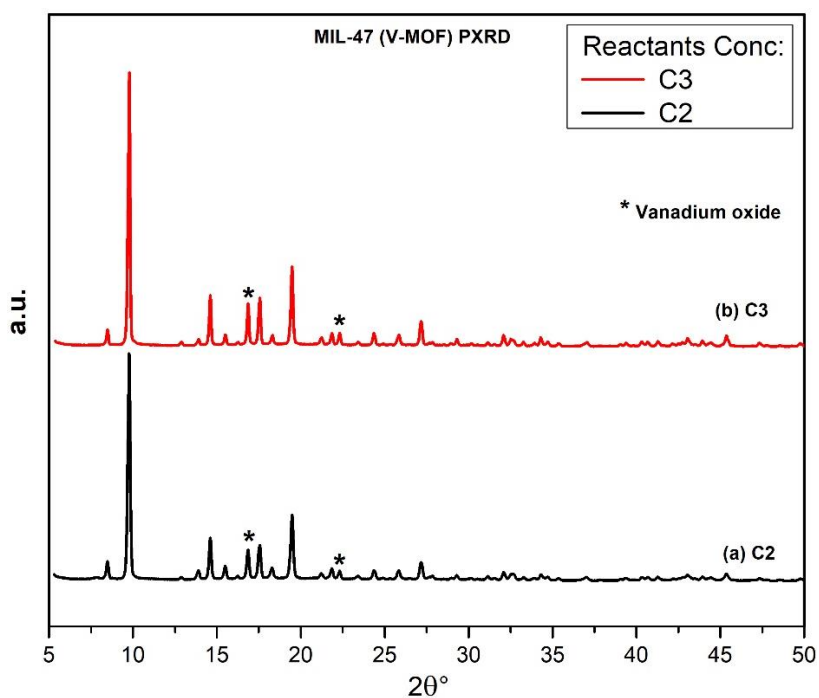


Figure 4.28 PXRD of MIL-47 MOF obtained at 160°C with different precursors concentrations in 5 days (a) C2 (M47-160-5-C2) (b) C3 (M47-160-5-C3)

It can be observed in Figure 4.28 that perfectly crystalline MIL-47 MOF is obtained at both C2 and C3 concentrations in 5 days at 160°C. The characteristic crystalline peaks were observed in PXRD patterns for both the MIL-47 samples. Some vanadium oxide formation was also observed in both samples as can be seen in Figure 4.28. Thus, MIL-47 synthesis was successful when the precursor concentrations were reduced to half or doubled with respect to C1 (see Table 3-3).

Figure 4.29a and Figure 4.29b show the FE-SEM images of MIL-47 synthesized at 160°C in 5 days with precursors concentrations C2 and C3.

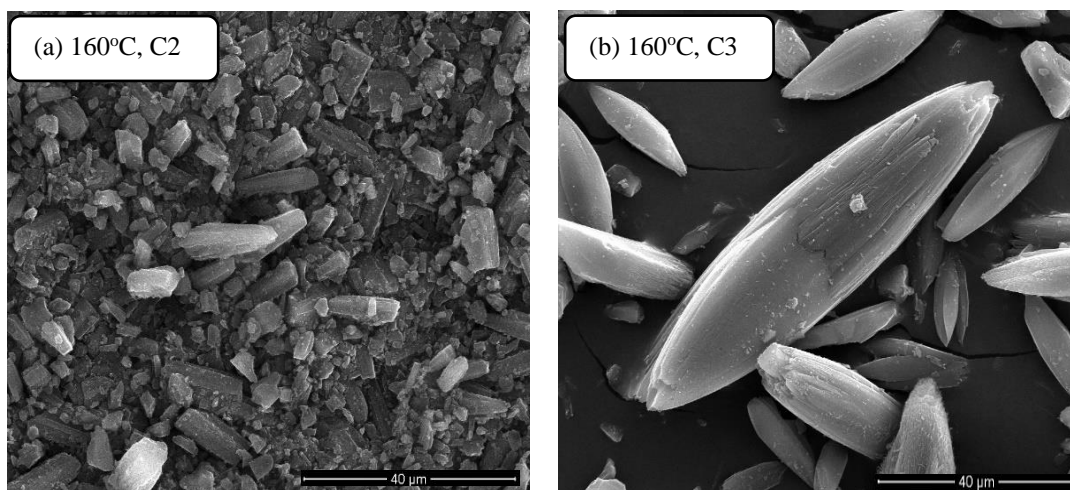


Figure 4.29 FE-SEM images of MIL-47 MOF obtained at 160°C with different precursors concentrations in 5 days (a) C2 (M47-160-5-C2) (b) C3 (M47-160-5-C3)

It can be seen in the FE-SEM image in Figure 4.29a that when the concentration of reactants was reduced to half (i.e. C2) of C1, half-grown MIL-47 crystals with no definite morphology were obtained. FE-SEM image for sample M47-160-5-C2 showed that some crystals have started to nucleate but could not fully grow into needle-like (or spindle-shaped) crystals, though some needle-like crystals were also observed in this sample. On the other hand, fully grown crystals were observed with C1 precursors concentrations at the same experimental conditions (see Figure 4.25c). Doubling the precursor concentrations (i.e. C3) compared to C1 resulted in discrete spindle-shaped crystals for MIL-47 MOF, as seen in Figure 4.29b. Some MOF crystals were observed to have grown from the same nucleation point (not shown here) as was previously seen at 220°C and C1 concentration in Figure 4.27a.

From the discussion on the effect of concentration on MIL-47 crystals, it is clear that at the same experimental conditions, fully grown spindle or needle-like crystals can be obtained at C1 and C2 precursor concentrations. At C2, though crystalline MIL-47 was synthesized at low concentration, the crystal could not grow to a fully formed

spindle or needle-shaped, which suggests that the growth phase of crystallization is lacking at low concentration.

The previous research works about MIL-47 are very obscure, and not much research work has been carried out related to MIL-47 MOF, specifically when it comes to its synthesis. The previous studies on MIL-47 are mostly focused on its functionalization and applications [22], [84] or theoretical studies [57]. This is probably the first study that focuses on the effect of temperature, concentrations, and reaction time on the crystallization and crystal morphology of MIL-47.

4.4 Activation, surface characterization, and thermogravimetric analysis of UiO-66, MIL-125, and MIL-47

As-synthesized MOFs usually contain DMF, organic linkers, or unreacted precursors in their pores. Before using MOFs for any application, the occluded molecules (or guest molecules) in the pores should be removed to access the porous structure of MOFs. The process of removal of occluded or guest molecules from the pores of the MOFs is called activation. The activation process for MOFs is discussed in the section in Chapter 3. One sample was chosen from each MOF based on the PXRD and FE-SEM results. All three as-synthesized MOFs were activated under vacuum at 150°C for 3 hours. All three MOFs were characterized by the nitrogen adsorption-desorption technique to get information about the porous structure of the framework. For UiO-66 MOF, the U66-80-C1 sample was chosen for nitrogen adsorption-desorption isotherm analysis. Figure 4.30 compares the nitrogen adsorption-desorption isotherm for as-synthesized and activated UiO-66 MOF.

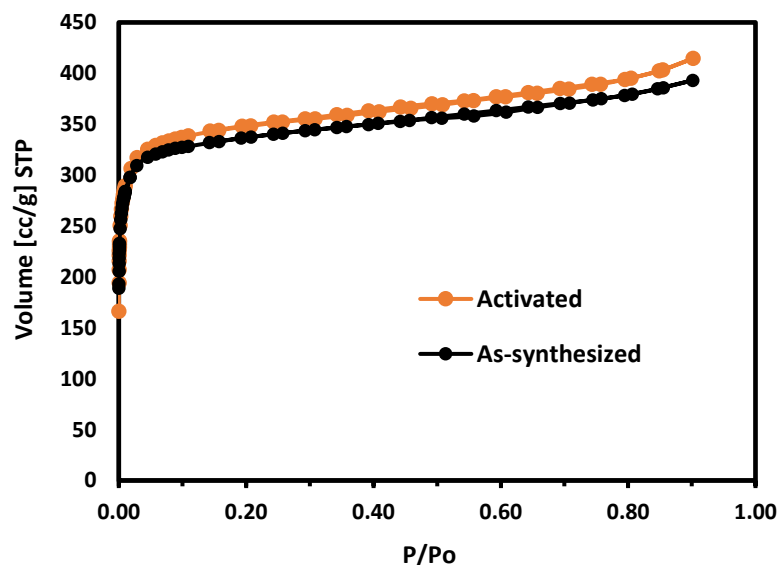


Figure 4.30 Nitrogen adsorption-desorption isotherm for as-synthesized (black) and activated (orange) UiO-66 (U66-80-C1 sample)

Figure 4.30 shows that Type-1 isotherm was obtained for UiO-66 which is a typical isotherm for microporous materials. It can be deduced from the isotherms in Figure 4.30 that the activation process did not affect the microporous structure of the UiO-66 framework. The multi-point BET surface areas calculated from nitrogen isotherm for as-synthesized and activated UiO-66 samples were 1308 m²/g and 1345 m²/g, respectively. The activated UiO-66 showed an increase in BET surface area, which was expected as the removal of solvents or organic linkers from the pores after activation allowed the nitrogen molecules to reach inside some of the inaccessible pores. A slight increase in the micropore volume was also observed for the activated UiO-66 MOF. The nitrogen isotherm for UiO-66 in this study matches the isotherms observed in the literature[13], [53]. The results from the nitrogen isotherm are shown in Table 4-2.

Figure 4.31 shows the nitrogen adsorption-desorption isotherm for as-synthesized and activated MIL-125 MOF (sample M125-150-3)

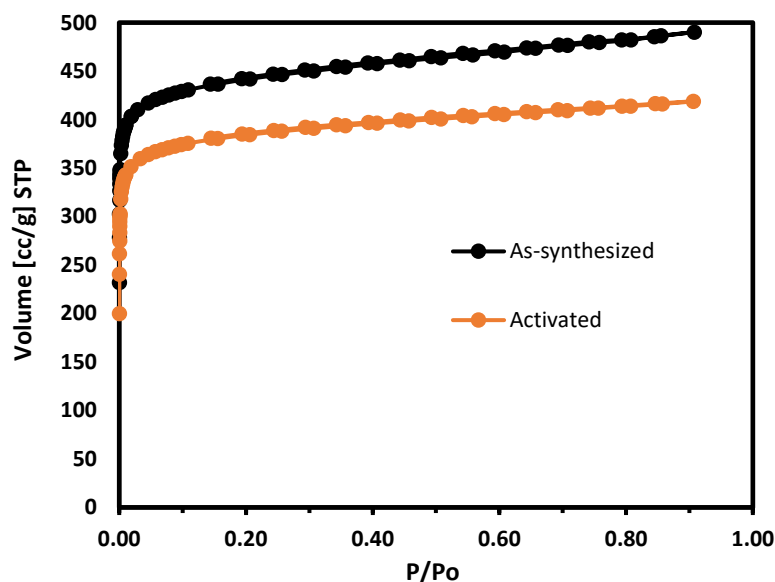


Figure 4.31 Nitrogen adsorption-desorption isotherm for as-synthesized (black) and activated (orange) MIL-125 (M125-150-3 sample).

Nitrogen adsorption-desorption isotherms obtained for both as-synthesized and activated MIL-125 MOF were type-I isotherms (Figure 4.31) which are typical for microporous materials. MIL-125 isotherms shown in Figure 4.31 suggests that the microporous structure is maintained after the activation of MOF. The multi-point BET surface areas were 1701 m²/g and 1464 m²/g for as-synthesized and activated MIL-125, which is interesting because the activated MOF should have a high surface area. The reason for this decrease in surface area after activation is not known. The surface areas of MIL-125 obtained in this work are comparable with the values reported in several studies [24], [25], [90]. Nitrogen adsorption-desorption results of MIL-125 MOF are shown in Table 4-2.

Figure 4.32 shows the nitrogen adsorption-desorption isotherm for as-synthesized and activated MIL-47 (M47-160-5).

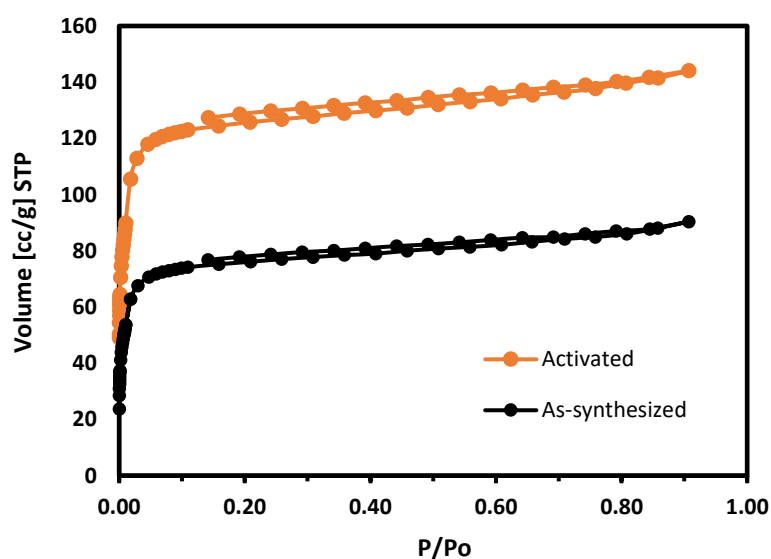


Figure 4.32 Nitrogen adsorption-desorption isotherm for as-synthesized (black) and activated (orange) MIL-47 (M47-160-5 sample)

Figure 4.32 shows that Type-I isotherm was observed for MIL-47 MOF. Hysteresis was observed in the adsorption isotherm of MIL-47, which is possibly due to the

presence of mesopores in MIL-47 or the formation of pores due to the evaporation of trapped DMF in the crystals. The possible reason for the presence of mesopores in MIL-47 could be the organic linker defects which may have increased the size of some of the pores in the MIL-47 framework. BET multi-point surface area of 304 m²/g and 493 m²/g was calculated from the nitrogen isotherm for as-synthesized and activated MIL-47 MOF, respectively. A considerable increase in the surface area for activated MIL-47 was observed, signaling the removal of solvents from the framework pores after activation. The activation of MIL-47 seems more successful compared to the other two MOFs (UiO-66 and MIL-125) probably the 1-D pores in its structure could easily be evacuated from the guest molecules. In prior studies, a wide range of surface area values are reported for MIL-47. i.e. from 350 m²/g to 1000 m²/g [19], [21], [56], and the surface areas calculated in this study fall in that range. Nitrogen adsorption-desorption results of MIL-125 MOF are shown in Table 4-2.

Table 4-2 Surface characterization results from N₂ adsorption-desorption isotherm data of UiO-66, MIL-125, and MIL-47

MOFs	Activation status	BET surface area (m²/g)	Micropore volume (cm³/g)	Micropore surface area (m²/g)
UiO-66 (U66-80-C1)	As-synthesized	1308	0.46	1164
	Activated	1345	0.47	1183
MIL-125 (M125-150-3)	As-synthesized	1701	0.61	1530
	Activated	1464	0.54	1343
MIL-47 (M47-160-5)	As-synthesized	304	0.10	270
	Activated	493	0.17	447

The isotherms of all three MOFs (UiO-66, MIL-125, and MIL47) show a small linear increase in the adsorbed volume of nitrogen gas as the relative pressure (P/P^0) increases, which indicates the presence of some macropores in the MOF samples. For pure microporous materials, this kind of increase is usually not observed and the isotherm shows a plateau at higher relative pressure values (P/P^0). The presence of macropores can also be hypothesized from the difference in the BET multi-point and micropore surface areas of MOFs (Table 4-2). These macropores were probably the void spaces formed between the agglomerated crystals of MOFs. The agglomeration for these MOFs samples was not visible in the FE-SEM images.

The particle size distribution of the three MOFs samples (U66-80-C1, M125-150-3, and M47-160-5) were obtained using Zeta potential and Dynamic Light scattering (DLS) spectroscopy. Particle size distribution of UiO-66, MIL-125, and MIL-47 are shown in Figure A. 1, Figure A. 2, and Figure A. 3, respectively, in Appendix A. The mean particle size of UiO-66 from zeta potential analysis was observed to be 342 nm which is considerably high compared to the mean size measured from FE-SEM images via ImageJ software [117] i.e 125 nm. The reason for the bigger zeta potential value for UiO-66 particle size may be the agglomeration of the UiO-66 crystals. The agglomeration of crystals was not seen in the section of the UiO-66 sample analyzed in FE-SEM (Figure 4.2a). The crystal sizes of MIL-125 and MIL-47 MOFs were expected to be more than 1 micron, so particle size distribution was obtained by Dynamic Light scattering (DLS) spectroscopy. The peaks obtained in the Particle size distribution curves of MIL-125 and MIL-47 were consistent with the crystal sizes observed from the FE-SEM images, which suggests that there was no crystal agglomeration in MIL-125 and MIL-47 samples.

Thermogravimetric analysis (TGA) was carried out to ascertain the thermal stability of all three MOFs synthesized in this study. The same MOF samples were chosen for TGA as was done for surface characterization i.e. samples U66-80-C1, M125-150-3, and M47-160-5 for UiO-66, MIL-125, and MIL-47, respectively. Figure 4.33 shows the TGA curves obtained for all three activated MOFs.

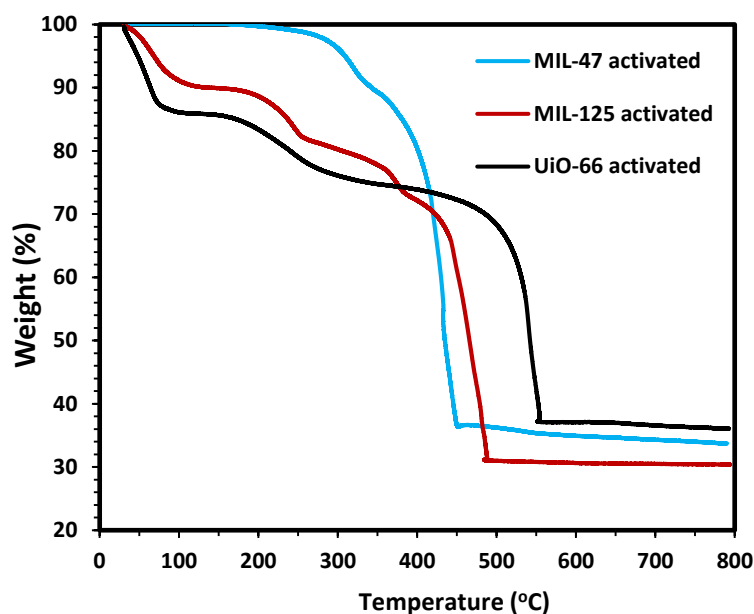


Figure 4.33 TGA curves of activated UiO-66 (black), MIL-125 (red), and MIL-47 (blue) MOFs. Samples are U66-80-C1, M125-150-3, and M47-160-5, respectively

The TGA curve of activated UiO-66 is shown in Figure 4.33 (black curve). Figure 4.33 shows that three weight loss steps were observed for activated UiO-66. This first weight loss step was observed from room temperature to 80°C, which is due to the volatilization of moisture and ethanol from the pores. The weight loss in this step for UiO-66 was 14%. The second weight loss step (8%) between 130°C-290°C was observed due to the removal of DMF, solvent, unreacted organic linker, and dihydroxylation (removal of -OH group). For the activated UiO-66 sample, the 8% weight reduction observed in the second step suggests that some of the unreacted precursors remained in the pores even after activation. The third weight loss step (~33%) for UiO-66 was observed between ~500°C-565°C. At ~500°C the decomposition of organic linkers started, and the framework of UiO-66 completely collapsed at around ~565°C leaving just zirconium oxide as the final product [13], [53]. These results in general can be told to agree with the literature data suggesting a relatively high thermal stability up to ~565°C [2], [13].

TGA curve activated MIL-125 show four distinct weight loss steps as shown in Figure 4.33 (red curve). First weight loss step (~9%) for MIL-125 was observed between room temperature and around 100°C due to volatilization of methanol solvent and water (moisture). The second weight loss step (~10%) from around 170°C to 250°C was due to the removal of DMF and organic linker trapped inside the pores of the MIL-125 framework. From 350°C to 390°C, partial degradation of MIL-125 framework occurred to form TiO₂ (anatase) which resulted in a small third weight loss step (~3%). The decomposition of the organic linker in the MIL-125 framework started around ~400°C and the framework completely collapsed at around ~480°C (~39%). The TGA characterization results of MIL-125 reasonably agree with the work in the literature [24], [25].

The TGA curve of activated MIL-47 shows two weight loss steps as shown in Figure 4.33 (blue curve). No weight loss was observed until around 250°C in the activated MIL-47 TGA curve which suggests the complete removal of moisture, methanol, and DMF from the pores of MIL-47 during the activation procedure. A small weight loss step (~10%) was observed between 260°C-345°C in the MIL-47 TGA curve, which corresponds to the evacuation of pores due to the removal of the residual organic linker. The decomposition of organic linker started around ~370°C and the complete collapse of the MIL-47 framework occurred at around ~450°C (~51%) leaving behind just the oxides of vanadium as the final product. The TGA results of MIL-47 agree with those obtained in the previous studies [19], [122].

In summary, the TGA results show that UiO-66 is the thermally most stable MOF among these three MOFs. UiO-66 can keep the integrity of its framework up to ~500°C compared to ~400°C and ~370°C for MIL-125 and MIL-47, respectively. UiO-66 is unique among the MOFs due to its high thermal stability as most of the MOFs are stable only up to 350°C-400°C. The high thermal stability of UiO-66 MOF is due to the strong interaction between the inorganic metal clusters and the organic linkers. Furthermore, UiO-66 has the highest coordination number in the MOF family i.e. the metal clusters are connected by 12 organic linkers. The structure of

UiO-66 is explained in detail in chapter 1 and shown in Figure 1.2, Figure 1.4, Figure 1.5, and Figure 1.6.

Besides its thermal stability, UiO-66 is also very stable in a wide variety of solvents, corrosive chemicals, and water for an extended period compared to other MOFs [13]. Keeping in view its solvent stability, UiO-66 water adsorption capacity was tested for potential application in water harvesting from atmospheric moisture.

4.5 Water adsorption (uptake) by UiO-66

UiO-66 is one of those few MOFs that remain stable in water for a prolonged period [13]. Recently, interest has been developed for water harvesting from the atmosphere using MOF as an adsorbent [49]. The water adsorption capacity of UiO-66 MOF was also tested in this study.

UiO-66 samples synthesized at 80°C with C1 precursors concentrations (U66-80-C1) without a modulator and with an HCl modulator were tested for water uptake. The activated MOF samples were exposed to a controlled climate at 25°C with relative humidity (%Rh) of 30% in a climate chamber. The bar chart in Figure 4.34 shows the water capacity of the U66-80-C1 sample synthesized without and with the HCl modulator.

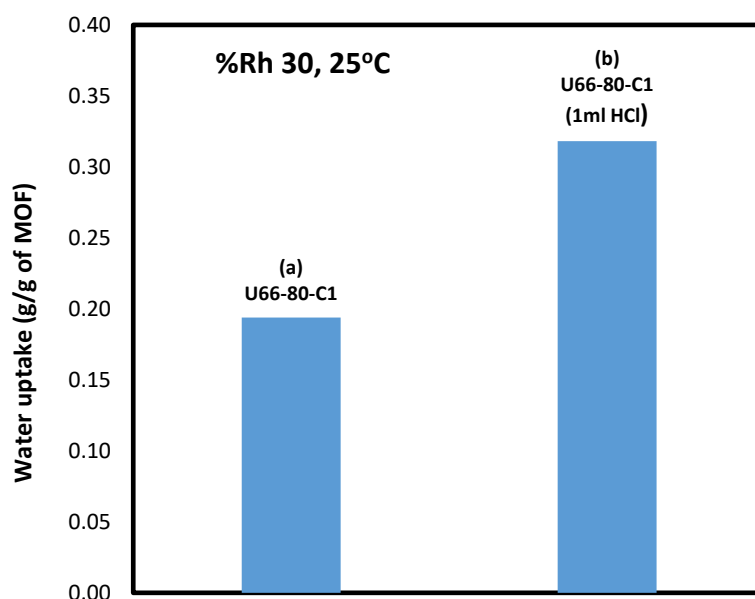


Figure 4.34 The water uptake bar chart of U66-80-C1 (a) without and (b) with HCl modulator

As can be seen in Figure 4.34, the water uptake capacity for UiO-66 (U66-80-C1) synthesized without a modulator and with HCl (1 ml in reacting solution) modulator was observed to be 0.19 g/g and 0.32 g/g of UiO-66 (or kg/kg of MOF), respectively. Almost a 65% increase in the water capacity was observed for the sample synthesized in the presence of HCl under the same conditions. The possible reason for this increase in water uptake could be the defects induced in the framework of UiO-66 by the HCl modulator. A previous study has shown the induction of defects in the UiO-66 framework by using HCl as a modulator [15]. The defects create vacant positions on the metal clusters which could act as attaching points for water molecules in the framework of UiO-66 [36], [124] which could be the reason for higher water uptake in HCl modulated UiO-66.

Due to its higher water uptake capacity, the U66-80-C1 sample synthesized with an HCl modulator was tested for relative humidity (%Rh) range of 25-80% at 30°C (this temperature was selected to mimic the real-world ambient conditions). The whole

isotherm was obtained in the %Rh range of 25-80% for U66-80-C1 (HCl) as shown in Figure 4.35.

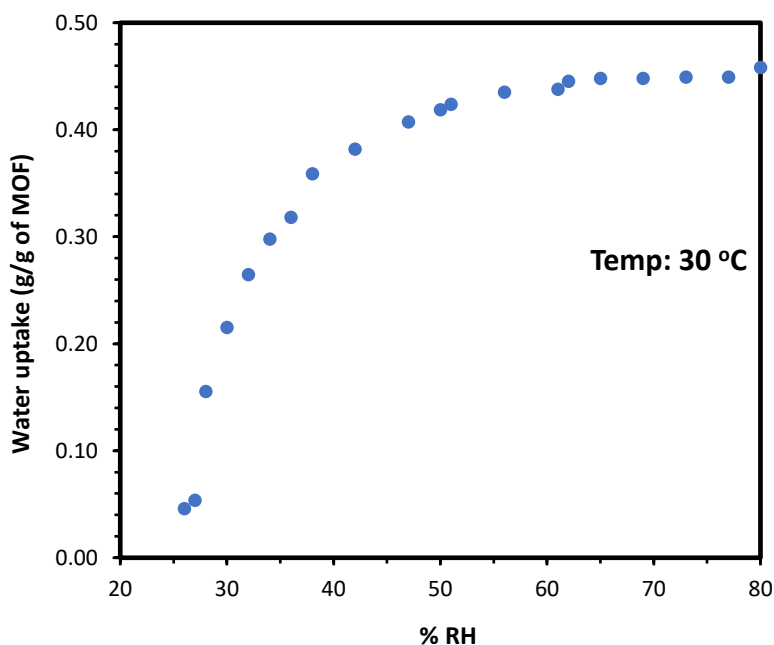


Figure 4.35 Water adsorption isotherm obtained at 30°C of U66-80-C1 synthesized in the presence of an HCl modulator.

From Figure 4.35 it can be deduced that at 30°C the water uptake capacity of HCl modulated UiO-66 MOF reached more than 40% at a relative humidity of 50% (or 0.43 kg/kg of MOF). The water uptake capacity plateaued at around 60% relative humidity. These results showed that UiO-66 MOF can be used for water harvesting in places where there is water scarcity but the relative humidity usually fluctuates between 40-60%. A prototype of scalable technologies for water harvesting has already been employed that uses MOFs as sorbent and the water adsorb can be harvested using only solar energy [49]. The HCl modulated UiO-66 MOFs could also potentially be used as sorbent coating on the condensers of the air conditioning systems to reduce the latent heat load (which can be up to 30% of total energy

consumption by residential AC systems) by absorbing the moisture from the inlet air. This type of prototype technology has been tried for other MOFs [32].

The water uptake capacity was also measured for the UiO-66 samples synthesized in the presence of acid-base co-modulation (for details see section 4.1.2.1). The bar chart for water adsorption capacities of acid-base modulated UiO-66 samples is shown in Figure 4.36.

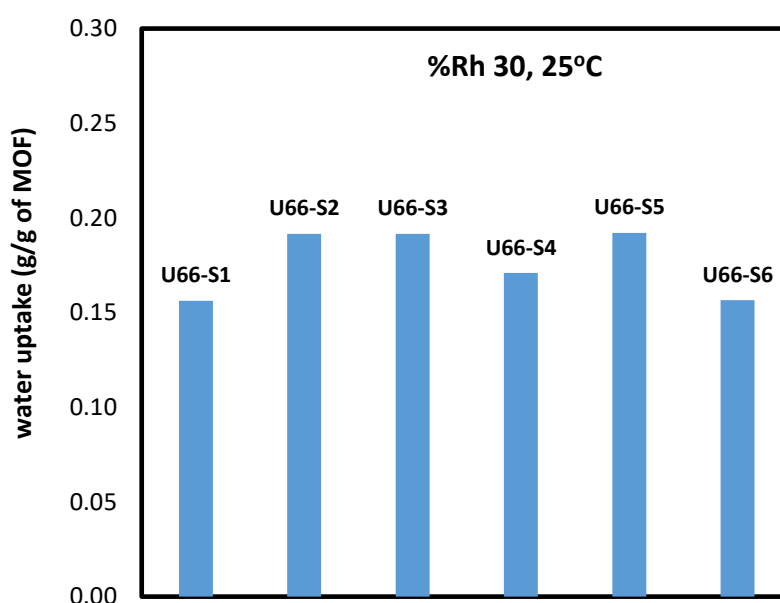


Figure 4.36 Water adsorption capacities of UiO-66 synthesized in the presence of AA-TEA modulators (see Table 3-2)

As can be seen in Figure 4.36 the water adsorption capacities of all the AA-TEA modulated UiO-66 samples are less than the sample synthesized in the presence of HCl at 80°C (U66-80-C1). The water capacities are AA-TEA modulated UiO-66 samples are comparable to the sample synthesized without an HCl modulator. This shows that capacities were not much affected by the change in TEA concentration in the synthesis solution. The possible reason could be fewer defects in the samples synthesized in the presence of acid-base modulators at 120°C. The high synthesis

temperature and presence of TEA have both been previously observed to have reduced defects in the UiO-66 framework [53], [54]. The average water capacity for samples synthesized in the presence of an AA-TEA modulator was observed to be 0.18 g/g of MOF.

From the discussion on the water uptake capacity of UiO-66 MOF, it can be deduced that HCl modulated MOF sample has considerably higher water capacity compared to the pristine and AA-TEA modulated UiO-66. HCl could induce more defects in the MOF framework and on the other hand, AA-TEA seems to have not generated many defective sites for water molecules to attach. HCl modulated UiO-66 could potentially be employed in water harvesting applications.

CHAPTER 5

SUMMARY, CONCLUSIONS, AND SUGGESTIONS

5.1 Summary and Conclusions

Three types of MOFs were synthesized in this study by the solvothermal method, UiO-66, a zirconium-based MOF (Zr-MOF), MIL-125, a titanium-based MOF (Ti-MOF), and MIL-47, a vanadium-based MOF (V-MOF). The effect of synthesis temperature, synthesis time, precursor concentrations, and the effect of modulators on these three MOFs were studied in this work.

UiO-66 MOF was synthesized with different mean crystal sizes and morphologies at various temperatures and in the presence of modulators. Cubic and octahedral crystal morphologies were obtained depending on the synthesis temperature and the use of a modulator. Moreover, UiO-6 was also successfully synthesized with no definite crystal morphology in the presence of HCl acid as a modulator. It was seen that synthesis temperature and the use of a modulator could drastically affect the shape and mean size of UiO-66 crystals. Furthermore, increasing the synthesis temperature can reduce the crystallization time of UiO-66. Modulators like HCl, AA, and TEA were observed to have significantly decreased the crystallization time of UiO-66. Modulator use was also tested to show that it affects the water uptake of UiO-66. The effect of AA-TEA versus using AA alone as a modulator can be suggested to be of further interest in future research based on specific application areas.

MIL-125 MOF was synthesized at different synthesis temperatures, synthesis times, and Ti-source concentrations. It was observed that all the experimental parameters considerably affected the final MIL-125 product. The variation in experimental parameters significantly affects the shape, size, and morphology of the MIL-125 crystals. In this study, both disc-shaped and truncated octahedral crystal morphologies were obtained by controlling the synthesis time and concentration of

the precursor. Synthesis temperature was observed to have affected the mean size of the crystal.

Titanium-based MOFs are generally very difficult to synthesize because of the reactive nature of the titanium sources. The highly reactive nature of the titanium source makes MIL-125 very difficult to synthesize. Special care is needed to handle the precursors while synthesizing MIL-125 or any other Ti-based MOF. A lot of unsuccessful attempts were made before the successful synthesis of MIL-125. In this study, the preparation of the synthesis solution for MIL-125 was carried out under ambient conditions without any glove box, which made it very hard to achieve the successful synthesis of MIL-125. The reproducibility of MIL-125 MOF in small batches was very low. When the batch size was increased, the successful synthesis of MIL-125 was achieved even without the use of a glove box. Despite the success, without the glove box, there was less control over MIL-125 synthesis. Even in bigger batches, the formation of impurities like TiO_2 could not be avoided and that affected the synthesis of MIL-125. That is why, sometimes the change in crystal shape, and sizes was observed from batch to batch under the same experimental conditions. Consequently, because of these reasons, the use of a glove box is strongly recommended for the synthesis of MIL-125 or any other Ti-based MOF.

MIL-47 was synthesized at different synthesis temperatures, synthesis times, and precursor concentrations. Spindle shape, needle-like, and rod-shaped crystals were observed under different experimental conditions. An increase in temperature can decrease the time for the crystallization of MIL47 MOF. On the other hand, the time of the reaction can affect the morphology of the synthesized MIL-47 crystals, moreover, precursor concentration can also affect the morphology of the crystals.

In all the three MOFs studied in this work, UiO-66 synthesis was found to be more well-regulated because UiO-66 was more responsive to the changes in experimental conditions, i.e., its synthesis can be carefully controlled via process parameters like T, time, etc. UiO-66 can be synthesized at a wide range of temperatures, and precursor concentrations and a variety of acid or base modulators could be used for

its synthesis. Furthermore, it is easy to engineer a variety of crystal morphologies for UiO-66, which can be employed in various applications. On the other hand, MIL-125 and MIL-47 are relatively difficult to synthesize, and it is difficult to control their synthesis by controlling the experimental parameters.

In general, there is still too much room to investigate and controllably tailor the MOFs structures based on synthesis methodologies as summarized in this thesis, which is believed to shape the future of advanced applications.

5.2 Suggestions for future work

- UiO-66, MIL-125, and MIL-47 can be synthesized using different types of precursors.
- Various experimental conditions and their effect on the MOFs can be tried in the future.
- A variety of acid or base modulators could be employed for the synthesis of all three MOFs i.e. benzoic acid, formic acid, and other acids or bases.
- The crystal morphology and size of these MOFs could be tailored for various applications by using different modulators.
- DMF is the solvent of choice for most of the MOFs synthesis but it is a toxic solvent. Other environmentally friendly solvents could be used for the synthesis of these MOFs. Moreover, the effect of solvents on MOFs could be studied.
- Different functional groups (e.g. -NH₂, -Cl, -Br, -OH) could be attached to the organic linker for tuning the properties of these MOFs e.g. electronic and magnetic properties.
- Other metal ions could be incorporated by the ion exchange method to tailor these MOFs for specific applications, for example, catalysis and gas adsorption.
- MIL-125 can be employed in photocatalytic applications.
- The potential role of MIL-47 as capacitors can be further studied.

REFERENCES

- [1] P. Z. Moghadam *et al.*, “Development of a Cambridge Structural Database Subset: A Collection of Metal-Organic Frameworks for Past, Present, and Future,” *Chemistry of Materials*, vol. 29, no. 7. pp. 2618–2625, 2017.
- [2] A. J. Howarth, A. W. Peters, N. A. Vermeulen, T. C. Wang, J. T. Hupp, and O. K. Farha, “Best practices for the synthesis, activation, and characterization of metal–organic frameworks,” *Chemistry of Materials*, vol. 29, no. 1. pp. 26–39, 2017.
- [3] C. A. Trickett, K. J. Gagnon, S. Lee, F. Gándara, H. B. Bürgi, and O. M. Yaghi, “Definitive Molecular Level Characterization of Defects in UiO-66 Crystals,” *Angew. Chemie - Int. Ed.*, vol. 54, no. 38, pp. 11162–11167, 2015.
- [4] M. A. Syzgantseva, C. P. Ireland, F. M. Ebrahim, B. Smit, and O. A. Syzgantseva, “Metal Substitution as the Method of Modifying Electronic Structure of Metal-Organic Frameworks,” *J. Am. Chem. Soc.*, vol. 141, no. 15, pp. 6271–6278, 2019.
- [5] O. M. Yaghi and H. Li, “Hydrothermal Synthesis of a Metal-Organic Framework Containing Large Rectangular Channels,” *J. Am. Chem. Soc.*, vol. 117, no. 41, pp. 10401–10402, 1995.
- [6] S. R. Batten *et al.*, “Coordination polymers, metal-organic frameworks and the need for terminology guidelines,” *CrystEngComm*, vol. 14, no. 9, pp. 3001–3004, 2012.
- [7] A. Li, R. Bueno-Perez, S. Wiggin, and D. Fairen-Jimenez, “Enabling efficient exploration of metal–organic frameworks in the Cambridge Structural Database,” *CrystEngComm*, vol. 22, no. 43, pp. 7152–7161, 2020.
- [8] S. R. Batten *et al.*, “Terminology of metal-organic frameworks and coordination polymers (IUPAC recommendations 2013),” *Pure Appl. Chem.*,

vol. 85, no. 8, pp. 1715–1724, 2013.

- [9] R. E. Morris and L. Brammer, “Coordination change, lability and hemilability in metal–organic frameworks,” *Chem. Soc. Rev.*, vol. 46, no. 17, pp. 5444–5462, 2017.
- [10] H. Furukawa, K. E. Cordova, M. O’Keeffe, and O. M. Yaghi, “The Chemistry and Applications of Metal-Organic Frameworks,” *Science (80-.)*, vol. 341, no. 6149, p. 1230444, 2013.
- [11] O. M. Y. Hailian Li, Mohammed Eddaoudi, M.O’Keeffe, “Design and synthesis of an exceptionally stable and highly porous metal-organic framework,” vol. 402, no. November, pp. 276–279, 1999.
- [12] H. C. Zhou, J. R. Long, and O. M. Yaghi, “Introduction to metal-organic frameworks,” *Chem. Rev.*, vol. 112, no. 2, pp. 673–674, 2012.
- [13] J. H. Cavka *et al.*, “A new zirconium inorganic building brick forming metal organic frameworks with exceptional stability,” *J. Am. Chem. Soc.*, vol. 130, no. 42, pp. 13850–13851, 2008.
- [14] “ChemTube3D.” [Online]. Available: <https://www.chemtube3d.com/mof-UiO66>.
- [15] M. J. Katz *et al.*, “A facile synthesis of UiO-66, UiO-67 and their derivatives,” *Chem. Commun.*, vol. 49, no. 82, pp. 9449–9451, 2013.
- [16] S. Chavan *et al.*, “H₂ storage in isostructural UiO-67 and UiO-66 MOFs,” *Phys. Chem. Chem. Phys.*, vol. 14, no. 5, pp. 1614–1626, 2012.
- [17] S. Yuan *et al.*, “Stable Metal–Organic Frameworks: Design, Synthesis, and Applications,” *Adv. Mater.*, vol. 30, no. 37, 2018.
- [18] Y. Han *et al.*, “Facile synthesis of morphology and size-controlled zirconium metal-organic framework UiO-66: the role of hydrofluoric acid in crystallization,” *CrystEngComm*, vol. 17, no. 33, pp. 6434–6440, 2015.

- [19] D. Riou and K. Barthelet, "A Breathing Hybrid Organic-Inorganic Solid with Very Large Pores and High Magnetic Characteristics," no. 2, pp. 281–284, 2002.
- [20] N. L. Rosi, J. Kim, M. Eddaoudi, B. Chen, M. O’Keeffe, and O. M. Yaghi, "Rod Packings and Metal–Organic Frameworks Constructed from Rod-Shaped Secondary Building Units," *J. Am. Chem. Soc.*, vol. 127, no. 5, pp. 1504–1518, Feb. 2005.
- [21] A. Phan, A. U. Czaja, F. Gándara, C. B. Knobler, and O. M. Yaghi, "Metal-organic frameworks of vanadium as catalysts for conversion of methane to acetic acid," *Inorg. Chem.*, vol. 50, no. 16, pp. 7388–7390, 2011.
- [22] K. Leus *et al.*, "Synthesis, characterization and sorption properties of NH₂-MIL-47," *Phys. Chem. Chem. Phys.*, vol. 14, no. 44, pp. 15562–15570, 2012.
- [23] H. Leclerc *et al.*, "Influence of the Oxidation State of the Metal Center on the Flexibility and Adsorption Properties of a Porous Metal Organic Framework: MIL-47(V)," *J. Phys. Chem. C*, vol. 115, no. 40, pp. 19828–19840, Oct. 2011.
- [24] M. Dan-Hardi *et al.*, "A new photoactive crystalline highly porous titanium(IV) dicarboxylate," *J. Am. Chem. Soc.*, vol. 131, no. 31, pp. 10857–10859, 2009.
- [25] S. Kim, J. Kim, H. Kim, H. Cho, and W. Ahn, "Adsorption/catalytic properties of MIL-125 and NH₂-MIL-125," *Esi*, vol. 204, pp. 85–93, 2013.
- [26] H. L. Nguyen, "Perspectives on titanium-based metal–organic frameworks," *J. Phys. Energy*, vol. 3, no. 2, p. 21003, 2021.
- [27] E. Yılmaz, E. Sert, and F. S. Atalay, "Synthesis and sulfation of titanium based metal organic framework; MIL-125 and usage as catalyst in esterification reactions," *Catal. Commun.*, vol. 100, no. June, pp. 48–51, 2017.
- [28] Y. Fang, Y. Ma, M. Zheng, P. Yang, A. M. Asiri, and X. Wang, "Metal–organic frameworks for solar energy conversion by photoredox catalysis,"

Coord. Chem. Rev., vol. 373, pp. 83–115, Sep. 2017.

- [29] L. G. da Trindade *et al.*, “SPEEK-based proton exchange membranes modified with MOF-encapsulated ionic liquid,” *Mater. Chem. Phys.*, vol. 236, no. April, 2019.
- [30] Y. Ren, G. H. Chia, and Z. Gao, “Metal-organic frameworks in fuel cell technologies,” *Nano Today*, vol. 8, no. 6. pp. 577–597, 2013.
- [31] Z. Song, N. Cheng, A. Lushington, and X. Sun, “Recent progress on MOF-Derived nanomaterials as advanced electrocatalysts in fuel cells,” *Catalysts*, vol. 6, no. 8, 2016.
- [32] S. Cui *et al.*, “Metal-Organic Frameworks as advanced moisture sorbents for energy-efficient high temperature cooling,” *Sci. Rep.*, vol. 8, no. 1, pp. 2–10, 2018.
- [33] A. R. Millward and O. M. Yaghi, “Metal-organic frameworks with exceptionally high capacity for storage of carbon dioxide at room temperature,” *J. Am. Chem. Soc.*, vol. 127, no. 51, pp. 17998–17999, 2005.
- [34] M. Usman, A. Helal, M. M. Abdelnaby, A. M. Alloush, M. Zeama, and Z. H. Yamani, “Trends and Prospects in UiO-66 Metal-Organic Framework for CO₂ Capture, Separation, and Conversion,” *Chem. Rec.*, vol. 21, no. 7, pp. 1771–1791, Jul. 2021.
- [35] D. Yang and B. C. Gates, “Catalysis by Metal Organic Frameworks: Perspective and Suggestions for Future Research,” *ACS Catal.*, vol. 9, no. 3, pp. 1779–1798, Mar. 2019.
- [36] X. L. i X. Cirujano, F G, “Tuning the Catalytic Properties of UiO-66 Metal – Organic Frameworks: From Lewis to Defect-Induced Brønsted Acidity,” *J. Phys. chmeistry Lett.*, vol. 11, pp. 4879–4890, 2020.
- [37] C. S. Diercks, Y. Liu, K. E. Cordova, and O. M. Yaghi, “The role of reticular chemistry in the design of CO₂ reduction catalysts,” *Nat. Mater.*, vol. 17, no.

- 4, pp. 301–307, 2018.
- [38] S. Hu *et al.*, “Solvothermal synthesis of NH₂-MIL-125(Ti) from circular plate to octahedron,” *CrystEngComm*, vol. 16, pp. 9645–9650, 2014.
- [39] C. Gomes Silva, I. Luz, F. X. Llabrés i Xamena, A. Corma, and H. García, “Water Stable Zr–Benzenedicarboxylate Metal–Organic Frameworks as Photocatalysts for Hydrogen Generation,” *Chem. – A Eur. J.*, vol. 16, no. 36, pp. 11133–11138, Sep. 2010.
- [40] M. B. Chambers *et al.*, “Maximizing the Photocatalytic Activity of Metal–Organic Frameworks with Aminated-Functionalized Linkers: Substoichiometric Effects in MIL-125-NH(2).,” *J. Am. Chem. Soc.*, vol. 139, no. 24, pp. 8222–8228, Jun. 2017.
- [41] G. W. Peterson *et al.*, “Tailoring the Pore Size and Functionality of UiO-Type Metal–Organic Frameworks for Optimal Nerve Agent Destruction,” *Inorg. Chem.*, vol. 54, no. 20, pp. 9684–9686, Oct. 2015.
- [42] A. Dhakshinamoorthy, A. Santiago-Portillo, A. M. Asiri, and H. Garcia, “Engineering UiO-66 Metal Organic Framework for Heterogeneous Catalysis,” *ChemCatChem*, vol. 11, no. 3, pp. 899–923, Feb. 2019.
- [43] J. Lee, O. K. Farha, J. Roberts, K. A. Scheidt, S. T. Nguyen, and J. T. Hupp, “Metal–organic framework materials as catalysts,” *Chem. Soc. Rev.*, vol. 38, no. 5, pp. 1450–1459, 2009.
- [44] Y. He, W. Zhou, G. Qian, and B. Chen, “Methane storage in metal–organic frameworks,” *Chem. Soc. Rev.*, vol. 43, no. 16, pp. 5657–5678, 2014.
- [45] D. Britt, H. Furukawa, B. Wang, T. G. Glover, and O. M. Yaghi, “Highly efficient separation of carbon dioxide by a metal-organic framework replete with open metal sites.,” *Proc. Natl. Acad. Sci. U. S. A.*, vol. 106, no. 49, pp. 20637–20640, Dec. 2009.
- [46] D. A. Gomez-Gualdron *et al.*, “Computational Design of Metal–Organic

- Frameworks Based on Stable Zirconium Building Units for Storage and Delivery of Methane,” *Chem. Mater.*, vol. 26, no. 19, pp. 5632–5639, Oct. 2014.
- [47] V. A. Online, “BASF Metal Organic Frameworks (MOFs): Innovative Fuel Systems for Natural Gas Vehicles (NGVs),” *Chem. Soc. Rev.*, vol. 43, no. 16, pp. 6173–6174, 2014.
- [48] S. Øien-Ødegaard, “Preparation, structure and reactivity of functionalized zirconium metal organic frameworks,” University of Oslo, 2016.
- [49] H. Kim *et al.*, “Water harvesting from air with metal-organic frameworks powered by natural sunlight,” *Science (80-.)*, vol. 356, no. 6336, pp. 430 LP – 434, Apr. 2017.
- [50] Y. Ren, G. H. Chia, and Z. Gao, “Metal–organic frameworks in fuel cell technologies,” *Nano Today*, vol. 8, no. 6, pp. 577–597, 2013.
- [51] M. R. DeStefano, T. Islamoglu, S. J. Garibay, J. T. Hupp, and O. K. Farha, “Room-Temperature Synthesis of UiO-66 and Thermal Modulation of Densities of Defect Sites,” *Chem. Mater.*, vol. 29, no. 3, pp. 1357–1361, 2017.
- [52] M. Sitarz, P. Jelen, A. Ko, A. Pajdak, Z. Majka, and A. Boguszewska-czubara, “Cracking the Chloroquine Conundrum: The Application of Defective UiO-66 Metal – Organic Framework Materials to Prevent the Onset of Heart Defects-In Vivo and In Vitro’,” 2020.
- [53] Y. Zhao, Q. Zhang, Y. Li, R. Zhang, and G. Lu, “Large-Scale Synthesis of Monodisperse UiO-66 Crystals with Tunable Sizes and Missing Linker Defects via Acid/Base Co-Modulation,” *ACS Appl. Mater. Interfaces*, vol. 9, no. 17, pp. 15079–15085, 2017.
- [54] G. C. Shearer *et al.*, “Tuned to perfection: Ironing out the defects in metal-organic framework UiO-66,” *Chem. Mater.*, vol. 26, no. 14, pp. 4068–4071, 2014.

- [55] L. Jiao, J. Y. R. Seow, W. S. Skinner, Z. U. Wang, and H.-L. Jiang, “Metal–organic frameworks: Structures and functional applications,” *Mater. Today*, vol. 27, pp. 43–68, 2019.
- [56] J. F. M. D. and P. V. D. V. Shyam Biswas, Danny E. P. Vanpoucke, Toon Verstraelen, Matthias Vandichel, Sarah Couck Karen Leus, Ying-Ya Liu, Michel Waroquier, Veronique Van Speybroeck, “New Functionalized Metal–Organic Frameworks MIL-47-X Synthesis, Characterization, and CO₂ Adsorption Properties.” *J. Phys. Chem. C*, pp. 22784–22796, 2013.
- [57] D. E. P. Vanpoucke, “Linker Functionalization in MIL-47(V)-R Metal–Organic Frameworks: Understanding the Electronic Structure,” *J. Phys. Chem. C*, vol. 121, no. 14, pp. 8014–8022, 2017.
- [58] B. Dhara *et al.*, “Increase in Electrical Conductivity of MOF to Billion-Fold upon Filling the Nanochannels with Conducting Polymer,” *J. Phys. Chem. Lett.*, vol. 7, no. 15, pp. 2945–2950, Aug. 2016.
- [59] M. Fuentes-Cabrera, D. M. Nicholson, B. G. Sumpter, and M. Widom, “Electronic structure and properties of isorecticular metal-organic frameworks: The case of M-IRMOF1 (M=Zn, Cd, Be, Mg, and Ca),” *J. Chem. Phys.*, vol. 123, no. 12, p. 124713, Sep. 2005.
- [60] Y. R. Lee, J. Kim, and W. S. Ahn, “Synthesis of metal-organic frameworks: A mini review,” *Korean J. Chem. Eng.*, vol. 30, no. 9, pp. 1667–1680, 2013.
- [61] H. Xu, S. Sommer, N. L. N. Broge, J. Gao, and B. B. Iversen, “The Chemistry of Nucleation: In Situ Pair Distribution Function Analysis of Secondary Building Units During UiO-66 MOF Formation,” *Chem. - A Eur. J.*, vol. 25, no. 8, pp. 2051–2058, 2019.
- [62] M. Taddei, J. A. van Bokhoven, and M. Ranocchiari, “Influence of Water in the Synthesis of the Zirconium-Based Metal–Organic Framework UiO-66: Isolation and Reactivity of [ZrCl(OH)₂(DMF)₂]Cl,” *Inorg. Chem.*, vol. 59, no. 11, pp. 7860–7868, Jun. 2020.

- [63] G. M. Pound and V. K. La Mer, "Kinetics of Crystalline Nucleus Formation in Supercooled Liquid Tin^{1,2}," *J. Am. Chem. Soc.*, vol. 74, no. 9, pp. 2323–2332, May 1952.
- [64] M. Avrami, "Kinetics of Phase Change. I General Theory," *J. Chem. Phys.*, vol. 7, no. 12, pp. 1103–1112, Dec. 1939.
- [65] J. De Yoreo, "More than one pathway," *Nat. Mater.*, vol. 12, no. 4, pp. 284–285, 2013.
- [66] O. M. Yaghi, M. O’Keeffe, N. W. Ockwig, H. K. Chae, M. Eddaoudi, and J. Kim, "Reticular synthesis and the design of new materials," *Nature*, vol. 423, no. 6941, pp. 705–714, 2003.
- [67] M. G. Goesten *et al.*, "Evidence for a chemical clock in oscillatory formation of UiO-66," *Nat. Commun.*, vol. 7, no. May, pp. 1–8, 2016.
- [68] E. A. Tomic, "Thermal stability of coordination polymers," *J. Appl. Polym. Sci.*, vol. 9, no. 11, pp. 3745–3752, Nov. 1965.
- [69] B. F. Hoskins and R. Robson, "Design and construction of a new class of scaffolding-like materials comprising infinite polymeric frameworks of 3D-linked molecular rods. A reappraisal of the zinc cyanide and cadmium cyanide structures and the synthesis and structure of the diamond-rela," *J. Am. Chem. Soc.*, vol. 112, no. 4, pp. 1546–1554, Feb. 1990.
- [70] J. Bedia, V. Muelas-Ramos, M. Peñas-Garzón, A. Gómez-Avilés, J. J. Rodríguez, and C. Belver, "A review on the synthesis and characterization of metal organic frameworks for photocatalytic water purification," *Catalysts*, vol. 9, no. 1, 2019.
- [71] O. M. Y. Jesse L.C. Rowsell, "Metal–organic frameworks a new class of porous material," *Micro porous Mesoporous Mater.*, vol. 73, pp. 3–14, 2004.
- [72] O. K. Farha *et al.*, "Metal–Organic Framework Materials with Ultrahigh Surface Areas: Is the Sky the Limit?," *J. Am. Chem. Soc.*, vol. 134, no. 36, pp.

15016–15021, Sep. 2012.

- [73] T. Ogawa, K. Iyoki, T. Fukushima, and Y. Kajikawa, “Landscape of research areas for zeolites and metal-organic frameworks using computational classification based on citation networks,” *Materials (Basel)*, vol. 10, no. 12, pp. 1–20, 2017.
- [74] V. V. Butova, M. A. Soldatov, A. A. Guda, K. A. Lomachenko, and C. Lamberti, “Metal-organic frameworks: Structure, properties, methods of synthesis and characterization,” *Russ. Chem. Rev.*, vol. 85, no. 3, pp. 280–307, 2016.
- [75] R. Seetharaj, P. V. Vandana, P. Arya, and S. Mathew, “Dependence of solvents, pH, molar ratio and temperature in tuning metal organic framework architecture,” *Arab. J. Chem.*, vol. 12, no. 3, pp. 295–315, 2019.
- [76] K. Sumida *et al.*, “Carbon Dioxide Capture in Metal–Organic Frameworks,” *Chem. Rev.*, vol. 112, no. 2, pp. 724–781, Feb. 2012.
- [77] M. O. & O. M. Y. Hailian Li, Mohamed Eddaoudi, “Design and synthesis of an exceptionally stable and highly,” *Lett. to Nat.*, vol. 402, no. November, pp. 276–279, 1999.
- [78] S. Biswas and P. Van Der Voort, “A General Strategy for the Synthesis of Functionalised UiO-66 Frameworks: Characterisation, Stability and CO₂ Adsorption Properties,” *Eur. J. Inorg. Chem.*, vol. 2013, no. 12, pp. 2154–2160, Apr. 2013.
- [79] A. Schaate *et al.*, “Modulated Synthesis of Zr-Based Metal–Organic Frameworks: From Nano to Single Crystals,” *Chem. – A Eur. J.*, vol. 17, no. 24, pp. 6643–6651, Jun. 2011.
- [80] G. C. Shearer, S. Chavan, S. Bordiga, S. Svelle, U. Olsbye, and K. P. Lillerud, “Defect Engineering: Tuning the Porosity and Composition of the Metal–Organic Framework UiO-66 via Modulated Synthesis,” *Chem. Mater.*, vol.

28, no. 11, pp. 3749–3761, Jun. 2016.

- [81] H. Wu *et al.*, “Unusual and Highly Tunable Missing-Linker Defects in Zirconium Metal–Organic Framework UiO-66 and Their Important Effects on Gas Adsorption,” *J. Am. Chem. Soc.*, vol. 135, no. 28, pp. 10525–10532, Jul. 2013.
- [82] M. Taddei *et al.*, “Band gap modulation in zirconium-based metal-organic frameworks by defect engineering,” *J. Mater. Chem. A*, vol. 7, no. 41, pp. 23781–23786, 2019.
- [83] D. M. Venturi, F. Campana, F. Marmottini, F. Costantino, and L. Vaccaro, “Extensive screening of green solvents for safe and sustainable UiO-66 synthesis,” *ACS Sustain. Chem. Eng.*, vol. 8, no. 46, pp. 17154–17164, 2020.
- [84] Y. Yan, Y. Luo, J. Ma, B. Li, H. Xue, and H. Pang, “Facile Synthesis of Vanadium Metal-Organic Frameworks for High-Performance Supercapacitors,” *Small*, vol. 14, no. 33, pp. 1–8, 2018.
- [85] E. Stavitski *et al.*, “Complexity behind CO₂ Capture on NH₂-MIL-53(Al),” *Langmuir*, vol. 27, no. 7, pp. 3970–3976, Apr. 2011.
- [86] K. Yue *et al.*, “Recent advances in strategies to modify MIL-125 (Ti) and its environmental applications,” *J. Mol. Liq.*, vol. 335, p. 116108, 2021.
- [87] Q. Huang, Y. Hu, Y. Pei, J. Zhang, and M. Fu, “In situ synthesis of TiO₂@NH₂-MIL-125 composites for use in combined adsorption and photocatalytic degradation of formaldehyde,” *Appl. Catal. B Environ.*, vol. 259, no. August, p. 118106, 2019.
- [88] H. L. Nguyen, “The chemistry of titanium-based metal–organic frameworks,” *New J. Chem.*, vol. 41, no. 23, pp. 14030–14043, 2017.
- [89] C. Zlotea *et al.*, “Effect of NH₂ and CF₃ functionalization on the hydrogen sorption properties of MOFs,” *Dalt. Trans.*, vol. 40, no. 18, pp. 4879–4881, 2011.

- [90] Y. Zhao, W. Cai, J. Chen, Y. Miao, and Y. Bu, "A Highly Efficient Composite Catalyst Constructed From NH₂-MIL-125(Ti) and Reduced Graphene Oxide for CO₂ Photoreduction," *Front. Chem.*, vol. 7, p. 789, 2019.
- [91] V. V Butova, A. P. Budnyk, K. M. Charykov, K. S. Vetlitsyna-Novikova, C. Lamberti, and A. V Soldatov, "Water as a structure-driving agent between the UiO-66 and MIL-140A metal-organic frameworks," *Chem. Commun.*, vol. 55, no. 7, pp. 901–904, 2019.
- [92] Y. Feng, Q. Chen, M. Jiang, and J. Yao, "Tailoring the Properties of UiO-66 through Defect Engineering: A Review," *Ind. Eng. Chem. Res.*, vol. 58, no. 38, pp. 17646–17659, 2019.
- [93] F. G. Cirujano, A. Corma, and F. X. Llabrés i Xamena, "Conversion of levulinic acid into chemicals: Synthesis of biomass derived levulinate esters over Zr-containing MOFs," *Chem. Eng. Sci.*, vol. 124, pp. 52–60, 2015.
- [94] S. Øien *et al.*, "Detailed structure analysis of atomic positions and defects in zirconium metal-organic frameworks," *Cryst. Growth Des.*, vol. 14, no. 11, pp. 5370–5372, 2014.
- [95] A. E. Platero-Prats *et al.*, "Structural Transitions of the Metal-Oxide Nodes within Metal-Organic Frameworks: On the Local Structures of NU-1000 and UiO-66," *J. Am. Chem. Soc.*, vol. 138, no. 12, pp. 4178–4185, 2016.
- [96] M. Taddei, "When defects turn into virtues: The curious case of zirconium-based metal-organic frameworks," *Coord. Chem. Rev.*, vol. 343, pp. 1–24, 2017.
- [97] K. Hendrickx *et al.*, "Understanding Intrinsic Light Absorption Properties of UiO-66 Frameworks: A Combined Theoretical and Experimental Study," *Inorg. Chem.*, vol. 54, no. 22, pp. 10701–10710, Nov. 2015.
- [98] C. H. Hendon *et al.*, "Engineering the Optical Response of the Titanium-MIL-125 Metal-Organic Framework through Ligand Functionalization," *J. Am.*

Chem. Soc., vol. 135, no. 30, pp. 10942–10945, Jul. 2013.

- [99] S. Hu *et al.*, “Effects of monocarboxylic acid additives on synthesizing metal-organic framework NH₂-MIL-125 with controllable size and morphology,” *Cryst. Growth Des.*, vol. 17, no. 12, pp. 6586–6595, 2017.
- [100] F. Vermoortele *et al.*, “Synthesis Modulation as a Tool To Increase the Catalytic Activity of Metal–Organic Frameworks: The Unique Case of UiO-66(Zr),” *J. Am. Chem. Soc.*, vol. 135, no. 31, pp. 11465–11468, Aug. 2013.
- [101] S. J. D. Smith, B. P. Ladewig, A. J. Hill, C. H. Lau, and M. R. Hill, “Post-synthetic Ti Exchanged UiO-66 Metal-Organic Frameworks that Deliver Exceptional Gas Permeability in Mixed Matrix Membranes,” *Sci. Rep.*, vol. 5, no. 1, p. 7823, 2015.
- [102] N. T. T. Van, L. C. Loc, N. Tri, and H. T. Cuong, “Synthesis, characterisation, adsorption ability and activity of Cu,ZnO@UiO-66 in methanol synthesis,” *Int. J. Nanotechnol.*, vol. 12, no. 5–7, pp. 405–415, Jan. 2015.
- [103] B. M. Connolly *et al.*, “Tuning porosity in macroscopic monolithic metal-organic frameworks for exceptional natural gas storage,” *Nat. Commun.*, vol. 10, no. 1, pp. 1–11, 2019.
- [104] J. Zhang *et al.*, “Emerging porous materials in confined spaces: From chromatographic applications to flow chemistry,” *Chem. Soc. Rev.*, vol. 48, no. 9, pp. 2566–2595, 2019.
- [105] Z. Yan *et al.*, “Preparation and evaluation of silica-UIO-66 composite as liquid chromatographic stationary phase for fast and efficient separation,” *J. Chromatogr. A*, vol. 1366, pp. 45–53, Oct. 2014.
- [106] N. Chang and X.-P. Yan, “Exploring reverse shape selectivity and molecular sieving effect of metal-organic framework UIO-66 coated capillary column for gas chromatographic separation,” *J. Chromatogr. A*, vol. 1257, pp. 116–124, 2012.

- [107] S.-L. Li and Q. Xu, “Metal–organic frameworks as platforms for clean energy,” *Energy Environ. Sci.*, vol. 6, no. 6, pp. 1656–1683, 2013.
- [108] C. Dey, T. Kundu, B. P. Biswal, A. Mallick, and R. Banerjee, “Crystalline metal-organic frameworks (MOFs): synthesis, structure and function,” *Acta Crystallogr. Sect. B*, vol. 70, no. 1, pp. 3–10, Feb. 2014.
- [109] M. Rubio-Martinez, C. Avci-Camur, A. W. Thornton, I. Imaz, D. Maspoch, and M. R. Hill, “New synthetic routes towards MOF production at scale,” *Chem. Soc. Rev.*, vol. 46, no. 11, pp. 3453–3480, 2017.
- [110] M. A. Abdelkareem, Q. Abbas, M. Mouselly, H. Alawadhi, and A. G. Olabi, “High-performance effective metal–organic frameworks for electrochemical applications,” *J. Sci. Adv. Mater. Devices*, vol. 7, no. 3, p. 100465, 2022.
- [111] G. Zahn *et al.*, “Insight into the mechanism of modulated syntheses: in situ synchrotron diffraction studies on the formation of Zr-fumarate MOF,” *CrystEngComm*, vol. 16, no. 39, pp. 9198–9207, 2014.
- [112] H. Li *et al.*, “Crystal-Growth-Dominated Fabrication of Metal–Organic Frameworks with Orderly Distributed Hierarchical Porosity,” *Angew. Chemie - Int. Ed.*, vol. 59, no. 6, pp. 2457–2464, 2020.
- [113] K. A. S. Usman *et al.*, “Downsizing metal–organic frameworks by bottom-up and top-down methods,” *NPG Asia Mater.*, vol. 12, no. 1, p. 58, 2020.
- [114] D. Erdemir, A. Y. Lee, and A. S. Myerson, “Nucleation of crystals from solution: Classical and two-step models,” *Acc. Chem. Res.*, vol. 42, no. 5, pp. 621–629, 2009.
- [115] P. Chammingkwan *et al.*, “Modulator-free approach towards missing-cluster defect formation in Zr-based UiO-66,” *RSC Adv.*, vol. 10, no. 47, pp. 28180–28185, 2020.
- [116] J. Qiu, Y. Feng, X. Zhang, M. Jia, and J. Yao, “Acid-promoted synthesis of UiO-66 for highly selective adsorption of anionic dyes: Adsorption

- performance and mechanisms,” *J. Colloid Interface Sci.*, vol. 499, pp. 151–158, 2017.
- [117] U. Wayne Rasban, National Institute of Health (NIH), “ImageJ,” 1997. [Online]. Available: www.imagej.net.
- [118] M. Miyamoto, S. Kohmura, H. Iwatsuka, Y. Oumi, and S. Uemiya, “In situ solvothermal growth of highly oriented Zr-based metal organic framework UiO-66 film with monocrystalline layer,” *CrystEngComm*, vol. 17, no. 18, pp. 3422–3425, 2015.
- [119] P. Wang, J. Lang, D. Liu, and X. Yan, “TiO₂ embedded in carbon submicron-tablets: synthesis from a metal–organic framework precursor and application as a superior anode in lithium-ion batteries,” *Chem. Commun.*, vol. 51, no. 57, pp. 11370–11373, 2015.
- [120] N. A. Rodríguez, R. Parra, and M. A. Grela, “Triethylamine as a tuning agent of the MIL-125 particle morphology and its effect on the photocatalytic activity,” *SN Appl. Sci.*, vol. 2, no. 11, p. 1881, 2020.
- [121] P. Yang, Y. Huang, Z. W. Zhang, N. Li, and Y. Fan, “Shape-controlled synthesis of the metal-organic framework MIL-125 towards a highly enhanced catalytic performance for the oxidative desulfurization of 4,6-dimethyldibenzothiophene,” *Dalt. Trans.*, vol. 49, no. 29, pp. 10052–10057, 2020.
- [122] M. Y. Zorainy, M. Sheashea, S. Kaliaguine, M. Gobara, and D. C. Boffito, “Facile solvothermal synthesis of a MIL-47(V) metal-organic framework for a high-performance Epoxy/MOF coating with improved anticorrosion properties,” *RSC Adv.*, vol. 12, no. 15, pp. 9008–9022, 2022.
- [123] A. Centrone, T. Harada, S. Speakman, and T. A. Hatton, “Facile synthesis of vanadium metal-organic frameworks and their magnetic properties,” *Small*, vol. 6, no. 15, pp. 1598–1602, 2010.

- [124] M. C. Lawrence and M. J. Katz, “Analysis of the Water Adsorption Isotherms in UiO-Based Metal–Organic Frameworks,” *J. Phys. Chem. C*, vol. 126, no. 2, pp. 1107–1114, 2022.

APPENDICES

A. Particle size distribution of UiO-66, MIL-125, and MIL-47

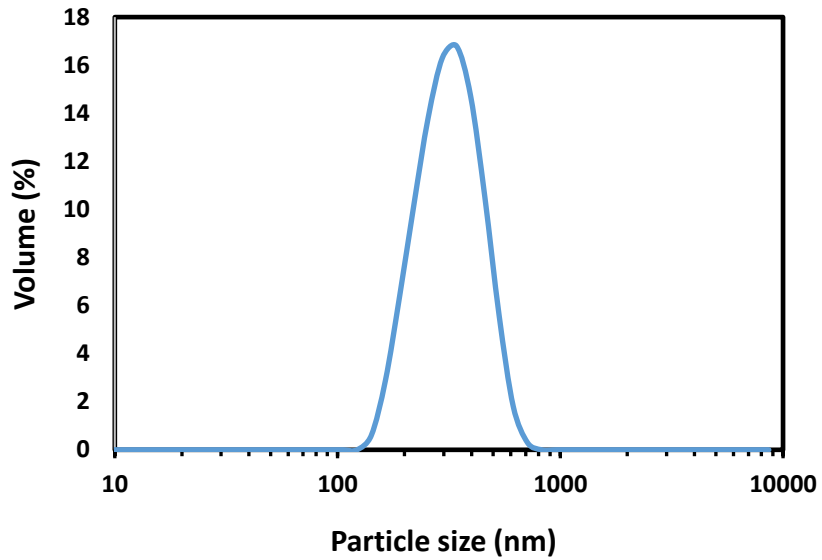


Figure A. 1 Particle size distribution curve of UiO-66 (sample U66-80-C1) obtained via Zeta potential analysis.

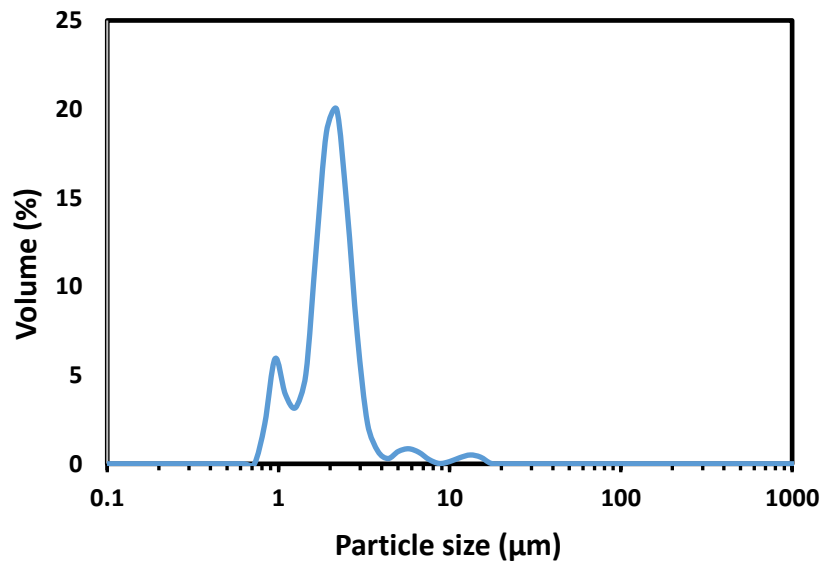


Figure A. 2 Particle size distribution curve of MIL-125 (sample M125-15-3) obtained via DLS

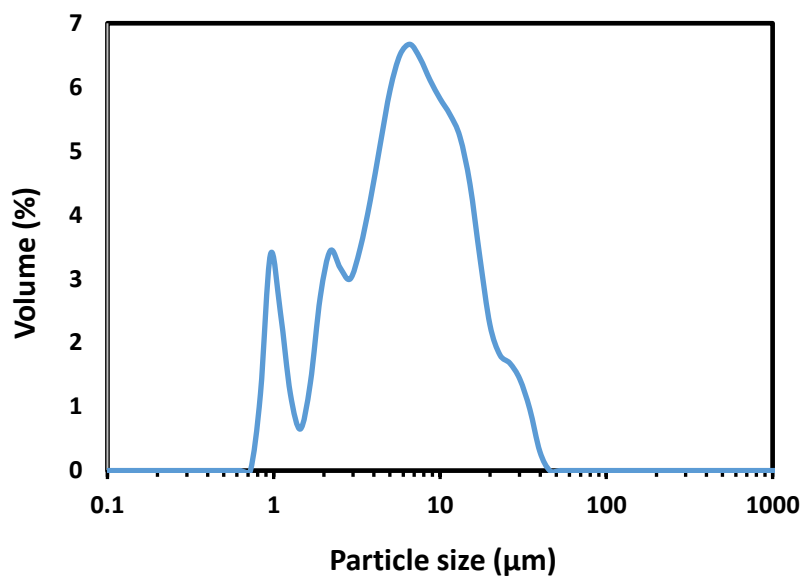


Figure A. 3 Particle size distribution curve of MIL-47 (sample M47-160-5) obtained via DLS.